Elsevier Editorial System(tm) for Gondwana Research
Manuscript Draft

Manuscript Number:

Title: New insights into the geodynamics of Neo-Tethys in the Makran area: Evidence from age and petrology of ophiolites from the Coloured Mélange Complex (SE Iran)

Article Type: SI:TETHYAN OROGENS

Corresponding Author: Professor Emilio Saccani,

Corresponding Author's Institution: Dipartimento di Fisica e Scienze della Terra

First Author: Emilio Saccani

Order of Authors: Emilio Saccani; Morteza Delavari; Asghar Dolati; Michele Marroni; Luca Pandolfi; Marco Chiari; Edoardo Barbero

Abstract: The Coloured Mélange Complex is part of the North Makran domain (SE Iran) and consists of an assemblage of metric-to decametric-thick slices mainly represented by volcanic rocks, locally stratigraphically associated with radiolarian cherts. In this paper, we present new geochemical data on volcanic rocks and biochronological data on the associated cherts. Our data indicate the occurrence of a wide range of volcanic rocks-types, which are: 1) normal-type mid-ocean ridge basalts (N-MORB); 2) oceanic plateau basalts (OPB); 3) alkaline basalts; 4) calc-alkaline basalts, basaltic andesites, andesites, and dacites; 5) volcanic arc tholeiitic basalts and dacites, and high pressure-low temperature metabasalts formed in deep levels of an accretionary wedge. The volcanic arc tholeiites range from Early (late Hauterivian-early Aptian) to Late (latest Cenomanian-lower late Campanian) Cretaceous, whereas the calc-alkaline rocks and OPBs are Late Cretaceous in age (early Coniacian-Santonian and early Turonian-early Campanian, respectively). Alkaline basalts, OPBs, and N-MORBs represent remnants of the Mesozoic Neo-Tethys oceanic branch located between the Arabian plate and the Lut block. In this paper we document that this oceanic sector was characterized by the development of an oceanic plateau in the Late Cretaceous. In contrast, calc-alkaline and volcanic arc tholeiitic rocks represent remnants of a continental volcanic arc and forearc, respectively, developed onto the southernmost realm of the Lut block. The petrogenesis and age of volcanic rocks allow us to propose a new tectono-magmatic model for the evolution of the convergent margin developed in the northern sector of the Neo-Tethys from Early to Late Cretaceous. This model is basically constrained by the collision of the oceanic plateau with the continental arc, which led to the jump of the subduction toward the south, as well as to the formation of the imbricate pile of different units today observed in the North Makran area.

Suggested Reviewers: Alastair Robertson
Scool of GeoSciences, University of Edinburgh, UK
Alastair.Robertson@ed.ac.uk
High level of expertise in the geodynamic evolution of the Neo-Tethys. Excellent knowledge of the Middle East ophiolites, as well as good

aptitude for evaluating magmatic processes. He will certainly be able to evaluate all different multidisciplinary aspects of the manuscript.

Yildirim Dilek
Department of Geology & Environmental Earth Science, Miami University, Oxford, OH, USA
dileky@miamioh.edu
Excellent expertise on both petrogenetic processes of magmatic rocks and geodynamic evolution of the Neo-Tethys

Cemal M. Göncüoglu
Geological Engineering Department06531, Anka, Middle East Technical University, Ankara, Turkey
mcgoncu@metu.edu.tr
High level of expertise in magmatic and tectonic processes, as well as in regional geology. Excellent aptitude for multidisciplinary (tectonics, stratigraphy, petrology, etc) approach.

Marc Sosson
Facultés des Sciences, Géoazur, Université de Nice Sophia Antipolis, France
sosson@geoazur.unice.fr
He has worked extensively on ophiolites and convergent margins in the Caucasus. He is a petrologist with, however, an excellent aptitude for multidisciplinary (tectonics, stratigraphy, geodynamics, etc) approach.

Hubert Whitechurch
Institut de Géologie, Université de Strasbourg (UdS), France
hubert.whitechurch@unistra.fr
He has worked extensively on Iranian ophiolites. He has all the necessary expertize for evaluating multidisciplinary studies

Opposed Reviewers:

Manuscript: "New insights into the geodynamics of Neo-Tethys in the Makran area: Evidence from age and petrology of ophiolites from the Coloured Mélange Complex (SE Iran)"
Authors: Emilio Saccani, Morteza Delavari, Asghar Dolati, Michele Marroni, Luca Pandolfi, Marco Chiari, and Edoardo Barbero

Submitted to GR Special Issue on "Tectono-Magmatic Evolution and Metallogenesis in the eastern Tethyan orogens"

COVER LETTER

Dear Editors,
We are very pleased to contribute to the GR SI on eastern Tethyan ophiolites, which will certainly be of great scientific impact.

We contribute with a paper on the Makran ophiolites. We think that this contribution will fully match the aim of the SI. In fact, The Makran ophiolites though representing the link between the Turkish-Zagros and Himalayan ophiolites are still almost totally unknown. This paper is innovative as it presents a comprehensive multidisciplinary study on the mélange complex at the base of the Makran ophiolites. Mélange complexes are particularly useful for reconstructing the geodynamic history of an oceanic basin and surrounding continental margins, as they incorporate different rock-types formed in distinct tectonic setting. In this paper, the tectonic setting of the mélange, the tectono-magmatic significance of volcanic rocks and biochronological data on radiolarian cherts are discussed in order to define the evolution of the Neo-Tethys Ocean in the Oman-Iran sector. As a major result, we document for the fist time the occurrence of an oceanic plateau within this oceanic sector, as well as the existence of a continental volcanic arc in the southern rim of the Lut block. It is widely recognized that the collision of oceanic plateau with a continental arc has a great impact on the tectonics of the whole oceanic basin and its continental margins. Therefore, we propose a new geodynamic model for the Neo-Tethys branch south of the Lut block based on oceanic plateau-arc collision.
This paper has the potential to be of timely significance and broad interest for researchers working on Alpine orogenic belts. The results obtained in this paper can also represent a valid support for future studies on stratigraphy, petrogenesis, tectonics, and biochronology on the Iranian-Oman ophiolites. In particular, the occurrence of an oceanic plateau within the Neo-Tethys may represent a robust constrain for explaining the widespread occurrence of enriched (plume MORB) and alkaline basalts in many Iranian ophiolitic complexes. Finally, our data indicate that the oceanic plateau-arc collision is coeval with the emplacement of the Oman ophiolites onto the Arabian margin. This evidence may also be of great interest for future geodynamic reconstructions.

The data presented in this paper have not been submitted to any other Journal by any of the authors or have been published or are in review or in press.

I specify that all authors have been involved with the work, have approved the manuscript, and agree to its submission.

Thank you very much for your consideration
Sincerely yours
Emilio Saccani
(On behalf of co-authors)

*Graphical Abstract

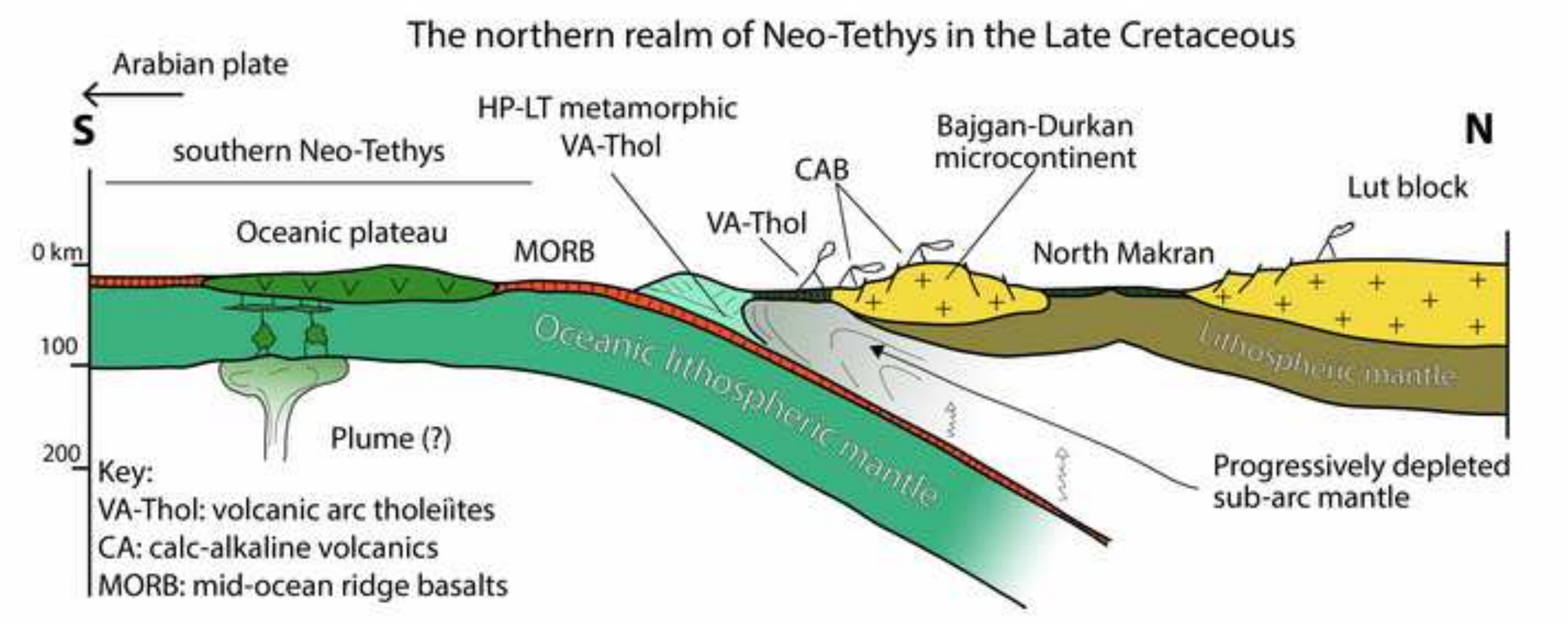

***Highlights (for review)**

Manuscript: "New insights into the geodynamics of Neo-Tethys in the Makran area: Evidence from age and petrology of ophiolites from the Coloured Mélange Complex (SE Iran)"
Authors: Emilio Saccani, Morteza Delavari, Asghar Dolati, Michele Marroni, Luca Pandolfi, Marco Chiari, and Edoardo Barbero

Submitted to GR Special Issue on "Tectono-Magmatic Evolution and Metallogenesis in the eastern Tethyan orogens"

HIGHLIGHTS

- Oceanic plateau basalts are documented for the first time in the eastern Neo-Tethys
- In Late Cretaceous, the oceanic plateau clogged with a volcanic arc
- This collision had a great impact on the geodynamics at a regional scale

New insights into the geodynamics of Neo-Tethys in the Makran area: Evidence from age and petrology of ophiolites from the Coloured Mélange Complex (SE Iran)

Emilio Saccani[a], Morteza Delavari[b], Asghar Dolati[b], Michele Marroni[c], Luca Pandolfi[c], Marco Chiari[d] and Edoardo Barbero[a]

a. Dipartimento di Fisica e Scienze della Terra, Università di Ferrara, Via Saragat 1, 44123 Ferrara, Italy

b. Faculty of Earth Sciences, Kharazmi University, Shahid Mofatteh St. 43, Tehran, Iran

c. Dipartimento di Scienze della Terra, Università di Pisa, Via S. Maria 53, 56126 Pisa, Italy

d. CNR, Istituto di Geoscienze e Georisorse, Via La Pira 4, 50121 Florence, Italy

Corresponding author:

Dr. Emilio Saccani

E-mail: sac@unife.it

Phone: +39 0532 974719

ABSTRACT

The Coloured Mélange Complex is part of the North Makran domain (SE Iran) and consists of an assemblage of metric-to decametric-thick slices mainly represented by volcanic rocks, locally stratigraphically associated with radiolarian cherts. In this paper, we present new geochemical data on volcanic rocks and biochronological data on the associated cherts. Our data indicate the occurrence of a wide range of volcanic rocks-types, which are: 1) normal-type mid-ocean ridge basalts (N-MORB); 2) oceanic plateau basalts (OPB); 3) alkaline basalts; 4) calc-alkaline basalts, basaltic andesites, andesites, and dacites; 5) volcanic arc tholeiitic basalts and dacites, and high pressure-low temperature metabasalts formed in deep levels of an accretionary wedge. The volcanic arc tholeiites range from Early (late Hauterivian-early Aptian) to Late (latest Cenomanian-lower late Campanian) Cretaceous, whereas the calc-alkaline rocks and OPBs are Late Cretaceous in age (early Coniacian-Santonian and early Turonian-early Campanian, respectively). Alkaline basalts, OPBs, and N-MORBs represent remnants of the Mesozoic Neo-Tethys oceanic branch located between the Arabian plate and the Lut block. In this paper we document that this oceanic sector was characterized by the development of an oceanic plateau in the Late Cretaceous. In contrast, calc-alkaline and volcanic arc tholeiitic rocks represent remnants of a continental volcanic arc and forearc, respectively, developed onto the southernmost realm of the Lut block. The petrogenesis and age of volcanic rocks allow us to propose a new tectono-magmatic model for the evolution of the convergent margin developed in the northern sector of the Neo-Tethys from Early to Late Cretaceous. This model is basically constrained by the collision of the oceanic plateau with the continental arc, which led to the jump of the subduction toward the south, as well as to the formation of the imbricate pile of different units today observed in the North Makran area.

KEYWORDS: ophiolite, mélange, Neo-Tethys, Makran, Iran, Cretaceous

1. Introduction

Most of the modern and fossil accretionary prisms are characterized by the widespread occurrence of mélanges (e.g., Festa et al., 2010), i.e. mappable units or bodies of mixed rocks including blocks of different ages and origin (e.g., Raymond, 1984). Owing to the lack of internal continuity of rock bodies deriving from high stratal disruption, these units are regarded as a result of different processes, such as tectonic shearing during accretion, mass transport in front of the accretionary prism or mud diapirism inside it.

Most of the mélanges in the accretionary prisms are characterized by blocks of incomplete ophiolitic sequences or ophiolitic rocks. These mélanges may incorporate a wide range of different ophiolitic rock-types, including: 1) continental margin ophiolites generated at the ocean-continent transition zone; 2) Mid-ocean ridge type and plume type ophiolites generated in subduction-unrelated oceanic settings; 3) supra-subduction type ophiolites generated at intra-oceanic arc settings; 4) volcanic arc ophiolites forming in long lasting arc settings onto polygenetic crust and showing island arc tholeiitic to calc-alkaline geochemical signatures (see Dilek and Furnes, 2011 for a detailed definition of the ophiolitic types). In other words, these mélanges may incorporate rocks forming at different tectonic settings and in different times. These rock-types can therefore be used for determining the nature and tectonic significance of the magmatic events that occurred in an oceanic basin and surrounding areas from the early oceanic spreading phase to the oceanic consumption in a subduction setting and development of backarc settings.

In the Makran region, SE Iran, (Figs.1a, b) one of the largest worldwide accretionary wedges is exposed (McCall and Kidd, 1982; Burg et al., 2013; Dolati and Burg, 2013). This accretionary wedge is regarded as the result of the northward subduction of the oceanic lithosphere of the Oman Sea beneath the Lut and Afghan continental blocks (McQuarrie et al.

2003; Masson et al. 2007). To the North, the accretionary wedge is bounded by the north Makran domain that can be regarded as the backstop of the accretionary wedge. The North Makran domain is represented by an imbricate stack of continental and oceanic units (McCall, 1985; 2002; Hunziker et al., 2015), including, the Coloured Mélange Complex (McCall and Kidd, 1982; McCall, 1985), also referred as the Imbricate Zone (Burg et al., 2013). The Coloured Mélange Complex, in turn, includes blocks of volcanic rocks of different origin locally showing primary relationships with their sedimentary cover, which is usually represented by radiolarian cherts. Unfortunately, no data on the geochemistry and tectono-magmatic significance of volcanic rocks, as well as on the biochronology of the associated cherts are up to now available. However, these data are crucial for recognizing the nature and age of the magmatic events that occurred in the oceanic basin and surrounding areas, thus providing robust constraints in the reconstruction of the geodynamic history of Makran sector of the Neo-Tethys during Cretaceous times. The aim of this paper is therefore to present new petrological, biostratigraphical, and tectonic data on volcanic and metavolcanic blocks included into the Coloured Mélange Complex of Makran. Such a multidisciplinary study is fundamental for providing robust constraints in the reconstruction of the geodynamic history of the Makran sector of the Neo-Tethys during Cretaceous times.

2. Overview of the Makran geology

The E-W trending Makran accretionary wedge extends between the Minab dextral transform fault (to the west) and the sinistral Chaman transform fault (to the east) with a width of 300–350 km. More than half of the accretionary wedge is exposed on land (Figs.1a, 2a) (McCall and Kidd, 1982; Dercourt et al., 1986; Burg et al., 2008; 2013; Dolati and Burg, 2013). The active, submarine frontal part is located southward in the Oman Sea where the ongoing subduction of the oceanic lithosphere shows a rate of about 2 cm/a in a roughly south-to-north direction (McQuarrie et al. 2003; Masson et al. 2007).

The accretionary wedge has been divided by Burg et al. (2013) into three main tectono-stratigraphic domains (Figs.2a, b), each representing different segments known as the Inner, Outer and Coastal Makran. The boundaries between these domains are represented by N-dipping, low-angle thrusts showing progressively younger ages from the north to the south (Burg et al., 2013). Northward, these domains are bounded by the North Makran domain, which is represented by an imbricate stack of continental and oceanic units, and it can be regarded as the backstop of the accretionary wedge (McCall, 1985; 2002; Hunziker et al., 2015). To the north, the North Makran domain is bounded by the Jaz Murian depression (Fig. 2b) that is considered as a forearc basin opened at the southern rim of the Lut block as a consequence of the Makran subduction (McCall and Kidd, 1982; McCall, 1985; 1997; Glennie, 2000; Burg et al., 2008; 2013). In contrast, to the Inner, Outer and Coastal Makran domains, which resulted from a northward subduction that was established since the Eocene times, the North Makran domain preserves remnants of the pre-Eocene geodynamic history.

The North Makran consists of several tectonic units, described in the literature as geotectonic provinces, each bounded by high-angle shear zones (McCall and Kidd, 1982; McCall, 1985; 1997; Glennie, 2000; Burg et al., 2008; 2013; Dolati and Burg, 2013; Hunziker et al., 2015). The relationships among the different units of the North Makran are sealed by Early Eocene sedimentary deposits, which are widespread along the whole width of the North Makran domain (McCall, 1997; 2002, Burg et al., 2013). The units of North Makran are thrust over the tectonic units of the Inner Makran (Figs. 2a, b) consisting of Late Eocene to Early Miocene siliciclastic turbidites at the top of Paleocene to Middle Eocene pelagic sediments and volcanic rocks (Burg et al., 2013). The boundary between the North and Inner Makran is represented by the Bashakerd thrust (Fig. 3), a main fault zone separating two geologically different domains.

From south to the north and from bottom to the top, four tectonic units have been identified in the North Makran (Figs. 2, 3): 1) The Coloured Mélange Complex (McCall and Kidd, 1982; McCall, 1985) also referred as Imbricate Zone (Burg et al., 2013), 2) the southern ophiolites, 3) the Bajgan and Durkan Complexes (McCall, 1985; 2002) and, finally, 4) the northern ophiolites. The North Makran Ophiolites represent the remnants of a Cretaceous oceanic basin located between a microcontinental block, today represented by the Bajgan-Durkan Complex, and the Lut continental block. This oceanic basin was subsequently destroyed by the collision between the Bajgan-Durkan microcontinental block and the Lut block leading to the building in the Early Tertiary of the present-day tectonic setting of the North Makran.

The Coloured Mélange Complex will be described in detail in the next paragraph, however it is important to outline that in the Makran accretionary wedge, two different types of mélanges have been found: 1) The Coloured Mélange Complex and 2) the Inner Makran mélange (McCall, 1983). The Coloured Mélange Complex is derived by tectonic processes leading to a fabric consisting of blocks bounded by shear zones and devoid of any matrix. In contrast, Burg et al. (2008) suggested that the Inner Makran mélange consist of a giant body emplaced by sedimentary gravitational processes during Tortonian–Messinian times (between 11.8 and 5.8 Ma). This sedimentary body includes blocks of ophiolites and oceanic sediments derived from the Coloured Mélange Complex. According to Burg et al. (2008) the chaotic nature of this mélange with blocks of any size and lithology and the weak, soft-sediment deformation of the matrix strongly support the sedimentary origin of this mélange.

The southern ophiolites are represented by Sorkhband and Rudan ophiolites that occur in the shear zone between the Coloured Mélange Complex and the Bajgan Complex (McCall, 2002; Delavari et al., 2016). Data about the Rudan ophiolite are lacking, but the Sorkhband ophiolite have been studied by Delavari et al. (2016). This ophiolite includes two different tectonic slices; the upper one is characterized by gabbros, whereas the lower one consists of mantle peridotite with remnants of its associated lower crust. The petrographic and geochemical data indicate that gabbros forming the upper tectonic slice were generated at mid-ocean ridge setting, whereas mantle peridotites of the lower tectonic slice were generated at SSZ setting. Therefore, the Sorkhband ophiolite seems to be derived from two different oceanic domains representing two different geodynamic settings. The age of this ophiolite is unknown, but a Mesozoic age for the ophiolite sequences seems to be the most probable (Delavari et al., 2016).

The Bajgan Complex is a metamorphic assemblage of schists, paragneisses, amphibolites and marbles. Metamorphism ranges from greenschists to amphibolite facies, but scattered occurrence of glaucophane is reported (McCall, 2002). Devonian fossils are reported in the Bajgan Complex by McCall (1985). The age of the metamorphism is unknown, but the occurrence of undeformed Jurassic deposits that lies unconformably over the Bajgan Complex (McCall, 2002) suggests a Paleozoic, or even older, age. In addition, scattered occurrence of serpentinites in uncertain tectonic position is also reported (McCall, 2002). To the east, the Bajgan Complex shows a transition to the Durkan Complex, which consists of a ~250 km-long and ~40 km-wide slice of continental crust (McCall, 1985) made up of an assemblage of Jurassic plutonic bodies associated with Cretaceous lavas, as well as shallow and deep marine, Permian to Cretaceous sedimentary rocks (Hunziker et al., 2015 and quoted references). To the west, the Bajgan Complex continues in the Sanandaj-Sirjan zone (Fig.1b) consisting in a ~1500 km-long metamorphic belt that extends from the northwest (Sanandaj) to southeast (Sirjan) Iran, parallel to the Zagros Fold and Thrust belt (Ghazi and Moazzen, 2015 and quoted references).

The North Makran Ophiolites are represented by several ophiolitic complexes including Band-e-Zeyarat / Dar Anar (Ghazi et al., 2004), Ganj (Shaker-Ardakani et al., 2009), Remeshk-Mokhtarabad (Moslempour et al., 2015), and Fanuj-Maskutan (Desmons and Beccaluva, 1983). Available data on these ophiolites are scarce. The best known sequences are those belonging to Band-e-Zeyarat / Dar Anar and Fanuj-Maskutan ophiolites. According to Ghazi et al. (2004), the Band-e-Zeyarat / Dar Anar ophiolites only consists of upper crustal section, including cumulate layered gabbros, isotropic gabbros, and pillow-lava basalts interbedded with pelagic sediments. The geochemistry of basalts from the Band-e-Zeyarat / Dar Anar ophiolites show enriched mid-ocean ridge (E-MORB) affinity. The ^{40}Ar–^{39}Ar ages are about 140–143 Ma (i.e., Berriasian, Early Cretaceous). In contrast, the Fanuj-Maskutan ophiolites shows a complete sequence from mantle peridotites to pillow-lava basalts and sedimentary cover (Moslempour et al., 2015). Based on the geochemistry of basalts, these authors have interpreted the Fanuj-Maskutan ophiolites as remnants of a back-arc basin formed in a supra-subduction basin during the Late Cretaceous. So, also the North Makran Ophiolites seem to be derived from different oceanic domains representing different geodynamic settings.

3. The Coloured Mélange Complex

The Coloured Mélange Complex (Gansser, 1955; McCall, 1983), which corresponds to the Imbricate Zone, as defined by Burg et al. (2013), consists of an assemblage of blocks i.e. metric- to decametric-thick slices with lozenge-type shape (Figs. 4a, b). The boundaries of the blocks are represented by cm-to dm-thick shear zones represented by foliated cataclasites. No evidence of sedimentary matrix has been recognized at the contact with the different slices. The blocks mainly consist (in order of volumetric abundance) of volcanic rocks, cherts, limestones, serpentinites, gabbros, and shales. Other ophiolitic blocks are represented by mantle serpentinites and serpentinized cumulate peridotites. McCall (1983) described blocks of dunites, harzburgites, wherlites, lherzolites, and websterites. In addition, blocks of layered peridotites with layers of gabbro, pyroxenites, and chromitites also occur. Blocks of gabbros and plagiogranites have also been locally recognized. Blocks of limestone are widespread as well. McCall (1983) reported the occurrence of well-bedded limestones consisting of Globotruncana-bearing biomicrites and Orbitolina-bearing reefal limestones of Albian age. However, the most important occurrence is represented by blocks of Globigerinids-bearing limestones of Early Paleocene age indicating that the processes leading to the origin of the Coloured Mélange took place in the late Paleocene. The occurrence of Eocene deposits unconformably lying at its top also support this conclusion. In addition, blocks of metamorphic rocks consisting of massive, recrystallized limestones and metavolcanic rocks have also been identified. Close to the basal Bashakerd thrust, a block with thick-bedded to massive recrystallized limestone intercalated within strongly sheared metabasalts has been found (Fig. 4c). Metavolcanic blocks are represented by high pressure-low temperature metamorphic rocks with abundant sodic amphibole (Fig. 4d). These blocks are enveloped by blocks of non-metamorphic sedimentary and magmatic rocks that correspond to the definition of 'knockers' of Karig (1980).

In the Coloured Mélange Complex a strong strain partitioning can be observed (Delavari et al., 2016). At the top of this complex, close to the contact with the southern ophiolites and/or the Bajgan Complex, an increase of the deformation has been detected. This intense deformation resulted in about 100 m-thick highly strained band, where the different slices display very different shape and size. This band is characterized by m-thick elongated and boudinaged bodies of marbles, metabasalts and serpentinized peridotites. The sense of shear in this band range from top-to-SW to top-to-S. In contrast, Bashakerd thrust at the base of the Coloured Mélange Complex is represented by a brittle shear zone with a thickness of about 1 km. It consists of an imbricate stack of less than 100 m-thick slices of Oligo-Miocene turbidites and 5 to 10 m-thick blocks derived from the Coloured Mèlange.

4. Field evidence and sampling

Volcanic and metavolcanic blocks were systematically sampled throughout the Mélange Complex. In contrast, radiolarian cherts have been collected in those outcrops where their primary stratigraphic relationships with volcanic rocks can unequivocally be recognized. This sampling method allows us to determine the age of the different magmatic events, providing thus important constraints for the geodynamic reconstruction. Cherts stratigraphically associated with volcanic rocks are however rare. Nonetheless, we found four blocks preserving the primary relationships between volcanic rocks and their sedimentary cover, which mainly consist of radiolaria-bearing cherts and siliceous mudstones. The location of these blocks is indicated in Fig. 3. One block has been recognized in the Manujan area along the road Bandar Abbas-Kahnuj (Kahmij-e-Balo section), whereas the others three blocks crop out in the Gorevi area, close to the road Ghaleh-Ganj-Sardasht (Gorevi 1, 2, and 3 sections). We have logged these blocks and their stratigraphic columns, as well as the position of samples are here described (Fig. 5).

4.1. *Kahmij-e-Balo section*

In this block a thick sequence of basalts (more than 80 m) is capped by ca.14 m of thin-bedded red cherts. The section is overturned (Fig. 5). The basalts are mainly pillow lavas and minor pillow breccia. In the uppermost part of the basalts sequence discontinuous red siliceous shales can be recognized (Fig. 6a) below the contact with the cherts. The sedimentary cover (Fig. 6b) is made up of cm-thick alternance of porcellanaceous red to violet radiolarian-bearing strata and siliceous red shales. The cherts/shales ratio is close to one. The sequence is very uniform and is more than 14 m-thick.

4.2. Gorevi 1 section

This is a 74 m-thick sequence of volcanic and sedimentary rocks showing intercalation of three levels of basalts and two levels of cherts (Fig. 5). From bottom to the top the block stratigraphy is represented by 25 m of pillow lavas capped by 4.4 m of pillow breccias showing primary relationships with 21 m of red cherts. The cherts consist of cm-thick alternance of porcellanaceous red cherts and siliceous red shales (Fig. 6c) and are capped by 2 m of thin bedded red cherty-limestones. A 4 m-thick layer of pillow lava basalts cover the first level of cherts and pass to the second cherts level formed by 5.6 m of thin-bedded alternance of cherts ribbons and siliceous dark shales. In this second level the cherts/shale ratio is less than one. These cherts are covered by the third level of pillow lava, which is more than 12 m-thick.

4.3. Gorevi 2 section

This small block is characterized by a 18 m-thick sequence of volcanic rocks and its sedimentary cover (Fig. 5). The volcanic sequence is represented by pillow lavas showing interpillow red siliceous shales, which are particularly abundant in the uppermost 3 m (Fig. 6d). The basalts are capped by 5.2 m of thin-bedded radiolarian cherts formed by radiolarian bearing cherts and siliceous mudstones with a cherts/shale ratio close to one. The cherts are covered by 3.8 m of dark thin bedded limestones and siliceous marls. The marls have been sampled for nannofossils but the samples were barren.

4.4. Gorevi 3 section

This is a 22 m-thick sequence of volcanic and sedimentary rocks consisting in the alternance of two levels of basaltic rocks with one level of siliceous shales (Fig. 5). The block stratigraphy is represented by 6.2 m of pillow breccia capped by 2.7 m of red siliceous shale with minor ribbons of radiolaria-bearing red cherts. The chert ribbons are discontinuous and less than 5 cm in thickness. The siliceous shales pass to 5 m of pillow lava and then to a 7.1 m-thick level of pillow breccia (Figs. 6e, f).

5. Radiolarian biostratigraphy

A total of ten radiolarian cherts samples were etched with hydrochloric and hydrofluoric acid at different concentrations following the method described by Dumitrica (1970) and Pessagno and Newport (1972). The residues of the different treatments have been observed at the optical microscope, whereas micrographs of the radiolarian species were taken at the scanning electron microscope (SEM). Unfortunately, some of them were barren or yielded radiolarians with poor preservation. Six sample were however suitable for biostratigraphical analysis. The principal radiolarian markers are illustrated in Figure 7. Furthermore, in the following paragraphs, we report the range of some taxa that we utilized for the age determinations of the samples.

5.1. Kahmij-e-Balo section

Sample MK63 gave an early Turonian - early Campanian (Late Cretaceous) age for the presence of *Afens liriodes* Riedel and Sanfilippo with *Archaeospongoprunum bipartitum* Pessagno.

Afens liriodes range: early Turonian (*Superbum* Zone after O'Dogherty, 1994) - late Campanian (lower part *Amphipyndax tylotus* Zone after Sanfilippo and Riedel, 1985).

Archaeospongoprunum bipartitum range: early Turonian (Erbacher, 1994; Bragina, 2016) - early Campanian (Vishnevskaya, 1987; Popova-Goll et al., 2005).

5.2. Gorevi 1 section

Sample MK152 gave a latest Cenomanian-lower late Campanian (Late Cretaceous) age for the presence of *Acanthocircus hueyi* (Pessagno).

Acanthocircus hueyi range: (Pessagno) latest Cenomanian (Salvini and Marcucci Passerini, 1998) - lower late Campanian (*Phaseliforma carinata* Subzone of *Crucella espartoensis* Zone after Pessagno, 1976).

Sample MK154 gave a latest Cenomanian-lower late Campanian (Late Cretaceous) age for the presence of *Acanthocircus hueyi* (Pessagno). This sample contains a poorly-preserved specimen indicated as *Theocampe* (?) sp. cf. *T. urna* (Foreman). If we take in consideration the range of *Theocampe* (?) *urna* it could be possible to indicate a more precise age of early Coniacian-lower late Campanian for this sample.

Sample MK155 gave an early Coniacian-Santonian (Late Cretaceous) age for the presence of *Theocampe* (?) *urna* (Foreman) with *Crucella cachensis* Pessagno.

5.3. Gorevi 2 section

Sample MK145 reseulted late Hauterivian - early Aptian (Early Cretaceous) in age for the presence of *Pantanellium masirahense* Dumitrica with *Orbiculiformella titirez* (Jud).

Pantanellium masirahense range: Hauterivian (Dumitrica et al., 1997) - early Aptian (*Turbocapsula costata* Subzone of *Turbocapsula* Zone after O'Dogherty, 1994 in Aguado et al., 2014).

Orbiculiformella titirez range: late Hauterivian (UAZ 20, after Baumgartner et al., 1995) - early Aptian (*Gongylothorax verbeeki* Subzone of *Turbocapsula* Zone after O'Dogherty, 1994 in Aguado et al., 2014).

5.4. Gorevi 3 section

Sample MK146 gave a early Coniacian-Santonian (Late Cretaceous) age for the presence of *Theocampe* (?) *urna* (Foreman) with *Crucella cachensis* Pessagno.

Crucella cachensis range: latest Cenomanian (Thurow, 1988; Salvini and Marcucci Passerini, 1998) - Santonian (Vishnevskaya, 2010; Bragina et al., 2014).

Theocampe (?) *urna* range: early Coniacian (*Theocampe urna* Zone after Sanfilippo and Riedel, 1985) - late Campanian (*Amphipyndax pseudoconulus* Zone after Sanfilippo and Riedel, 1985).

6. Petrography and geochemistry of volcanic rocks

6.1. Analytical methods

Whole-rock major and some trace element were analyzed by X-ray fluorescence (XRF) on pressed-powder pellets, using an ARL Advant-XP automated X-ray spectrometer. The matrix correction methods proposed by Lachance and Trail (1966) were applied. Volatile contents were determined as loss on ignition (L.O.I.) at 1000°C. In addition, Rb, Sr, Zr, Y, Nb, Hf, Ta, Th, U, and the rare earth elements (REE) were determined by inductively coupled plasma-mass spectrometry (ICP-MS) using a Thermo Series X-I spectrometer. The results are shown in Table 1. Moreover, for the discussion of the geochemical characteristics major element composition has been re-calculated on L.O.I.-free bases.

The accuracy of the data for XRF and ICP-MS analyses were evaluated using results for international standard rocks run as unknown. The detection limits for XRF and ICP-MS analyses were evaluated using results from several runs of twenty-nine international standards. Results are given in Appendix B. All whole-rock analyses were performed at the Department of Physics and Earth Sciences, Ferrara University.

6.2. Petrography

Most of the studied rocks were affected by low temperature, ocean-floor alteration, which resulted in the replacement of primary minerals. Plagioclase is usually replaced by albite, whereas clinopyroxene is pseudomorphosed either by chlorite or actinolitic amphibole. Groundmass secondary phases mainly consist of chlorite, and clay minerals. Nonetheless, in these samples the primary igneous textures are well preserved. Therefore, regardless of the secondary mineralogical transformation, their petrographic description will be made on the bases of primary igneous phases. In contrast, a few samples show intense metamorphic transformations, which obliterated the primary textures and mineral assemblages. Due to the chaotic distribution of the different rock-types within the mélange, for a better understanding the following petrographic description will be made according to the geochemical groups described in the geochemistry section.

Basalt MK52 has vitrophyric texture with small laths of plagioclase and volcanic glass in interstitial position. Basalt MK69 has aphyric, microcrystalline sub-ophitic texture in which small laths of plagioclase and intergranular clinopyroxene can be recognized. This sample also shows a considerable amount of opaque minerals in interstitial position with respect to plagioclase. The crystallization order is: plagioclase + clinopyroxene ± Fe-Ti-oxides.

Group 2. All Group 2 basalts show vitrophyric texture with small laths of plagioclase and volcanic glass in interstitial position. Sample MK62 displays rare skeletal clinopyroxene.

Group 3. Basalt MK56 displays vitrophyric texture with small laths of plagioclase set in volcanic glass. This sample is characterized by a moderate amount of amygdules filled by calcite. In contrast, sample MK70 shows medium-grained doleritic texture with euhedral plagioclase and subhedral clinopyroxene forming the main mineral phases. Epidote, apatite, and relatively abundant opaque minerals occur as accessory phases. The crystallization order is: plagioclase + clinopyroxene ± Fe-Ti-oxides.

Group 4. Basaltic andesite MK144 shows porphyritic texture (PI = ~50). Phenocrysts mainly include plagioclase (0.5-1 mm in size) and hornblende with opacitic rims (0.3-1 mm in size), as well as minor clinopyroxene microphenocrysts (~0.3 mm in size), which are relatively fresh. Phenocrysts are set in a hyalopilitic groundmass. In contrast, basaltic andesite MK67, as well as andesite and dacite display aphyric, intergranular texture. Mineral phases include plagioclase and clinopyroxene in all samples and minor orthopyroxene in the dacite sample. Minor volumes of volcanic glass are found in interstitial position.

Group 5. Group 5 rocks show a wide range of textural features. Basalts MK149, MK150, MK156, and MK158 display aphyric intergranular texture with plagioclase laths and granular clinopyroxene. Minor amounts of glass can also be observed. In contrast, basalt MK143 has porphyritic texture (PI = ~20) with plagioclase and clinopyroxene phenocrysts set in a mycrocristalline, intergranular groundmass. Among phenocrysts, plagioclase is commonly ~2 mm in size, whereas clinopyroxene is comparatively smaller (0.7-1 mm in size). Dacite MK58 displays slightly porphyritic texture (PI = ~10) with microphenocrysts of plagioclase and clinopyroxene set in a hyalopilitic groundmass. The groundmass also shows a clear flow banding marked by bands having slightly different colours. The crystallization order is: clinopyroxene + plagioclase. Samples MK73, MK136, and MK139 show metamorphic textures. Metabasalts MK73 and MK136 have foliated texture. In sample MK73, the foliation is marked by the alignment of fine-grained chlorite and compositional segregation of quartz, albite, and epidote. In sample MK136 the foliation is marked by the alignment of chlorite ± actinolite-tremolite minerals and compositional segregation of quartz and albite. Minor clinopyroxene relicts are observed in both samples. The mineralogical paragenesis of this sample suggests low-grade greenschist-facies metamorphic conditions. In contrast, the metabasaltic andesite MK139 displays lepidoblastic texture, where the schistosity is defined by the alignment of sodic amphibole, whereas the mineralogical banding involves alternation of sodic amphibole with quartz and albite. This sample also contains significant amounts of crisscrossed pumpellyite crystals, as well as minor amounts of epidote. The occurrence of sodic amphibole and pumpellyite indicate blueschist-facies metamorphic condition.

6.3. Geochemistry

The geochemical features of the volcanic rocks from the Coloured Mélange Complex are described using those elements, which are virtually immobile during low-temperature alteration and metamorphism. They include many incompatible trace elements (e.g., Ti, P, Zr, Y, Sc, Nb, Ta, Hf, Th), middle (M) and heavy (H) REE, as well as some transition metals (e.g., Ni, Co, Cr, V). In contrast, large ion lithophile elements (LILE) and major elements are commonly mobilized during alteration (Pearce and Norry, 1979). Light REE (LREE) may also be affected to some degree by alteration-induced mobilization. Some mobility tests were therefore made for Ba, Rb, SiO_2, Al_2O_3, FeO, CaO, Na_2O, K_2O, La, and Ce by plotting these elements versus some immobile elements (e.g., Zr, Y) and then calculating the correlation coefficients (r^2) for the different groups of rocks (not shown). These tests indicate that Rb (r^2 vs Zr = 0.87-0.94), SiO_2 (r^2 vs Zr = 0.89-0.99), Al_2O_3 (r^2 vs Zr = 0.96-0.98), La (r^2 vs Zr = 0.93-0.97), and Ce (r^2 vs Zr = 0.81-0.96) show good correlation with immobile elements suggesting that the amount of mobilization of these elements was limited. FeO (r^2 vs Zr = 0.63-0.80) resulted moderately mobilized in all rock-types. In consequence, these elements can be used, thought with some caution. Tests on CaO and Ba returned different results depending on the rock-type. CaO was mobilized in all samples except those belonging to Group 2 (r^2 vs Zr = 0.99) and Group 4 (r^2 vs Zr = 0.94) rocks. Ba was little mobilized in samples of Group 4 (r^2 vs Zr = 0.90) and Group 5 (r^2 vs Zr = 0.79) rocks and moderately mobilized in Group 2 (r^2 vs Zr = 0.68) rocks. In contrast, Na_2O (r^2 vs Zr = 0.05-0.57) and K_2O (r^2 vs Zr = 0.02-0.53) were affected by high degrees of alteration-induced mobilization and therefore cannot be used.

The volcanic rocks included in the Coloured Mélange Complex show a wide range of geochemical characteristics (Table 1); in fact, five main geochemical groups can be identified.

6.3.1. Group 1 rocks

Group 1 rocks include one basalt and one Fe-basalt (Table 1). These rocks show a clear subalkaline nature with Nb/Y ratios < 0.12 (Fig. 8). The generally low MgO (5.49-6.08 wt.%), CaO (6.30-9.07 wt.%) contents, and Mg# (54.5-40.4), indicate a moderately fractionated nature for basalt MK52 and a rather fractionated nature for Fe-basalt MK69. These rocks show high to very high TiO_2 contents (1.41 - 2.95 wt.%), as well as generally high contents of FeO_t (11.13-16.75 wt.%) P_2O_5 (0.20 - 0.28 wt.%), Zr (110-194 ppm), and Y (37-62 ppm), where the highest contents of these elements are observed in the Fe-basalt. The Ti/V ratios displayed by Group 1 basalts range from 40 to 72 and cluster in the field for basalts generated at mid-ocean ridge settings (Shervais, 1982). Compatible element contents are decreasing from basalt to Fe-basalt (Table 1). The relative distribution of high field strength elements (HFSE) concentrations (Fig. 9a) indicates that these rocks share affinity with ocean-floor basalts. In fact, N-MORB (normal-type mid-ocean ridge basalt) normalized patterns are rather flat and range from ~1 to ~4 times N-MORB contents (Sun and McDonough, 1989) in basalt and Fe-basalt, respectively. REE patterns (Fig. 9b) are also consistent with N-MORB compositions, as they show LREE depletion (La_N/Sm_N = 0.55-0.82) and an overall enrichment for HREE of 20 - 40 times chondrite abundance. In the discrimination diagram in Figure 10 (Wood, 1980), these rocks plot in the field for basalts generated at mid-ocean ridge settings. Accordingly, in the discrimination diagram in Figure 11a (Saccani, 2015), the basaltic sample plots close to the composition of typical N-MORB (Sun and McDonough, 1989), whereas the Fe-basaltic sample plots in the field for N-MORB-type fractionated rocks. Both samples plot in the field for oceanic subduction-unrelated settings (Fig. 11b).

6.3.2. Group 2 rocks

Group 2 volcanic rocks are represented by basalts with SiO_2 ranging from 45.08 to 50.23 wt.% and Mg# ranging between 59.4 and 50.2, which suggest a variably fractionated nature of these rocks. They display a sub-alkaline, tholeiitic nature having low Nb/Y ratios (Table 1, Fig. 8). Group 6 basalts are relatively rich in TiO_2 (1.92-2.11 wt.%), P_2O_5 (0.24-0.29 wt.%) Zr (125-134 ppm), and Y (38-42 ppm). They are also relatively rich in Ni (39-61 ppm) and Cr (126-367 ppm). These rocks show rather flat N-MORB normalized incompatible element patterns from Th to Yb (Fig. 9a), with abundances ranging from ~1.5 to ~4 times N-MORB composition. The chondrite-normalized REE patterns of these rocks are very flat (Fig. 9b), with $(La/Yb)_N$ ranging from 0.93 to 1.25. These basalts show very uniform REE abundance, which is in the range 23-28 times chondrite composition. In the discrimination diagram in Figure 10, Group 2 basalts plot in the field for rocks formed at mid-ocean ridge settings. In the Th_N vs. Nb_N diagram (Fig. 11a), they plot close to the E-MORB composition (Sun and McDonough, 1989), as well as in the field for oceanic subduction-unrelated settings (Fig. 11b). These geochemical features, in particular the very flat REE patterns are very similar to those observed in oceanic plateau tholeiites from both peri-Caribbean ophiolitic complexes (e.g., Kerr et al., 1996; Hauff et al., 2000; Hastie et al., 2008) and modern oceanic settings (e.g., Fitton and Godard, 2004; Kerr, 2014). In particular, the Nb/Y (0.12 – 0.13) and Nb/Zr (0.03 – 0.04) ratios are very similar to those observed in the Ontong Java oceanic plateau tholeiites (Nb/Y = 0.12 – 0.17; Nb/Zr = 0.05 – 0.06) and significantly different from those of N-MORB (Nb/Y = 0.08; Nb/Zr = 0.03), E-MORB (Nb/Y = 0.38; Nb/Zr = 0.11), and alkaline ocean island basalt (OIB) (Nb/Y = 1.66; Nb/Zr = 1.17) (data from Sun and McDonough, 1989).

6.3.3. Group 3 rocks

Group 3 volcanic rocks are represented by a couple of basalts. The Nb/Y ratios (Table 1, Fig. 8) evidence the alkaline character of this rocks. Al_2O_3 (12.21-18.75 wt.%), MgO (4.37-12.33 wt.%), and CaO (5.02-10.52 wt.%) contents, and Mg# (65.6-49.6) show a wide range of variation in the studied samples, likely reflecting different degrees of fractionation. Sample MK70 is relatively primitive, whereas sample MK56 is rather fractionated. However, both samples are characterized by relatively high TiO_2 (2.04–2.54 wt.%), P_2O_5 (0.38–0.73 wt.%), and Zr (198–231 ppm) contents, as well as Ti/V ratios (47-78). The incompatible element abundance (Fig. 9c) is characterized by decreasing patterns, from Th to Yb, which are similar to those of typical oceanic within-plate alkali basalts (Sun and McDonough, 1989). No Th, Ta, and Nb anomalies can be seen. Group 2 rocks display significant LREE enrichment with respect to HREE (Fig. 9d), which is exemplified by their $(La/Yb)_N$ ratios, which are ~10.5 in both samples. The overall REE enrichment ranges from ~10 to ~150 times chondrite abundance for Yb and La, respectively. These chemical features are comparable to those of typical within-plate alkaline basalts, such as OIBs (e.g., Frey and Clague, 1983; Haase and Dewey, 1996). Accordingly, in both the discrimination diagrams shown in Figures 10 and 11a, these rocks plot in the fields for alkaline oceanic within-plate basalts and oceanic subduction-unrelated settings (Fig. 11b).

6.3.4. Group 4 rocks

Group 4 volcanic rocks include basaltic andesites, andesites, and dacites, with SiO_2 contents ranging between 52.61 and 59.89 wt.%. They display a clear sub-alkaline nature as testified by low Nb/Y ratios (Fig. 8). Mg# ranges between 74.3 and 56.5. Many elements show a wide compositional range, likely reflecting the different degrees of fractionation of these samples. TiO_2, Al_2O_3, and FeO_t show a mild decrease with increasing Mg# (here used as fractionation index). Compatible element contents in andesites and dacites are higher than in basaltic andesites. TiO_2 (0.59-0.79 wt.%) and Y (24-28 ppm) contents are generally low in all rock-types. In contrast, P_2O_5 content is fairly high in basaltic andesites (P_2O_5 = 0.21-0.36 wt.%), whereas is comparatively lower in andesites and dacites and (P_2O_5 = 0.13 wt.%) and is negatively correlated with Mg# and Zr. The incompatible element abundance (Fig. 9e) exhibits patterns, which are very similar to those of typical calc-alkaline basalts from both modern (e.g., Pearce, 1983; Elburg and Foden, 1998) and Mesozoic eastern Mediterranean (e.g., Bébien et al., 1994; Nicolae and Saccani, 2003; Saccani et al., 2008) convergent margins. In fact, these rocks display marked positive anomalies in Th, U, La, and Ce, and negative anomalies in Ta, Nb, and Ti. The chondrite-normalized REE abundances of the Group 4 volcanic rocks have patterns regularly decreasing from LREE to HREE (Fig. 9f) with $(La/Yb)_N$ ratios ranging from 6.41 to 10.96. La generally varies from ~66 to ~110 times chondrite abundance. The REE patterns (Fig. 9f) are consistent with a calc-alkaline affinity for these rocks (e.g., Pearce, 1983). Accordingly, in both the discrimination diagrams shown in Figures 10 and 11a these samples plot in the fields for calc-alkaline basalts generated at continental margin volcanic arc (Fig. 11b).

6.3.5. Group 5 rocks

Group 5 rocks include both volcanic and metavolcanic rocks. These rocks display a sub-alkaline, tholeiitic nature exemplified by generally low Nb/Y ratios (Fig. 8). Volcanic rocks are mainly represented by basalts with minor occurrences of dacites. In basaltic rocks, SiO_2 contents range between 44.18 and 54.89 wt.% and Mg# range between 76.4 and 50.0. They are characterized by variable, but generally low TiO_2 contents (0.64-1.65 wt.%). These rocks show relatively high P_2O_5 (0.19-0.30 wt.%) values and relatively low Zr (58-100 ppm) and Y (18-26 ppm) contents. However, the metabasaltic andesite MK139 shows relatively low P_2O_5 content (0.07 wt.%). Cr, as well as other compatible elements, contents are higher than in the other rock-groups if compared at similar incompatible element values (Table 1). In particular, Cr (1120 ppm), Ni (372 ppm), and Co (81 ppm) values are exceptionally high in basalt MK156. N-MORB normalized incompatible element patterns of both volcanic and metavolcanic rocks (Fig. 9g) show low or moderate Th relative enrichment (Th = 1.73 – 7.57 times N-MORB content in basalts) coupled with marked Ta and Nb negative anomalies. No Ti negative anomalies can be seen in basalts and metabasaltic rocks, whereas the dacitic sample shows a mild Ti negative anomaly, which is likely associated with its fractionated nature. HFSE abundance is generally low ranging from ~0.4 to ~2 times N-MORB abundance (Sun and McDonough, 1989). Except metabasalt MK73, all samples show REE patterns slightly decreasing from LREE to HREE (Fig. 9h) with $(La/Sm)_N$ ratios = 1.40-2.16 and (La/Yb)N ratios = 1.38-3.14.

Metabasalt MK73 has some chemical features that slightly differ from those of other Group 5 rocks (Table 1). This sample displays comparatively lower TiO_2, P_2O_5, and Zr contents, as well as Ti/V ratio (Table 1). The incompatible element abundance is characterized by a fairly depleted N-MORB normalized pattern (Fig. 9g) with a mild Th relative enrichment (Th_N = 1.73) and a marked Nb depletion (Nb_N = 0.42). In contrast to other Group 5 rocks, the chondrite-normalized REE pattern (Fig. 9h) displays LREE depletion with respect to MREE (medium REE) and HREE (heavy REE) with $(La/Sm)_N$ ratios = 0.71, $(Sm/Yb)_N$ ratios = 0.96, and $(La/Yb)_N$ ratios = 0.69.

In the discrimination diagram in Figure 10, both volcanic and metavolcanic rocks fall in the field for volcanic arc basalts, with the only exception of metabasalt MK73 that plots slightly outside this field. Accordingly, in the discrimination diagrams in Figure 11a all samples plot in the field for island arc tholeiites. The overall geochemical data of these rocks are very similar to those of oceanic island arc tholeiites (e.g., Pearce, 1983; Dilek et al., 2008; Saccani et al., 2011).

7. Discussion

7.1. Melt petrogenesis and mantle sources

As shown in the previous section, the Coloured Mélange Complex of Makran incorporates a wide range of different rock-types. These rock-types can be used for determining the nature and tectonic significance of the magmatic events that occurred in the Makran sector of the Neo-Tethys during Cretaceous times. In fact, according to Pearce and Norry (1979) and Pearce (1983), major element composition is defined mostly by fractional crystallization and rock assimilation, whereas trace element (particularly, incompatible element) composition depends on the composition of mantle source and the degree of its melting rather than shallow-level crustal processes. In consequence, it can be assumed that the trace element composition of the different magma-types is primarily related to different source characteristics that are associated, in turn, with distinct tectono-magmatic settings of formation. We will therefore focus our petrogenetic discussion to the identification of the possible mantle sources and related tectonic settings of formation of the six distinct rock-groups identified in the previous chapter. Unfortunately, the chemical variation due to fractional crystallization cannot be defined in detail, as the mélange nature of the sampled rocks prevents us to establish definite genetic relationships between rocks within each single chemical group. However, some trace elements contents (e.g., Nb, Th, and REE) and their degree of depletion or enrichment, as well as trace element ratios (e.g., Nb/Yb, Th/Ta, Th/Nb, Ba/Th) are moderately affected by fractional crystallization of predominantly olivine + clinopyroxene + plagioclase. Therefore, in presence of moderate amounts of fractionation, they are believed to represent the elemental ratios in the source (e.g., Beker et al., 1997). For this reason, the following discussion will be based on the relatively less fractionated basalts and basaltic andesites of the different magmatic groups.

A first discrimination of the possible mantle sources associated with the different lava groups can be seen in Figure 12a, which shows that Group 2 basalts were generated from an enriched-type mantle source, whereas, all other rock-groups were generated from depleted-types mantle sources. Figure 11a shows that the relatively less fractionated Group 1 (N-MORB), Group 2 (tholeiitic) and Group 3 (alkaline) basalts plot along the N-MORB-OIB array. Group 1 basalt is generally compatible with a genesis from primary magmas originating from depleted MORB-type suboceanic mantle sources, with no influence of either enriched OIB-type material or subduction-related chemical components, such as Th and LREE (see also Figs. 9a, b). In contrast, Group 3 basalts are compatible with a genesis from primary magmas originating from enriched within-plate oceanic mantle source, whereas Group 2 basalts are compatible with a genesis from primary magmas originating from oceanic mantle source slightly enriched with respect to N-MORB sources.

Basaltic rocks from Group 4 (calc-alkaline), and Groups 5 and 6 (volcanic arc tholeiites) show variable extents of Th enrichment relative to Nb, which suggest variable addition of subduction-derived components (Fig. 11a). These conclusions are fully supported by the Th/Ta ratios and Zr composition (Fig. 12b). In particular, this Figure shows that the influence from subduction components is moderate for Groups 5 and 6 volcanic and metavolcanic rocks and comparatively more significant for Group 4 basaltic andesites.

We have applied trace element modelling in order to find the mantle peridotite compositions that best fit with the compositions of the less fractionated basaltic rocks for each magmatic type. A rigorous quantification of the melting processes (i.e., composition of mantle sources and degrees of partial melting) generating the different rock-types is not possible as the mantle source compositions cannot be constrained in detail. However, semi-quantitative modellings of some trace elements can place some solid constraints and, to this purpose, we use different models. We present in Figure 13 melting model, using Th and Nb/Yb ratio. This diagram has the advantage to combine two types of information in a single plot. The abundance of Th and Nb is used to evaluate the enrichment of the source, whereas the Nb/Yb ratio is sensitive to the presence of residual garnet in the source. Another important feature of these plots is that mixing between different melt fractions will generate linear mixing arrays (e.g., Beker et al., 1997). This Figure is particularly useful for estimating the composition of mantle sources and the degrees of partial melting generating Group 1, Group 2, and Group 3 basalts. In contrast, the model in Figure 13 is not fully appropriate for modeling the possible mantle sources of Group 4, Group 5, and Group 6 basaltic rocks. In fact, calc-alkaline and island arc tholeiitic rocks are commonly interpreted as originating from partial melting of sub-arc residual peridotites that experienced Nb depletion during previous partial melting events followed by Th and LREE enrichment carried by subduction-derived fluids or melts (e.g., Pearce, 1982, 1983; Gribble et al., 1996; Parkinson and Pearce, 1998). In addition, the application of trace element models is dependent on the critical assumptions that the mantle source has a uniform composition. However, many modeling studies of peridotites have shown that in subduction-related settings this assumption is not fully valid because of fluid-influenced refertilization of the mantle source. In these settings, the extent and timing of fluid-induced refertilization is difficult to constrain, because the fluid flux from a subducted slab may be either localized or pervasive. Moreover, fluid-mobile trace elements may be added at every melting increment (see Barth et al, 2003). In addition, compositions and the amounts of subduction-related trace elements incorporated into the overlying mantle wedge depend on a number of factors, such as the mineralogical compositions of the subducting rocks (in turn, mostly depending on their alteration degrees), temperatures, pressures, and distance from a subduction zone (Parkinson and Pearce, 1998; Gribble et al., 1996; Dilek and Furnes, 2011). Again, the trade-off between the rate of extensional tectonics in the upper slab and the slab sinking is also important in facilitating fluid transfer (e.g., Flower and Dilek, 2003). Given these uncertainties, an alternative method for estimating the degree of depletion and degree of melting of the mantle source(s) is to plot a compatible versus an incompatible element, since compatible element abundance is not significantly modified during the progressive mantle source depletion, whereas abundance of incompatible elements is closely related to source depletion and degree of melting (Pearce, 1982; 1983). To this purpose, the Cr vs. Y diagram in Figure 14 (Pearce, 1983) is used for estimating the composition of mantle sources and the degrees of partial melting generating these rock-types. In Figure 14, three possible mantle are assumed according to Murton (1989): 1) source S1 represents a MORB-type mantle source; 2) source S2 represents a depleted mantle source residual after 15% MORB-type melt extraction; 3) source S3 represents a rather depleted mantle source residual after 10% melt extraction from source S2.

7.1.1. Group 1 rocks

Group 1 basalts have a chemistry suggesting melt generation from a depleted, sub-oceanic mantle source. Therefore, we assume as the possible mantle source of these rocks a depleted MORB mantle (DMM) source with Nb = 0.128 ppm, Th = 0.0068 ppm, Yb = 0.353 ppm (Workman and Hart, 2005). In addition, the $(Sm/Yb)_N$ ratios around 1 (Table 1, Fig. 9b) suggest no involvement of residual garnet in the source. In consequence, we assume that this mantle source underwent partial melting in the spinel-facies. In fact, Figure 13 shows that the composition of the relatively less fractionated Group 1 basalt is compatible with ~12% of partial melting of a DMM source at shallow levels. The estimation above takes into account that this basalt may have experienced ~25-30% of fractional crystallization. The model in Figure 14 is generally in agreement with the above conclusion. In fact, Group 1 basalts plot along the fractionation trend starting from primary melts generated from ~15% of partial melting of a DMM source and the relatively less fractionated basalt shows ~25% of fractional crystallization mainly involving plagioclase and clinopyroxene and minor olivine and spinel (Fig. 13).

7.1.2. Group 2 rocks

Group 2 basalts have incompatible element generally similar to those of N-MORB (Sun and McDonough, 1989). However, they also show some geochemical indicators (e.g., Zr/Y, Nb/Y, Th/Tb, Ce/Y), as well as very flat REE patterns, which are similar to those of oceanic plateau basalts. In particular, Nb/Y (0.12 -0.13), Nb/Zr (0.03 – 0.04), Th/Tb (0.60 – 0.55), Ce/Y (0.26 – 0.49) ratios are slightly higher than those observed in N-MORB (Nb/Y = 0.08, Nb/Zr = 0.03, Th/Tb = 0.17, Ce/Y = 0.27), but definitely lower than those of E-MORB (Nb/Y = 0.38, Nb/Zr = 0.11, Th/Tb = 1.13, Ce/Y = 0.68). Greater concentrations of Nb, Th, and LREE in the Group 2 basalts compared to N-MORB cannot simply be a result of smaller degree of partial melting of N-MORB-type source material or a result of fractional crystallization, because such processes would not significantly change the LILE/HFSE and LREE/HREE ratios with respect to the source composition. In fact, modeling using REE contents (not shown) indicates that the REE concentration in Group 2 basalts would be generated by an unreasonably low (<2.5 %) degree of partial melting of a DMM source. It follows that the source material of the Group 2 basalts was most likely a sub-oceanic mantle source slightly richer in Nb, Th, and LREE compared to the DMM source (e.g., Herzberg, 2004). For this reason, a fertile lherzolite source (E-DMM of Workman and Hart, 2005) with Nb = 0.246 ppm, Th = 0.016 ppm, Yb = 0.382 ppm, La = 0.253 ppm has been assumed as the possible mantle source of Group 2 basalts. Chazey and Neal (2004), Fitton and Godard (2004), and Herzberg (2004) calculated that primary magmas of Ontong Java Plateau result from 25 to 30% partial melting of a peridotite at temperature around 1500 °C to produce primary magmas containing 16–19 wt.% (or even more) MgO. Accordingly, the model in Figure 13 shows that the Th-Nb-Yb composition of the relatively less fractionated Group 2 basalt is compatible with very high degrees of partial melting (~27-30%) of the assumed mantle source in the spinel-facies. This estimation takes into account that these melts may have experienced ~40-45% of fractional crystallization of mainly olivine and plagioclase and minor clinopyroxene (Fig. 13).

7.1.3. Group 3 rocks

Group 3 basalts have high MREE/HREE ratios (Fig. 9d), which suggest an involvement of a garnet peridotite source. Moreover, the high La/Yb ratios imply a source significantly enriched in LREE compared to DMM. Therefore, in Figure 13 we assume an OIB-type source with Nb = 1.5 ppm, Th = 0.18 ppm, Yb = 0.353 ppm (Lustrino et al., 2002) in both garnet- and spinel-facies. The Th-Nb-Yb composition of the less fractionated Group 3 basalt cannot however be explained by partial melting of this mantle source either in the garnet- or in the spinel-facies. Therefore, the simplest model to account for the Th-Nb-Yb systematics of this basalt involves mixing of small melt fractions from garnet-facies enriched mantle with relatively larger melt fractions from spinel-facies (Fig. 13). In fact, the composition of this basalt is compatible with the calculated composition for 2.5% melting in the garnet-facies followed by 5% melting in the spinel-facies (polybaric melting), assuming mixing of ~70% of melt derived from spinel-facies mantle with ~30% melt from garnet-facies mantle.

7.1.4. Group 4 rocks

Group 4 rocks have high Th/Nb ratios (Fig. 11a) and are strongly LREE-enriched (Fig. 9f). The high abundance of LILE relative to N-MORB (Fig. 9e) clearly indicates imprints of subduction-related processes, whereas depletions in Nb, Ta, and Ti indicate a residual nature of the mantle source (Pearce, 1982). Accordingly, in the model shown in Figure 14, these rocks are compatible with about 15% partial melting from a depleted mantle source residual after 15% MORB-type melt extraction. The marked enrichments in Th and LREE indicate that the mantle source was significantly metasomatized by subduction-related components. In order to qualitatively evaluate the different chemical contributions from subduction components, the Ba/Th ratios are plotted vs. Th/Nb ratios (Fig. 15). This Figure shows that the subduction component in Group 4 basaltic andesites is predominantly influenced by sediment melt addition to their mantle sources. HREE/MREE depleted patterns (Fig. 9f) are consistent with melting of peridotite in the garnet-facies (McKenzie and O'Nions, 1991). It can therefore be postulated that the primitive magmas producing these rocks were originated deep in the mantle.

7.1.5. Group 5 rocks

Group 5 basalts and metabasalts have depleted Ta, Nb, and HFSE compositions (Fig. 9g) that are consistent with an origin from partial melting of refractory mantle sources, whereas Th enrichment relative to Nb (Fig. 11a) and LREE/HREE enrichments (Fig. 9h) observed in most samples suggest an arc signature. In particular, the relatively high Ba/Th ratios indicate enrichment by subduction-related fluids (Fig. 15). In fact, in the Cr-Y model (Fig. 14), most Group 5 basalts and metabasalts are compatible with about 12% partial melting from a depleted mantle source residual after 15% MORB-type melt extraction. However, compared to other Group 5 basalts, basalt MK73 shows a more depleted nature with lower Ta, Nb, and HFSE (Fig. 9g), as well as definitely low enrichment in Th (Fig. 11a) and LREE (Fig. 8h). The LREE depleted nature of this basalt suggests that hydration of the sub-arc mantle wedge was accompanied by a moderate transfer of LREE-enriched subduction zone components (e.g., Barth et al., 2003). The more depleted nature of this basalt with respect to other Group 5 rocks can be explained either by comparatively higher melting degrees of the same mantle source assumed for other Group 5 rocks (S2 in Fig. 14) or by partial melting of a more refractory mantle source. Figure 14 shows that the Cr-Y composition of this basalt is consistent with ~17% partial melting of the S2 mantle source. Alternatively, its composition can be explained by ~8% of partial melting of a very depleted mantle source that experienced multi-stage melt extraction (source S3 in Fig. 14). However, modeling using HREE contents (not shown) indicates that ~17% partial melting of the same mantle source assumed for Group 5 rocks would generate concentrations of HREE in the melt that are 1.5 times lower than values observed in all Group 5. In fact, basalt MK73 has HREE content similar to those of other Group 5 basalts (Fig. 9g) and therefore its HREE composition cannot be explained by higher degrees of partial melting of the S2 mantle source (Fig. 14). In contrast, HREE modeling assuming ~8% of partial melting of a mantle source more depleted than that hypothesized for Group 5 rocks would generate concentrations of HREE in the melt that are similar to those observed in basalt MK73. In consequence, we favour the hypothesis that this basalt was generated from moderate degrees of partial melting of a rather refractory mantle source. The low fractionation of HREE with respect to MREE observed in Group 5 rocks (Fig. 9h) is consistent with melting of peridotite in the spinel-facies. It can therefore be postulated that the primitive magmas producing these rocks were originated at shallow levels in the mantle.

7.2. Tectono-magmatic significance

The petrological evidence presented in the previous section allow to conclude that the geochemically distinct Groups of volcanic rocks in the Makran Coloured Mélange Complex are related to different mantle source compositions and partial melting degrees. The formation of Group 1 basalts (N-MORB) implies the occurrence of a MORB-type mantle source and therefore we suggest that they were originated in mid-ocean ridge setting with no influence of either enriched OIB-type components or subduction-related components.

The formation of Group 2 basalts implies the occurrence of a fertile lherzolite mantle source, which experienced very high degrees of partial melting (~27-30%). Such a high degree of partial melting requires temperature around 1500 °C (Herzberg, 2004). The data from this paper do not allow melting temperatures to be calculated in detail. The empirical model proposed by Niu and Batiza (1991) is the only one that can be used with the available data. Although this model is not fully robust because it is based on silica and iron contents, which can be mobilized to some extents by secondary alteration, temperature estimated for Group 2 samples is about 1450 °C. Such a mantle source condition is commonly observed below oceanic plateaus, where source temperatures are much greater than the potential temperature of ambient upper mantle (McKenzie and Bickle, 1988; Herzberg et al., 2007). It widely accepted that mantle plumes are one of the most effective means of carrying heat flux (on average, 200 °C hotter than ambient mantle) to the upper mantle (see Kerr, 2014 for an exhaustive review). The formation of Group 3 alkaline rocks implies the occurrence of mantle sources strongly metasomatized by OIB-type (plume type) components. Two alternative hypotheses can account for such OIB-type metasomatized mantle: 1) the existence of plume activity in the region during Cretaceous times and 2) the existence of deep mantle heterogeneously modified by previous mantle plume activity. In the first case, Group 3 basalts likely represent seamount material originated in an oceanic within-plate setting. In the second hypothesis, they may have been formed in a mid-ocean ridge setting by tapping strongly enriched local portions of a heterogeneous mantle, as documented in some Mediterranean Tethys ophiolitic complexes (e.g., Bortolotti et al., 2017). Alternatively, they may represent volcanic rocks erupted at ocean-continent transition zones during the continental rift phase preceding the oceanic spreading, as observed in many Mediterranean Tethys ophiolitic complexes (e.g., Saccani et al., 2003, 2015). Nonetheless, the petrogenetic mechanism for the formation of Group 3 rocks implies polybaric partial melting starting in the deep mantle and continuing in the shallow level mantle. Such a mechanism is commonly observed in within-plate tectonic settings and in continental rift settings, whereas is rarely observed in mid-ocean ridge settings. In addition, the conventional mantle plume model predicts that oceanic plateaus should be followed by a seamount chain or aseismic ridge (e.g., Kerr, 2014 and references therein). It follows that Group 3 alkaline basalts were likely formed in seamount setting and were associated with Group 2 oceanic plateau basalts thus supporting the hypothesis of the existence of mantle plume activity in the Makran sector of the Neo-Tethys. Finally, Group 1, Group 2, and Group 3 basalts have Nb-Th contents that are included in the MORB–OIB array (Fig. 11a) indicating no influence from continental crust material, as also shown in Figures 12b and 13. They therefore represent fragments of oceanic crust that were incorporated into the Coloured Mélange Complex from the subducting plate.

Group 4 and Group 5 rocks were formed from primary melts generated, in turn, from depleted mantle sources that experienced variable subduction-related metasomatisms prior to melting. Therefore, all these rocks were likely generated in volcanic arc tectonic settings. Nonetheless, the different nature of the inferred mantle sources associated with each single rock-group suggests that they likely represent different types or different portions of volcanic arc settings. The calc-alkaline nature and the marked influence from continental crust materials shown by Group 4 rocks (Figs. 11a, 13) suggest formation in a continental arc tectonic setting. In contrast, the island arc tholeiitic affinity of Group 5 rocks and their geochemical signature from subduction-related fluids suggest that these rocks were no or little influenced by continental crust material and likely formed in the oceanic side of a volcanic arc setting. The rather depleted nature of the mantle source inferred for metabasalt MK73 of Group 5, coupled with a limited influence from slab-derived fluids are consistent with a genesis in a forearc setting. In any case, Group 4 and Group 5 rocks represent materials incorporated into the Coloured Mélange Complex from the upper plate.

7.3. Geodynamic implications

In the previous section it has been shown that the Coloured Mélange Complex in the North Makran incorporated a wide range of volcanic and metavolcanic rocks formed in distinct tectonic settings. The great geochemical and petrological diversity of these rocks suggest that several distinct magmatic events took place in the Makran sector of the southern Neo-Tethys and its northern margin. N-MORBs, originated in an oceanic subduction-unrelated setting, whereas oceanic plateau basalts (OPBs) and alkaline basalts where originated in an oceanic plateau. Therefore, these rocks represent remnants of the oceanic subducting plate. In contrast, calc-alkaline rocks represent remnants of a volcanic arc located onto continental crust or onto polygenetic crust (see Dilek and Furnes, 2011; Saccani, 2015), whereas arc tholeiitic rocks likely derived from an oceanic arc or a forearc tectonic setting and therefore represent material derived from the upper plate. Biochronological data show that volcanic arc tholeiites were erupted in the Hauterivian-early Aptian and latest Cenomanian-lower late Campanian, whereas calc-alkaline volcanic rocks are early Coniacian-Santonian in age (Fig. 16). These data indicate the existence of a subduction setting in the northern realm of the Neo-Tethys since Early Cretaceous times. Our data also show that calc-alkaline magmatism started in the Late Cretaceous and that it was associated with volcanic arc tholeiitic magmatism. This conclusion is also supported by field evidence. In fact, a strict association of calc-alkaline and volcanic arc tholeiites has been found within a single outcrop.

Unfortunately, the N-MORB and alkaline magmatisms cannot be dated due to the lack of radiolarian cherts associated with these rocks-types. However, the radiolarian cherts associated with the OPBs indicate an early Turonian-early Campanian age (Fig. 16). This implies that oceanic plateau magmatism was active in the oceanic plate during the Late Cretaceous that is, much later than subduction initiation in the convergent margin.

A possible tectono-magmatic model that can explain the formation of the different volcanic rocks incorporated in the Coloured Mélange Complex is shown in Figure 17. In this model, a northward subduction is assumed according to regional data (e.g., Berberian et al. 1982; McCall and Kidd 1982). In this model, the subduction of the Neo-Tethys below the southern margin of the Lut block, today represented by the Bajgan-Durkan Complex, was already active during the Early Cretaceous (not shown). In this stage, volcanic arc tholeiites were erupted in a volcanic arc setting located in the southermost rim of the Lut continental block. The chemistry of volcanic arc tholeiites indicate that this volcanic arc setting was characterized by no or negligible chemical influence from continental crust components (Figs. 12, 15). This implies that volcanic arc tholeiites formed onto oceanic crust either in an island arc setting or in the forearc sector of a continental arc. Unfortunately the data presented in this paper do not allow a clear distinction of the tectonic setting of formation of these rocks to be made. According to Hunziker et al. (2015), a back-arc oceanic basin also opened in the Early Cretaceous leading to the separation of the Bajgan-Durkan domain from the Lut block. In fact, the North Makran Ophiolites are interpreted by these authors as remnants of this backarc basin.

During Late Cretaceous times (Fig. 17a) the oceanic plate was characterized by the formation of an oceanic plateau with eruption of oceanic plateau basalts and, most likely, alkaline basalts. In the same times, the subduction setting was characterized by the contemporaneous eruption of calc-alkaline and volcanic arc tholeiitic rocks in a arc-forearc setting. The chemistry of calc-alkaline volcanic rocks indicate that they have been strongly influenced by continental crust chemical components (Figs. 12, 15), suggesting that these rocks were erupted onto the southern realm of the Bajgan-Durkan domain. The formation of high pressure-low temperature metabasalts with volcanic arc tholeiitic affinity can be explained by processes of subduction erosion of the accretionary wedge (e.g. Huene and Scholl, 1991), as observed in some fossil convergent margins associated with the Eastern Mediterranean ophiolites (e.g., Bébien et al., 1994; Sayit et al., 2016). In fact, the forearc can be likely eroded and significant volumes of its basement can be tectonically removed, dragged in depth and exhumed as HP metamorphic slices. According to Huene and Scholl (1991), the basal erosion is largely controlled by the episodic collision of large topographic high, like a plateau, with the trench.

The model we propose fits very well with the available data on regional geology. In fact, several authors suggested that the subduction of the Neo-Tethys in the Makran sector was already active during the Late Cretaceous (e.g., Berberian et al. 1982; McCall and Kidd 1982). In addition, based on the age of the volcanic arc north of the Makran, as well as the age of the intra-arc extensional basin of the proto-Jaz Murian depression, Shahabpour (2010) suggested that this convergent margin was characterized by a northward subduction developed from Middle Jurassic to Late Cretaceous.

The deformation of this convergent margin and its change into an imbricate pile of different units, as today observed in the North Makran, requires a collision, i.e. a geodynamic event able to produce a relevant shortening of the convergent margin. The oceanic plateaus are more buoyant than oceanic crust formed at a mid-ocean ridge and therefore they have a greater potential to be 'peeled off' and accreted on to island arcs and active continental margins (e.g., Cloos, 1993). When an oceanic plateau clogs a subduction zone, a range of events can happen depending on the plate tectonic setting. Plateau collision with a continental arc results in the formation of a new subduction zone behind the accreted plateau (see Kerr, 2014 for an exhaustive discussion). Therefore, we propose that the collision between the oceanic plateau and the volcanic arc of the Bajgan-Durkan domain resulted in a subduction jump toward the south, as well as in the deformation of the oceanic basin from which the North Makran Ophiolites were originated (Fig. 17b).

Biochronological data indicate that the upper plate remained undeformed since early Coniacian-Santonian, probably up to the lower late Campanian. In addition, the youngest age of the blocks in the Coloured Mélange Complex can be referred as Early Paleocene in age (McCall, 1983). Thus, the deformation of the convergent margin probably was occurring since Late Campanian up to Late Paleocene. The upper limit of this deformation is provided by shallow-water Early Eocene deposits that unconformably seal the relationships between the different units of the North Makran domain. These constraints indicate an origin of the Coloured Mélange Complex from shortening of the convergent margin before the building of the present-day accretionary wedge, whose backstop is represented by the pile of the tectonic units of the North Makran. The model we propose can also explain the present day tectonic setting, where the North Makran Ophiolites and the Bajgan-Durkan Complex are imbricated with southward sense of displacement over the Coloured Mélange Complex (Fig. 17b).

The Sorkhband ophiolites, which are located between the Coloured Mélange Complex and the Bajgan-Durkan Complex (Fig. 3), consist of a tectonic slice of mantle harzburgites and very depleted harzburgites bearing dunite pods and chromitite ore deposits, as well as a tectonic slice made up of MORB-type gabbros (Delavari et al., 2016). According to the model in Figure 17a, the Sorkhband harzburgites likely represent sub-arc residual mantle subsequently incorporated into the mélange together with tectonic slices of gabbros derived from the lower, subducting plate. Therefore, it can be suggested that the tectonic slices in Sorkhband ophiolites are equivalent to those forming the Coloured Mélange Complex.

Finally, the collision of an oceanic plateau with a continental arc usually has an impact on the geodynamic evolution of an oceanic basin at a regional scale. (see Kerr, 2014). The Oman and Zagros ophiolites are interpreted as originated in the southern portion of the southern Neo-Tethys Ocean (Glennie, 2000; Allahyari et al., 2010, 2014; Saccani et al., 2013, 2014). It is worth to mention that the obduction in the Oman area started in the Late Cenomanian and was completed by the emplacement of the ophiolites onto the Arabian continental margin (Roberts et al., 2016). This event lasted from the Santonian-Campanian boundary up to the end of the Lower Maastrichtian, that is, almost at the same time lapse in which the oceanic plateau collided with the Lut continental margin. It can therefore be postulated that the emplacement of the Oman ophiolites in the southern side of Neo-Tethys may have been somewhat related with the collision of the oceanic plateau in the northern side of the same oceanic basin. Unfortunately, available data do not allow this hypothesis to be proved. However, this postulation is worth to be further investigated.

8. Conclusions

The North Makran domain (SE Iran) represents the backstop of the present-day Makran accretionary wedge and is represented by an imbricate stack of continental and oceanic units, including the Coloured Mélange Complex (McCall and Kidd, 1982). The Coloured Mélange Complex includes blocks of volcanic and metavolcanic rocks of different nature, locally showing primary relationships with radiolarian cherts. Geochemical and petrologic data on volcanic and metavolcanic rocks coupled with biochronological data on the associated radiolarian cherts allow us to draw the following conclusions.

1) A wide range of volcanic and metavolcanic rocks-types is incorporated within the mélange. They are: a) normal-type mid-ocean ridge basalts and Fe-basalts (N-MORB); b) oceanic plateau basalts (OPB); c) alkaline basalts; d) calc-alkaline basalts, basaltic andesites, andesites, and dacites; e) volcanic arc tholeiitic basalts and dacites, as well as metabasalts formed under high pressure-low temperature conditions in deep levels of the accretionary wedge.

2) The volcanic arc tholeiites range from Early (late Hauterivian-early Aptian) to Late (latest Cenomanian-lower late Campanian) Cretaceous. In contrast, the calc-alkaline rocks and OPBs are Late Cretaceous in age (namely, early Coniacian-Santonian and early Turonian-early Campanian, respectively).

3) N-MORBs, OPBs, and alkaline basalts represent remnants of the Neo-Tethys Ocean that developed between the Arabian plate and the Lut continental block. The occurrence of OPBs indicates that this Neo-Tethys branch was characterized by the development of an oceanic plateau during Late Cretaceous. In contrast, calc-alkaline and volcanic arc tholeiitic rocks represent remnants of a volcanic arc that was active in the southern realm of the Lut block from Early to Late Cretaceous. In this volcanic arc, calc-alkaline rocks were erupted onto

continental crust (now represented by the Bajgan-Durkan complexes), whereas arc tholeiitic volcanic rocks were erupted onto oceanic crust, most likely in a forearc setting.

4) A new tectono-magmatic model for the evolution of a convergent margin developed at the northern rim of the Neo-Tethys from Early to Late Cretaceous is proposed. This model is basically constrained by the collision of the oceanic plateau with the continental arc, which resulted in the jump of the subduction toward the south, as well as in the formation of the imbricate pile of different units (i.e., Coloured Mélange, Bajgan-Durkan Complexes, and North Makran ophiolites) today observed in the North Makran.

5) Finally, the Coloured Mélange Complex does not represent a simple tectonic mélange like those recognized in the fossil subduction zones (e.g., Meneghini et al., 2009; Göncüoglu et al., 2014; Ernst, 2016; Festa et al., 2016) but it can be regarded as an effective suture zone due to arc-plateau collision.

Acknowledgments

The research has been funded by Darius Project (Head M. Marroni). This research benefits also by grants from PRA project of University of Pisa (Head S. Rocchi) and from IGG-CNR, as well as from FIR-2016 Project of the Ferrara University. R. Tassinari (University of Ferrara) is acknowledged for technical support with chemical analyses. Constructive and thorough reviews for the journal by XXX and ZZZ have helped us improve the science and organization presented in the paper.

References

Aguado, R., de Gea, G. A., O'Dogherty, L., 2014. Integrated biostratigraphy (calcareous nannofossils, planktonic foraminifera, and radiolarians) of an uppermost Barremian-lower Aptian pelagic succession in the Subbetic Basin (southern Spain). Cretaceous Research 51, 153-173.

Allahyari, K., Saccani, E., Pourmoafi, M., Beccaluva, L., Masoudi F., 2010. Petrology of mantle peridotites and intrusive mafic rocks from the Kermanshah ophiolitic complex (Zagros belt, Iran): Implications for the geodynamic evolution of the Neo-Tethyan oceanic branch between Arabia and Iran. Ofioliti 35, 71–90.

Allahyari, K., Saccani, E., Rahimzadeh, B., Zeda, O., 2014. Mineral chemistry and petrology of highly magnesian ultramafic cumulates from the Sarve-Abad (Sawlava) ophiolites (Kurdistan, NW Iran): New evidence for boninitic magmatism in intra-oceanic fore-arc setting in the Neo-Tethys between Arabia and Iran. Journal of Asian Earth Sciences 79, 312–328.

Barth, M.G., Mason, P.R.D., Davies, G.R., Dijkstra, A.H., Drury, M.R., 2003. Geochemistry of the Othris Ophiolite, Greece: evidence for refertilization. Journal of Petrology 44, 1759–1785.

Baumgartner, P.O., O’Dogherty, L., Goričan, Š., Dumitrica-Jud, R., Dumitrica, P., Pillevuit, A., Urquhart, E., Matsuoka, A., Danelian, T., Bartolini, A., Carter, E.S., De Wever, P., Kito, N., Marcucci, M., Steiger, T.A., 1995. Radiolarian catalogue and systematics of Middle Jurassic to Early Cretaceous Tethyan genera and species. In: Baumgartner, P.O., O’Dogherty, L., Goričan, Š., Urquhart, E., Pillevuit, A., De Wever, P. (Eds.), Middle Jurassic to Lower Cretaceous Radiolaria of Tethys: occurrences, systematics, biochronology. Mémoires de Géologie (Lausanne), vol. 23, pp. 37-685.

Bébien, J., Platvoet, B., Mercier J., 1994. Geodynamic significance of the Paikon Massif in the Hellenides : contribution of the volcanic rock studies. Bulletin of the Geological Society of Greece 30, 63-67.

Beker, J.A., Menzies, M.A., Thirlwall, M.F., Macpherson, C.G., 1997. Petrogenesis of Quaternary intraplate volcanism, Sana'a, Yemen: Implications for plume-Lithosphere interaction and polybaric melt hybridization. Journal of Petrology 38, 1359–1390.

Berberian, F., Muir, I.D., Pankhurst, R.J., Berberian, M., 1982. Late Cretaceous and early miocene andean-type plutonic activity in northern makran and central Iran. Journal of the Geological Society of London 139, 605–614.

Bortolotti, V., Chiari, M., Göncüoglu, M.C., Principi, G., Saccani, E., Tekin, U.K., Tassinari, R., 2017. The Jurassic-Early Cretaceous Basalt-Chert association in the Ophiolites of the Ankara Mélange east of Ankara, Turkey: Age and Geochemistry. Geological Magazine in press.

Bragina, L.G., 2016. Radiolarian-Based Zonal Scheme of the Cretaceous (Albian-Santonain) of the Tethyan Regions of Eurasia. Stratigraphy and Geological Correlation 24, 141-166.

Bragina, L.G., Bragin, N. Yu., Djerić, N., Gajić, V., 2014. Late Cretaceous Radiolarians and Age of Flyschoid Sediments in the Struganik Section (Western Serbia). Stratigraphy and Geological Correlation 22, 202-218.

Burg, J.-P., Bernoulli, D., Smit, J., Dolati, A., Bahroudi, A., 2008. A giant catastrophic mud-and-debris flow in the Miocene Makran. Terra Nova 20, 188–193.

Burg, J.-P., Dolati, A., Bernoulli, D., Smit, J., 2013. Structural style of the Makran tertiary accretionary complex in SE Iran. In: Al Hosani, K., Roure, F., Ellison, R., Lokier, S. (Eds.), Lithosphere Dynamics and Sedimentary Basins: The Arabian Plate and

Analogues, Frontiers in Earth Sciences, Springer, Berlin, Heidelberg, vol. 5, pp. 239–259.

Chazey, W.J., Neal, C.R., 2004. Large igneous province magma petrogenesis from source to surface: platinum-group element evidence from Ontong Java Plateau basalts recovered during ODP Legs 130 and 192. In: Fitton, J.G., Mahoney, J.J., Wallace, P.J., Saunders, A.D. (Eds.), Origin and evolution of the Ontong Java Plateau, Geological Society of London Special Publication, vol. 229, pp. 219–238.

Cloos, M., 1993. Lithospheric buoyancy and collisional orogenesis: Subduction of oceanic plateaus, continental margins, island arcs, spreading ridges, and seamounts. Geological Society of America Bulletin 105, 715–737.

Cohen, K.M., Finney, S.C., Gibbard, P.L., Fan, J.-X., 2013. The ICS International Chronostratigraphic Chart. Episodes 36, 199-204.

Delavari, M., Dolati, A., Marroni, M., Pandolfi, L., Saccani, E., 2016. Association of MORB and SSZ ophiolites along the shear zone between Coloured Mélange and Bajgan Complexes (North Makran, Iran): evidence from the Sorkhband area. Ofioliti 41, 21-34, doi:10.4454/ofioliti.v41i1.440.

Dercourt, J., Zonenshian, L.P., Ricou, L.E., Kazmin, V.G., LePichon, X., Knipper, A.L., Grandjacquet, C., Sbortshikov, M., Geyssant, J., Lepvrier, C., Pechersky, D. H., Boulin, J., Sibuet, J.C., Savostin, L.A., Sorokhtin, O., Westphal, M., Bazhenov, M.L., Lauer, J.P., Biju-Duval, B., 1986. Geological evolution of the Tethys Belt from the Atlantic to the Pamirs since the Lias. Tectonophysics 123, 241–315.

Desmons, J., Beccaluva, L., 1983. Mid-oceanic ridge and island arc affinities in ophiolites from Iran: paleogeographic implication. Chemical Geology 39, 39–63.

1069 Dilek, Y., Furnes, H., Shallo, M., 2008. Geochemistry of the Jurassic Mirdita Ophiolite
1070 (Albania) and the MORB to SSZ evolution of a marginal basin oceanic crust, Lithos
1071 100, 174–209, doi:10.1016/j.lithos.2007.06.026

1072 Dilek, Y., Furnes, H., 2011. Ophiolite genesis and global tectonics: geochemical and tectonic
1073 fingerprinting of ancient oceanic lithosphere. Geological Society of America Bulletin
1074 123, 387–411. http://dx.doi.org/10.1130/B30446.1.

1075 Dolati, A., Burg, J.P, 2013. Preliminary fault analysis and paleostress evolution in the Makran
1076 Fold-and-Thrust Belt in Iran. In: Al Hosani, K., Roure, F., Ellison, R., Lokier, S. (Eds.),
1077 Lithosphere Dynamics and Sedimentary Basins: The Arabian Plate and Analogues,
1078 Frontiers in Earth Sciences, Springer, Berlin, Heidelberg, vol. 5, pp. 261-277.

1079 Dumitrica, P., 1970. Cryptocephalic and cryptothoracic Nassellaria in some Mesozoic
1080 deposits of Romania. Revue Roumaine de Géologie, Géophysique et Géographie (série
1081 de Géologie) 14, 45-124.

1082 Dumitrica, P., Immenhauser, A., Dumitrica-Jud, R., 1997. Mesozoic radiolarian
1083 biostratigraphy from Masirah ophiolite, Sultanate of Oman, Part 1. Middle Triassic,
1084 Uppermost Jurassic and Lower Cretaceous spumellarians and multisegmented
1085 nassellarians. Bulletin of the National Museum of Natural Sciences, Taiwan 9, 1-106.

1086 Erbacher, J., 1994. Entwicklung und Palaoozeanographie mittelkretazischer Radiolarien der
1087 westlichen Tethys (Italien) und des Nordatlantiks. Tubinger Mikropälaontologische
1088 Mitteilungen 12, 119.

1089 Ernst, W.G., 2016. Franciscan mélanges: coherent blocks in a low-density, ductile matrix.
1090 International Geology Review 58, 626-642.

1091 Festa, A., Pini, G.A., Dilek, Y., Codegone, G., 2010. Mélanges and mélange-forming
1092 processes: a historical overview and new concepts. International Geology Review 52,
1093 1040–1105.

Festa, A., Ogata, K., Pini, G.A., Dilek, Y., Alonso, J.L., 2016. Origin and significance of olistostromes in the evolution of orogenic belts: A global synthesis. Gondwana Research 29, 180-203.

Fitton, J.G., Godard, M., 2004. Origin and evolution of magmas on the Ontong Java Plateau. In: Fitton, J.G., Mahoney, J.J., Wallace, P.J., Saunders, A.D. (Eds.), Origin and evolution of the Ontong Java Plateau, Geological Society of London Special Publication, vol. 229, pp. 151–178.

Flower, M.F.J., Dilek, Y., 2003. Arc-trench rollback and forearc accretion: 1. A collision-induced mantle flow model for Tethyan ophiolites. In: Dilek, Y., Robinson, P.T. (Eds.), Ophiolites in Earth History, Geological Society of London Special Publication, vol. 218, pp.21–41.

Frey, F.A., Clague, D.A., 1983. Geochemistry of diverse basalt types from Loihi seamount, Hawaii. Earth and Planetary Science Letters 66, 337–355.

Gansser, A., 1955. New aspects of the geology in central Iran. Paper presented at 4th World Petroleum Congress, Rome, 279–300.

Ghazi, A.M., Hassanipak, A.A., Mahoney, J.J., Duncon, R.A., 2004. Geochemical characteristics, 40Ar-39Ar ages and original tectonic setting of the Band-e-Zeyarat/Dar Anar ophiolite, Makran accretionary Prism, S.E. Iran. Tectonophysics 193, 175–196.

Ghazi J.M., Moazzen, M. 2015. Geodynamic evolution of the Sanandaj-Sirjan Zone, Zagros Orogen, Iran. Turkish Journal of Earth Sciences 24, 513–528

Glennie, K.W., 2000. Cretaceous tectonic evolution of Arabia's Eastern plate margin: a tale of two oceans. SEPM Special Publication 69, 9–20.

Göncüoglu, M.C., Marroni, M., Pandolfi, L., Ellero, A. Ottria, G., Catanzariti, R., Tekin, U.K., Sayit, K., 2014. The Arkot Dağ Mélange in Araç area, central Turkey: Evidence of its origin within the geodynamic evolution of the Intra-Pontide suture zone. Journal of Asian Earth Sciences 85, 117-139.

Gribble, R.F., Stern, R.J., Bloomer, S.H., Stuben, D., O'Hearn, T., Newman, S., 1996. MORB mantle and subduction components interact to generate basalts in the southern Mariana Trough back-arc basin. Geochimica et Cosmochimica Acta 60, 2153–2166.

Haase, K.M., Devey, C.W., 1996. Geochemistry of lavas from the Ahu and Tupa volcanic fields, Easter Hotspot, southeast Pacific: Implications for magma genesis near a spreading axis. Earth and Planetary Science Letters 137, 129–143.

Hastie, A.R., Kerr, A.C., Mitchell, S.F., Millar, I.L., 2008. Geochemistry and petrogenesis of Cretaceous oceanic plateau lavas in eastern Jamaica. Lithos 101, 323–343.

Hauff, F., Hoernle, K., Bogaard, P.v.d., Alvarado, G., Garbe-Schonberg, D., 2000. Age and geochemistry of basaltic complexes in western Costa Rica: Contributions to the geotectonic evolution of Central America. Geochemistry, Geophysics, Geosystem 1. doi:10.1029/1999GC000020.

Herzberg, C., 2004. Partial melting below the Ontong Java Plateau. In: Fitton, J.G., Mahoney, J.J., Wallace, P.J., Saunders, A.D. (Eds), Origin and evolution of the Ontong Java Plateau, Geological Society of London Special Publication, vol. 229, pp. 179-183.

Herzberg, C., Asimow, P.D., Arndt, N., Niu, Y., Lesher, C.M., Fitton, J.G., Cheadle, M.J., Saunders, A.D., 2007. Temperatures in ambient mantle and plumes: Constraints from basalts, picrites, and komatiites. Geochemistry, Geophysics, Geosystems 8.

Huene, R., Scholl, D.W., 1991. Observations at convergent margins concerning sediment subduction, subduction erosion, and the growth of continental crust. Reviews of Geophysics 29, 279-316.

Hunziker, D., Burg, J.-P., Bouilhol, P., von Quadt, A., 2015. Jurassic rifting at the Eurasian Tethys margin: Geochemical and geochronological constraints from granitoids of North Makran, southeastern Iran. Tectonics 34, 571–593.

Karig, D.E., 1980. Material transport within accretionary prisms and the “Knocker” problem. The Journal of Geology 88, 27-39.

Kerr, A.C., 2014. Oceanic Plateaus. In: Holland, H.D., Turekian, K.K. (Eds.), Treatise on Geochemistry, Second Edition, vol. 4. Elsevier, Oxford, pp. 631–667.

Kerr, A.C., Tarney, J., Marriner, G.F., Klaver, G.T., Saunders, A.D., Thirlwall, M.F., 1996. The geochemistry and petrogenesis of the late-Cretaceous picrites and basalts of Curacao, Netherlands Antilles: a remnant of an oceanic plateau. Contribution to Mineralogy and Petrology 124, 29-43.

Kinzler, R.J., 1997. Melting of mantle peridotite at pressures approaching the spinel to garnet transition: application to mid-ocean ridge basalt petrogenesis. Journal of Geophysical Research 102, 853–874.

Lachance, G.R., Trail, R.J., 1966. Practical solution to the matrix problem in X-ray analysis. Canadian Spectroscopy 11, 43-48.

Lustrino, M., Melluso, L., Morra, V., 2002. The transition from alkaline to tholeiitic magmas: a case study from the Orosei–Dorgali Pliocene volcanic district (NE Sardinia, Italy). Lithos 63, 83–113.

Masson, F., Anvari, M., Djamour, Y., Walpersdorf, A., Tavakoli, F., Daignières, M., Nankali, H., Van Gorp, S., 2007. Large-scale velocity field and strain tensor in Iran inferred from GPS measurements: new insight for the present-day deformation pattern within NE Iran. Geophysical Journal International 170, 436–440.

McCall, G.J.H., 1983. Mélanges of the Makran, southeastern Iran. In: McCall, G.J.H. (Ed.), Ophiolitic and related mélanges, Benchmark Papers in Geology, Hutchinson Ross Publishing Company, Stroudsburg, Pennsylvania, 66, 292–299.

McCall, G.J.H., 1985. Explanatory text of the Minab Quadrangle Map; 1:250,000; No. J13. Geological Survey of Iran, Tehran, 530 pp.

McCall, G.J.H., 1997. The geotectonic history of the Makran and adjacent areas of southern Iran. Journal of Asian Earth Sciences 15, 517–531

McCall, G.J.H., 2002. A summary of the geology of the Iranian Makran. In: Clift, P.D., Kroon, F.D., Gaedecke, C., Craig, J. (Eds.), The tectonic and climatic evolution of the Arabian Sea Region, Geological Society of London Special Publication, vol. 195, pp. 147–204

McCall, G.J.H., Kidd, R.G.W., 1982. The Makran southeastern Iran: the anatomy of a convergent margin active from Cretaceous to present. In: Leggett, J.K. (Eds), Trench-forearc geology: sedimentation and tectonics of modern and ancient plate margins, Geological Society of London Special Publication, vol. 10, pp. 387–397.

McKenzie, D., Bickle, M.J., 1988. The volume and composition of melt generated by extension of the lithosphere. Journal of Petrology 29, 625–679.

McKenzie, D., O'Nions, R.K., 1991. Partial melt distributions from inversion of rare earth element concentrations. Journal of Petrology 32, 1021–1091.

McQuarrie, N., Stock, J.M., Verdel, C., Wernicke, B.P., 2003. Cenozoic evolution of Neotethys and implications for the causes of plate motions. Geophysical Research Letters 30, 2036. doi:10.1029/2003GL017992.

Meneghini, F., Marroni, M., Moore, J.C., Pandolfi, L., Rowe, C.D., 2009. The processes of underthrusting and underplating in the geologic record: structural diversity between the

Franciscan Complex (California), the Kodiak Complex (Alaska) and the Internal Ligurian Units (Italy). Geological Journal 44, 126-152.

Moslempour, M.E., Khalatbari-Jafari, M., Ghaderi, M., Yousefi, H., Shahdadi, S., 2015. Petrology, Geochemistry and Tectonics of the Extrusive Sequence of Fannuj-Maskutan Ophiolite, Southeastern Iran. Journal of Geological Society of India 85, 604-618.

Murton, B.J., 1989. Tectonic controls on boninite genesis. In: Saunders, A.D., Norry, M.J. (Eds.), Magmatism in the Ocean Basins, Geological Society of London Special Publication, vol. 42, pp. 347-377.

Nicolae, I., Saccani, E., 2003. Petrology and geochemistry of the Late Jurassic calc-alkaline series associated to Middle Jurassic ophiolites in the South Apuseni Mountains (Romania). Swiss Journal of Petrology 83, 81-96.

Niu, Y., Batiza, R., 1991. An Empirical Method for Calculating Melt Compositions Produced Beneath Mid-Ocean Ridges: Application for Axis and Off-Axis (Seamounts) Melting. Journal of Geophysical Research 96, 21753-21777.

O'Dogherty, L., 1994. Biochronology and Paleontology of Mid-Cretaceous radiolarians from Northern Apennines (Italy) and Betic Cordillera (Spain). Mémoires de Géologie (Lausanne) 21, 1-413.

Parkinson, I.J., Pearce, J.A., 1998. Peridotites from the Izu-Bonin-Mariana forarc (ODP Leg 125): evidence for mantle melting and melt-mantle interaction in a suprasubduction zone setting. Journal of Petrology 39, 1577–1618.

Pearce, J.A., 1982. Trace element characteristics of lavas from destructive plate boundaries. In: Thorpe, R.S. (Eds.), Andesites, Wiley, New York, pp. 525–548.

Pearce, J.A., 1983. Role of the Sub-continenetal Lithosphere in Magma Genesis at Active Continental Margins. In: Hawkesworth C.J., Norry, M.J. (Eds.), Continental Basalts and Mantle Xenoliths, Nantwich, Shiva Publication, pp. 230-249.

Pearce, J.A., 1996. A user's guide to basalt discrimination diagrams. In: Bailes (Eds.), Trace element geochemistry of volcanic rocks; applications for massive sulphide exploration, Short Course Notes - Geological Association of Canada, 12, p. 79-113.

Pearce, J.A., Norry, M.J., 1979. Petrogenetic implications of Ti, Zr, Y, and Nb variations in volcanic rocks. Contributions to Mineralogy and Petrology 69, 33–47.

Pessagno, E.A.Jr., Newport, L.A., 1972. A technique for extracting Radiolaria from radiolarian chert. Micropaleontology 18, 231-234.

Pessagno, E.A.Jr., 1976. Radiolarian zonation and stratigraphy of the Upper Cretaceous portion of the Great Valley Sequence, California Coast Ranges. Micropaleontology Special Publication 2, 1-95.

Popova-Goll, I., Vishnevskaya, V., Baumgartner, P.O., 2005. Upper Cretaceous (Santonian-Campanian) radiolarians from Voronesh Anticline, southwestern Russia. Micropaleontology 51, 1-38.

Raymond, L.A., 1984. Classification of melanges. In:Raymond , L.A. (Ed.), Melanges: Their nature, origin and significance. Boulder, Colorado, Geological Society of America Special Paper vol. 198, pp. 7-20.

Roberts, N.M., Thomas, R.J., Jacobs, J., 2016. Geochronological constraints on the metamorphic sole of the Semail ophiolite in the United Arab Emirates. Geoscience Frontiers 7, 609-619.

Saccani, E., 2015. A new method of discriminating different types of post-Archean ophiolitic basalts and their tectonic significance using Th-Nb and Ce-Dy-Yb systematics. Geoscience Frontiers 6, 481-501. http://dx.doi.org/10.1016/j.gsf.2014.03.006.

Saccani, E., Padoa, E., Photiades, A., 2003. Triassic mid-ocean ridge basalts from the Argolis Peninsula (Greece): new constraints for the early oceanization phases of the Neo-Tethyan Pindos basin. Ophiolites in earth history. In: Dilek, Y., Robinson, P.T. (Eds.), Ophiolites in Earth History, Geological Society of London Special Publication, vol. 218, pp. 109-127.

Saccani, E., Bortolotti, V., Marroni, M., Pandolfi, L., Photiades, A., Principi, G., 2008. The Jurassic association of backarc basin ophiolites and calc-alkaline volcanics in the Guevgueli Complex (northern Greece): Implication for the evolution of the Vardar Zone. Ofioliti 33, 209-227.

Saccani, E., Beccaluva, L., Photiades, A., Zeda, O., 2011. Petrogenesis and tectono-magmatic significance of basalts and mantle peridotites from the Albanian–Greek ophiolites and sub-ophiolitic mélanges. New constraints for the Triassic–Jurassic evolution of the Neo-Tethys in the Dinaride sector. Lithos 124, 227–242.

Saccani, E., Allahyari, K., Beccaluva, L., Bianchini, G., 2013. Geochemistry and petrology of the Kermanshah ophiolites (Iran): Implication for the interaction between passive rifting, oceanic accretion, and plume-components in the Southern Neo-Tethys Ocean. Gondwana Research 24, 392-411.

Saccani, E., Allahyari, K., Rahimzadeh, B., 2014. Petrology and geochemistry of mafic magmatic rocks from the Sarve-Abad ophiolites (Kurdistan region, Iran): Evidence for interaction between MORB-type asthenosphere and OIB-type components in the southern Neo-Tethys Ocean. Tectonophysics 621, 132-147. DOI:10.1016/j.tecto.2014.02.011.

Saccani, E., Dilek, Y., Marroni, M., Pandolfi, L., 2015. Continental Margin Ophiolites of Neotethys: Remnants of Ancient Ocean-Continent Transition Zone (OCTZ) Lithosphere and Their Geochemistry, Mantle Sources and Melt Evolution Patterns. Episodes 38, 230-249.

Salvini, G., Marcucci-Passerini, M., 1998. The radiolarian assemblages of the Bonarelli Horizon in the Umbria-Marche Apennines and Southern Alps, Italy. Cretaceous Research 19, 777-804.

Samimi Namin, M., 1982. Geological map of Taherui 1:250000 scale. Geological survey of Iran.

Samimi Namin, M., 1983. Geological map of Minab 1:250000 scale. Geological survey of Iran.

Sanfilippo, A., Riedel, W.R., 1985. Cretaceous Radiolaria. In: Bolli, H.M., Saunders, J.B., Perch-Nielson, K. (Eds.), Plankton Stratigraphy, Cambridge University Press, pp. 573-630.

Sayit, K., Marroni, M., Göncüoglu, M.C., Pandolfi, L., Ellero, A., Ottria, G., Frassi, C., 2016. Geological setting and geochemical signatures of the mafic rocks from the Intra-Pontide Suture Zone: implications for the geodynamic reconstruction of the Mesozoic Neotethys. International Journal of Earth Sciences 105, 39-64.

Shahabpour, J., 2010. Tectonic implications of the geochemical data from the Makran igneous rocks in Iran. Island Arc 19, 676-689.

Shaker-Ardakani, A.R., Arvin, M., Oberhänsli, R., Mocek, B., Moeinzadeh, S.H., 2009. Morphology and Petrogenesis of Pillow Lavas from the Ganj Ophiolitic Complex, Southeastern Kerman, Iran. Journal of Sciences, Islamic Republic of Iran 20, 139-151.

Shervais, J.W., 1982. Ti-V plots and the petrogenesis of modern ophiolitic lavas. Earth and Planetary Science Letters 59, 101–118.

Sun, S.S., McDonough, W.F., 1989. Chemical and isotopic-systematics of oceanic basalts: implications for mantle composizion and processes. In: Saunders, A. D., Norry, M.J. (Eds.), Magmatism in Ocean Basins. Geological Society of London Special Publication, vol. 42, 313-345.

Taylor, S.R., McLennan, S.M., 1985. The Continental Crust: Its Composition and Evolution. Blackwell, Oxford, 312 pp.

Thurow, J., 1988. 22. Cretaceous radiolarians of the North Atlantic Ocean; ODP Leg 103 (Sites 638, 640 and 641) and DSDP legs 93 (site 603) and 47 B (site 398). In: Boillot, G., Winterer, E. L., et al. (Eds.), Proceedings of the Ocean Drilling Program, Scientific Results, vol. 103, pp. 379-418.

Vishnevskaya, V.S., 1987.Composition and age of the Cretaceous siliceous-volcanogenic formation of the Olutor Range. In: Tilman, S.M. (Eds.), Geology of Southern Koryak Highland, Nauka, Moscow, pp. 10-65 (in Russian).

Vishnevskaya, V.S., 2010. Upper Cretaceous Radiolarians of the East European Platform and Their Biostratigraphic Significance. Stratigraphy and Geological Correlation 18, 607-634.

Winchester, J.A., Floyd, P.A., 1977. Geochemical discrimination of different magma series and their differentiation products using immobile elements. Chemical Geology 20, 325-343.

Wood, D.A., 1980. The application of a Th-Hf-Ta diagram to problems of tectonomagmatic classification and to establishing the nature of crustal contamination of basaltic lavas of the British Tertiary volcanic province. Earth and Planetary Science Letters 50, 11-30.

Workman, R.K., Hart, S.R., 2005. Major and trace element composition of the depleted MORB mantle (DMM). Earth and Planetary Science Letters 231, 53-72.

Table Caption

Table 1. Major and trace element analyses of volcanic and metavolcanic rocks from the Makran Coloured Mélange Complex. The volcanic rocks stratigraphically associated with radiolarian cherts sampled in the Kahmij-e-Balo, Gorevi 1, Gorevi 2, and Gorevi 3 sections (see Fig. 5) are shown and age is reported. Abbreviations, bas: basalt; bas and: basaltic andesite; Fe-bas: ferrobasalt; and: andesite; dac: dacite; metavolc: metavolcanic rock. N-MORB: normal-type mid-ocean ridge basalt; Alk: alkaline oceanic within-plate; OPB: oceanic plateau basalt; VA-Th: volcanic arc tholeiite; CA: calc-alkaline; MLF: massive lava flow; pill. brec.: pillow breccia; E: Early; L: Late; Cr: Cretaceous; Tu: Turonian; Ca: Campanian; lCe: late Cenomanian; Sa: Santonian; Ha: Hauterivian; Ap; Aptian; Co: Coniacian; n.d.: not detected. Mg#=100xMg/(Mg+Fe). Fe_2O_3=0.15xFeO. Normalizing values for REE ratios are from Sun and McDonough (1989).

Figure Captions

Figure 1. Geographic and geological location of the study area. a) Satellite image; b) tectonic sketch map of Iran with location of the main ophiolite massifs (modified from Saccani et al., 2013). In both the figures the study area is boxed.

Figure 2. Tectonic sketch map of the Makran region (a) and related cross section (b). The location of the study area in the North Makran is shown. Modified after Burg et al. (2013).

Figure 3. Tectonic sketch map of the study area. Boxes indicate the location of sections with radiolarian cherts stratigraphically associated with volcanic rocks. (Modified from Samimi Namin, 1982, 1983).

Figure 4. a) and b) field occurrence of the Coloured Mélange in the Kahmij-e-Balo area (a) and Gorevi area (b). c) block of a metavolcanic rock in the Gorevi area. d) Photomicrograph of the metavolcanic rock shown in Panel c) showing the occurrence of glaucophane (Gln) and epidote (Ep).

Figure 5. Stratigraphic logs of the blocks of the Coloured Mélange Complex with radiolarian cherts stratigraphically associated with volcanic rocks. The stratigraphic position of samples is also shown. Field photos of the studied sections are shown in the three pictures. Boxes in the stratigraphic columns indicate the position of the pictures shown in Figure 6. Abbreviations, bas: basaltic rock; rad: radiolarian chert; bas-br: basaltic breccia; rad-sh: radiolarian-bearing siliceous shale

Figure 6. Field occurrence of the Coloured Mélange in the Kahmij-e-Balo and Gorevi areas. The position of these pictures with respect to the stratigraphic column is shown in Figure 5. a) Kahmij-e-Balo section: primary relationships between basalts (bas) and radiolarian cherts (rad), the arrow indicate a discontinuous red siliceous interpillow shale. b) Kahmij-e-Balo section: cm-thick alternance of porcellanaceous red to violet radiolaria-bearing strata and siliceous red shales. c) Gorevi 1 section: cm-thick alternance of porcellanaceous red cherts and siliceous red shales. d) Gorevi 2 section: interpillow red siliceous shales highlight the primary relationships between basalts and cherts. e) and f) Gorevi 3 section: pillow lava (e) and pillow breccia (f) in the upper part of the measured section.

Figure 7. Scanning electron micrographs of late Hauterivian to late Campanian radiolarians. 1) *Acanthocircus hueyi* (Pessagno), MK154; 2) *Afens liriodes* Riedel and Sanfilippo, MK63; 3) *Alievum* sp. cf. *A. gallowayi* (White), MK155; 4) *Alievum* sp., MK63; 5) *Archaeodictyomitra* sp., MK63; 6) *Archaeospongoprunum bipartitum* Pessagno, MK63; 7) *Crucella cachensis* Pessagno, MK155; 8) *Crucella* sp. cf. *C. angulata* Yang, MK154; 9) *Orbiculiformella titirez* (Jud), MK145; 10) *Pantanellium masirahense* Dumitrica, MK155; 11) *Praeconocaryomma* sp., MK145; 12) *Rhopalosyringium* sp. cf. *R. mangaleniense* Bragina, MK155; 13) *Thanarla* sp. cf. *T. brouweri* (Tan), MK145; 14) *Theocampe* (?) *urna* (Foreman), MK155; 15) *Theocampe* (?) sp. cf. *T.* (?) *urna* (Foreman), MK155; 16) *Theocampe* (?) sp. cf. *T.* (?) *urna* (Foreman), MK154. Scale bar = 50µm.

Figure 8. Nb/Y vs. Zr/Ti discrimination diagram of Winchester and Floyd (1977) modified by Pearce (1996) for volcanic and metavolcanic rocks from the Makran Coloured Mélange Complex. The composition of basalts from the Band-e-Zeyarat ophiolites in the North Makran domain are shown for comparison (data from Ghazi et al., 2004).

Figure 9. N-MORB normalized incompatible element patterns (left column) and chondrite-normalized REE patterns (right column) for volcanic and metavolcanic rocks from the Makran Coloured Mélange Complex. The compositional variation of oceanic plateau basalts from the peri-Caribbean ophiolites (Hauff et al., 2000; Hastie et al., 2008) and Ontong Java Plateau (Fitton and Godard, 2004), as well as basalts from the Band-e-Zeyarat ophiolites (B-e-Z) in the North Makran domain (Ghazi et al., 2004) are shown for comparison. The composition of modern normal-type (N-) and enriched-type (E-) mid-ocean ridge basalts (MORB), and alkaline ocean island basalt (OIB), as well as normalizing values are from Sun

and McDonough (1989).

Figure 10. Th, Ta, Hf/3 discrimination diagram of Wood (1980) for volcanic and metavolcanic rocks from the Makran Coloured Mélange Complex. Abbreviations, N-MORB: normal-type mid-ocean ridge basalt; E-MORB: enriched-type mid-ocean ridge basalt.

Figure 11. N-MORB-normalized Th vs. Nb discrimination diagram of Saccani (2015) for volcanic and metavolcanic rocks from the Makran Coloured Mélange Complex. a) rock-type discrimination, b) tectonic setting interpretation. Abbreviations, MORB: mid-ocean ridge basalt, N-: normal type, E-: enriched type, D-: depleted type, MTB: medium-Ti basalts, IAT: island arc tholeiite, CAB: calc-alkaline basalt; OIB: alkaline oceanic within-plate basalt, BABB: backarc basin basalt, SSZ-E: supra-subduction zone enrichment, AFC: assimilation-fractional crystallization, OIB-CE: OIB component enrichment, FC: fractional crystallization, backarc A: relatively immature backarc setting, backarc B: relatively mature backarc setting. The compositional variation of volcanic rocks and dykes from the Band-e-Zeyarat ophiolites in the North Makran domain (data from Ghazi et al., 2004) is shown for comparison. Normalization values, as well as the composition of typical modern N-MORB, EMORB, and OIB (stars) are from Sun and McDonough (1989).

Figure 12. a) Nb vs. Zr and b) Th/Ta vs. Zr diagrams for volcanic and metavolcanic rocks from the Makran Coloured Mélange Complex. Only the relatively less fractionated basaltic and metabasaltic rocks are plotted in b). Stars indicate the compositions of average pelitic sediments (APS), upper continental crust (UCC), average calc-alkaline basalts and basaltic andesites (CA-B-BA), average island arc tholeiitic basalts (IAT), normal-type mid-ocean ridge basalt (N-MORB), and alkaline ocean island basalt (OIB). Data source: N-MORB, E-

MORB, and OIB are from Sun and McDonough (1989); APS and UCC are from Taylor and McLennan (1985); IAT and CA-B-BA are calculated from 249 and 244 samples, respectively, of basaltic rocks from various ophiolitic complexes (see Table 1 in Saccani, 2015 for references).

Figure 13. Nb/Yb vs. Th diagram for relatively less fractionated Group 1, Group 2, and Group 3 basalts from the Makran Coloured Mélange Complex, as well as batch melting curves for: depleted MORB mantle (DMM) in the spinel stability field; fertile lherzolite in the spinel stability field; ocean island-type enriched source (OIB) in both garnet and spinel stability fields. The dashed line represents the mixing line of various melt fractions from garnet- and spinel-facies mantle. Ticks on the spinel-facies fertile lherzolite melting curve indicate the same percentages of melt fractions as shown for the other melting curves. Mantle source compositions, DMM: Nb = 0.128 ppm, Th = 0.0068 ppm, Yb = 0.353 ppm (Workman and Hart, 2005); fertile lherzolite: Nb = 0. 246 ppm, Th = 0.016 ppm, Yb = 0.382 ppm (E-DMM of Workman and Hart, 2005); OIB: Nb = 1.5 ppm, Th = 0.18 ppm, Yb = 0.353 ppm (Lustrino et al., 2002). Source modes and melting proportions for the garnet-facies are: $Ol_{0.57}$-$Opx_{0.21}$-$Cpx_{0.13}$-$Grt_{0.09}$ and $Ol_{0.04}$-$Opx_{-0.19}$-$Cpx_{1.05}$-$Grt_{0.11}$, respectively (Kinzler, 1997). Source modes and melting proportions for the spinel-facies are: $Ol_{0.53}$-$Opx_{0.27}$-$Cpx_{0.17}$-$Spl_{0.03}$ and $Ol_{-0.06}$-$Opx_{-0.28}$-$Cpx_{0.67}$-$Spl_{0.11}$, respectively (Kinzler, 1997). Fractional crystallization trends for DMM and fertile lherzolite primary melts are calculated assuming the crystallization of olivine (Ol), plagioclase (Pl), clinopyroxene (Opx), and spinel (Spl) in the proportions shown in Figure. Partition coefficients are from McKenzie and O'Nions (1991).

Figure 14. Cr vs. Y diagram (modified after Pearce, 1982) for Group 1, Group 4, and Group 5 volcanic and metavolcanic rocks from the Makran Coloured Mélange Complex.

Abbreviations, N-MORB: normal-type mid-ocean ridge basalt, IAT: island arc tholeiite, CA: calc-alkaline. Mantle source compositions and melting paths for incremental batch melting are calculated according to Murton (1989). S1: MORB-type mantle source; S2: residual mantle source after 15% MORB melt extraction from source S1; S3: residual mantle source after 10% melt extraction from source S2. The fractional crystallization trends for CA, IAT, and N-MORB melts are also shown (tick marks indicate 10% fractional crystallization steps).

Figure 15. Ba/Th vs. Th/Nb diagram for relatively less fractionated basaltic and metabasaltic rocks from the Makran Coloured Mélange Complex. Stars indicate the compositions of average pelitic sediments (APS), upper continental crust (UCC), average calc-alkaline basalts and basaltic andesites (CA-B-BA), average island arc tholeiitic basalts (IAT), normal-type mid-ocean ridge basalt (N-MORB), and alkaline ocean island basalt (OIB). Data source: N-MORB, E-MORB, and OIB are from Sun and McDonough (1989); APS and UCC are from Taylor and McLennan (1985); IAT and CA-B-BA are calculated from 249 and 244 samples, respectively, of basaltic rocks from various ophiolitic complexes (see Saccani, 2015 for references).

Figure 16. Summary of the biostratigraphic and geochemical data for basalts and associated radiolarian chert in the sections shown in Figure 5. Sample labels refer to radiolarian cherts. Abbreviations, OPB: oceanic plateau basalt; VA-Th: volcanic arc tholeiitic basalt; CAB: calc-alkaline basalt. Time scale after Cohen et al. (2013).

Figure 17. Two-dimensional geodynamic reconstruction of the southern Neo-Tethys-Lut Block section at Santonian-Early Campanian (a) and Paleocene times (b). In the Santonian-Early Campanian (a), the subduction of the Neo-Tethys Ocean below the Lut block and the

development of an accretionary prism were active. In the lower plate, oceanic plateau basalts (OPB) and alkaline basalts were erupted in these times, whereas in the upper plate a volcanic arc is developing on the southern rim of the Lut block, and a backarc basin (future north Makran ophiolites) was opening between the Lut Block and the Durkan-Bajgan microcontinent. In the Paleocene (b), the convergence led to the collision of the oceanic plateau with the continental arc that, in turn, triggered the subduction jump and the emplacement of both the Coloured Mélange and North Makran Ophiolites.

Figure 1 color

Click here to download high resolution image

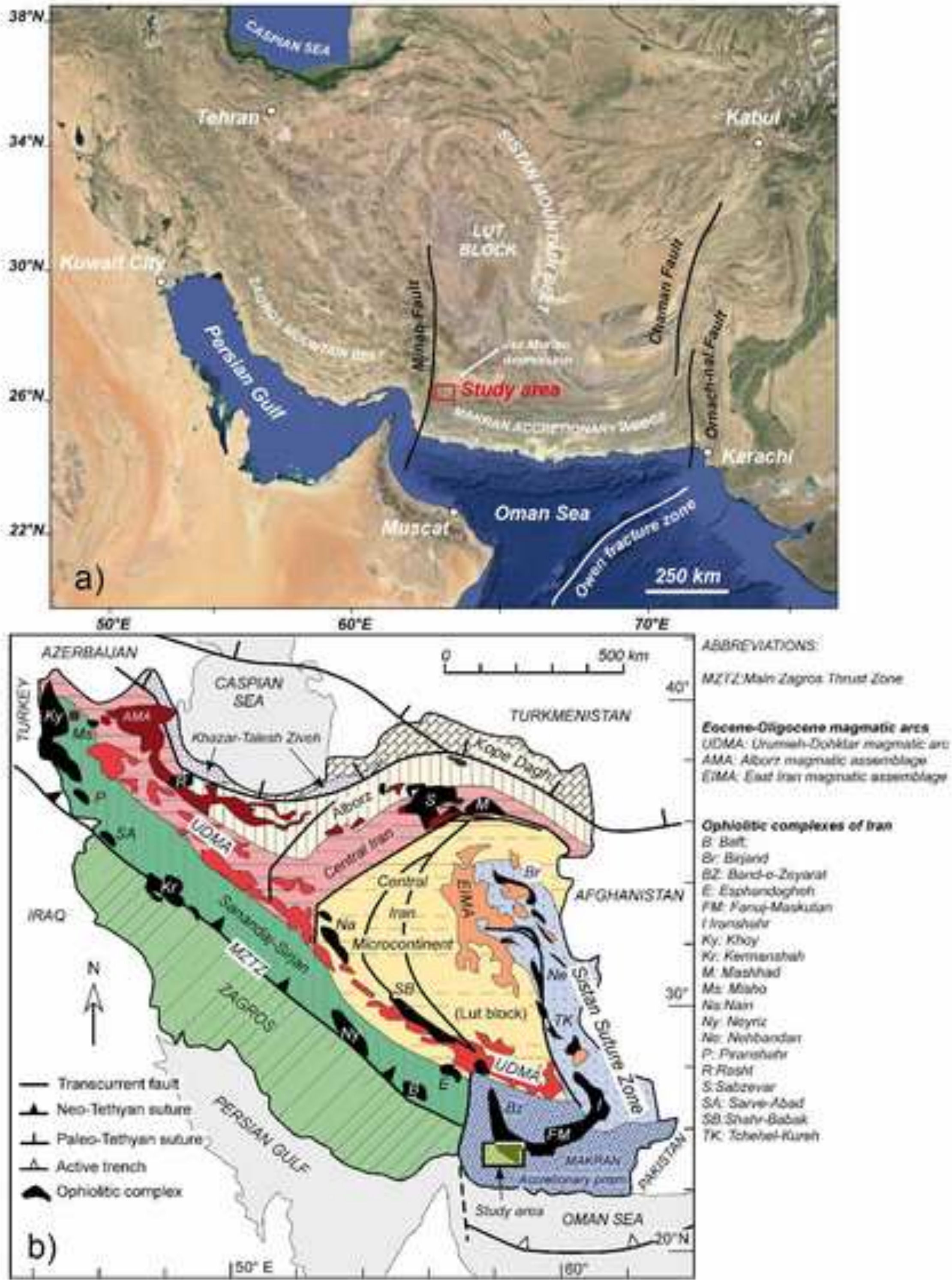

Figure 2 color

Click here to download high resolution image

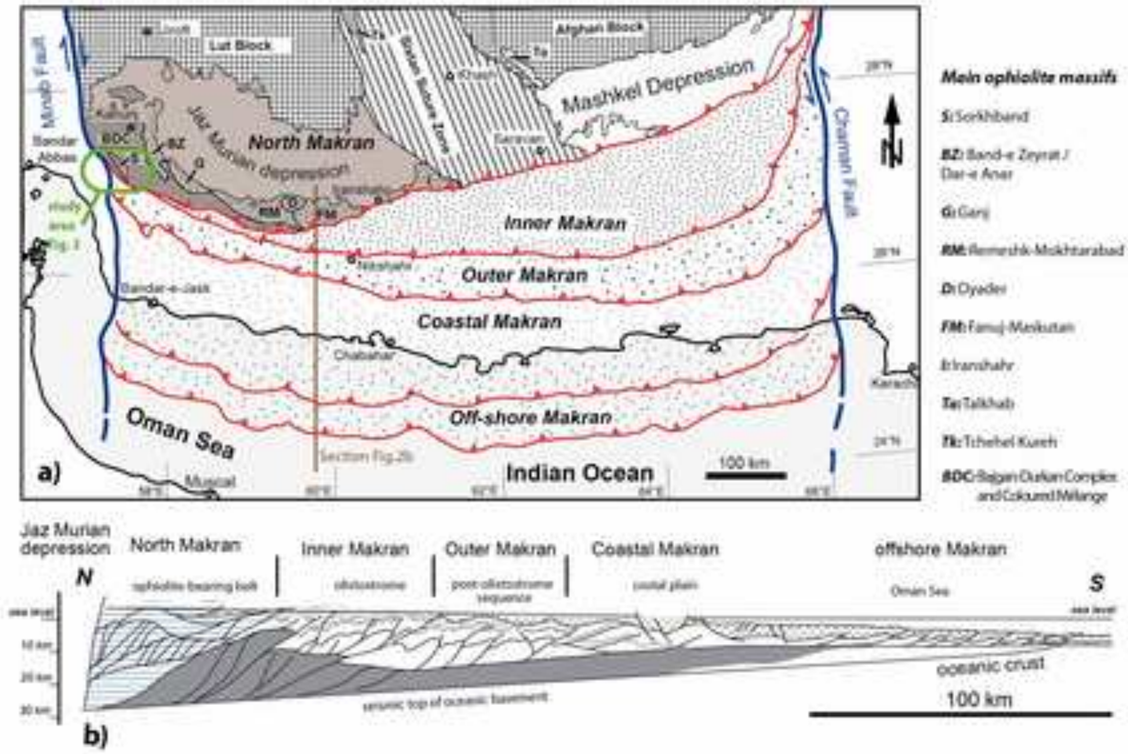

Figure 3 color

Click here to download high resolution image

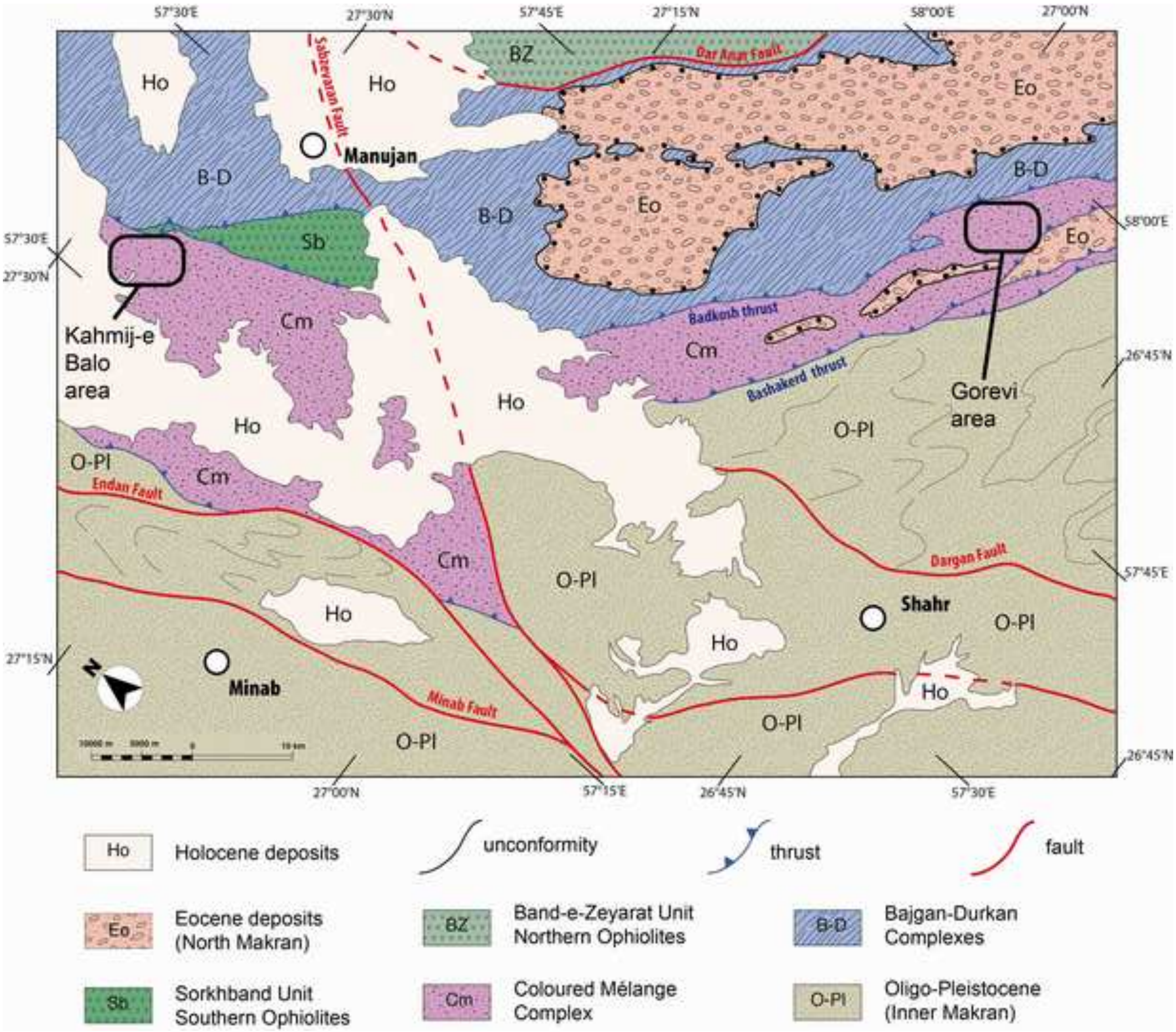

Figure 4 color
Click here to download high resolution image

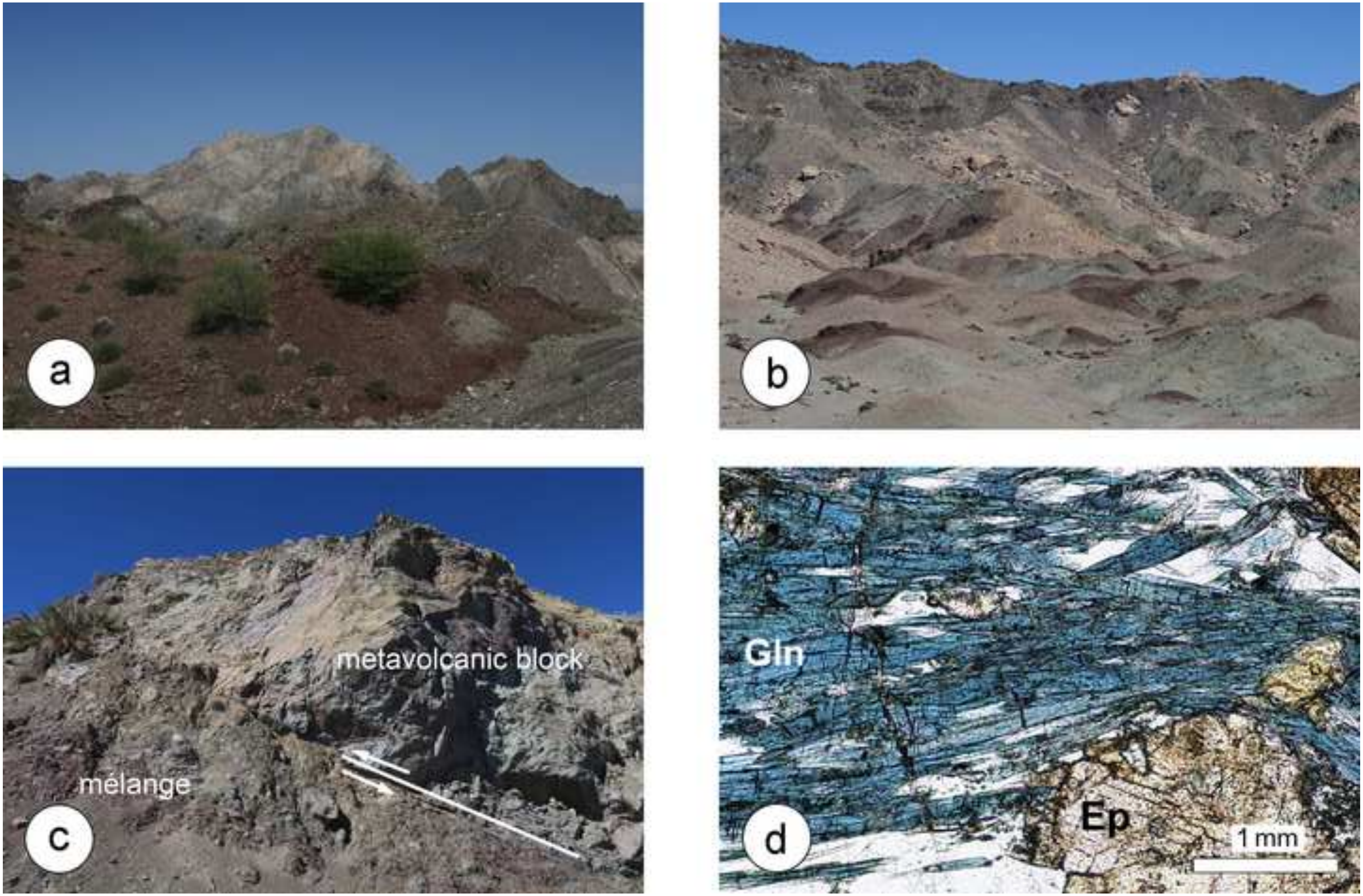

Figure 5 color

Click here to download high resolution image

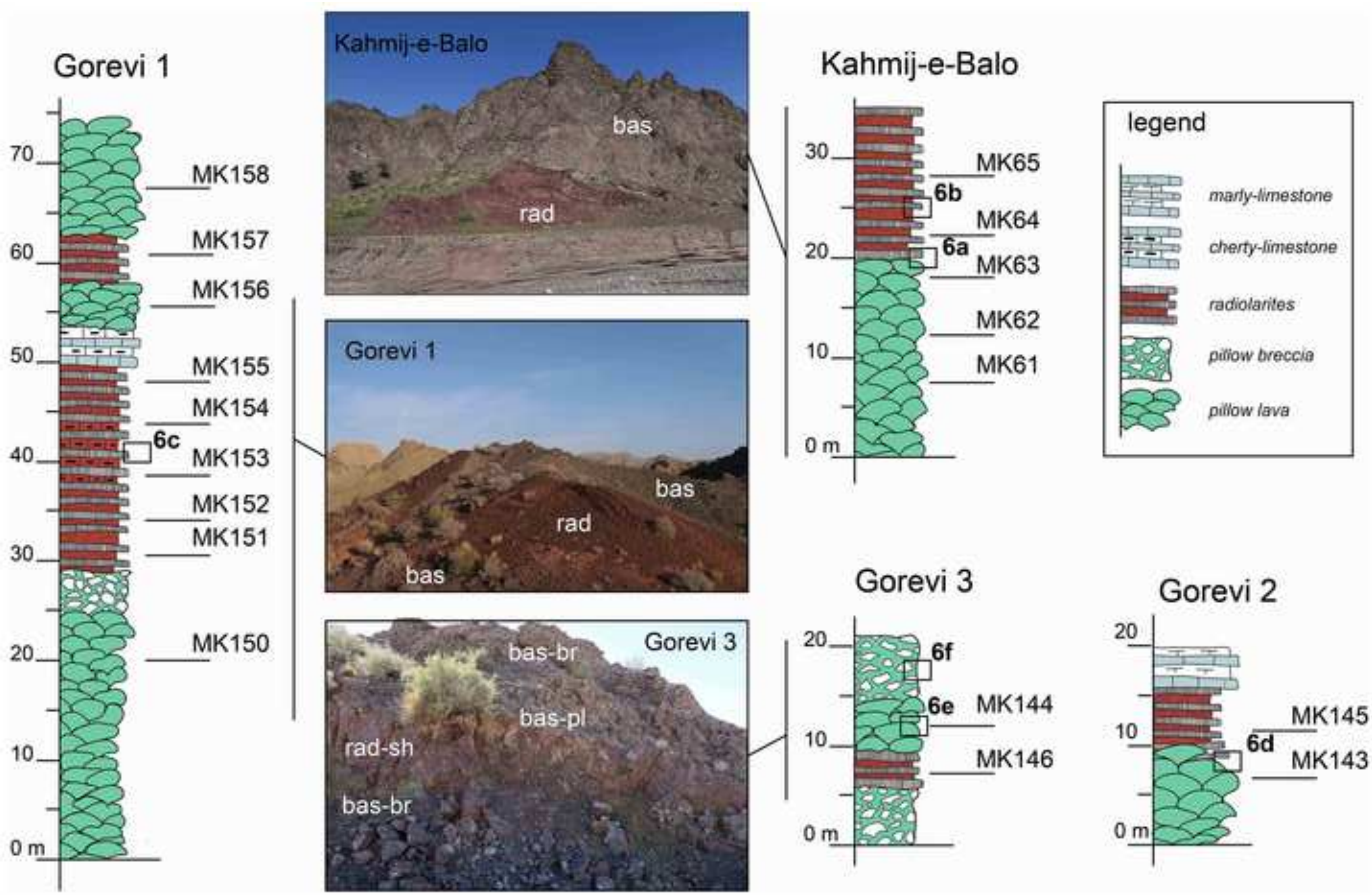

Figure 6 color
Click here to download high resolution image

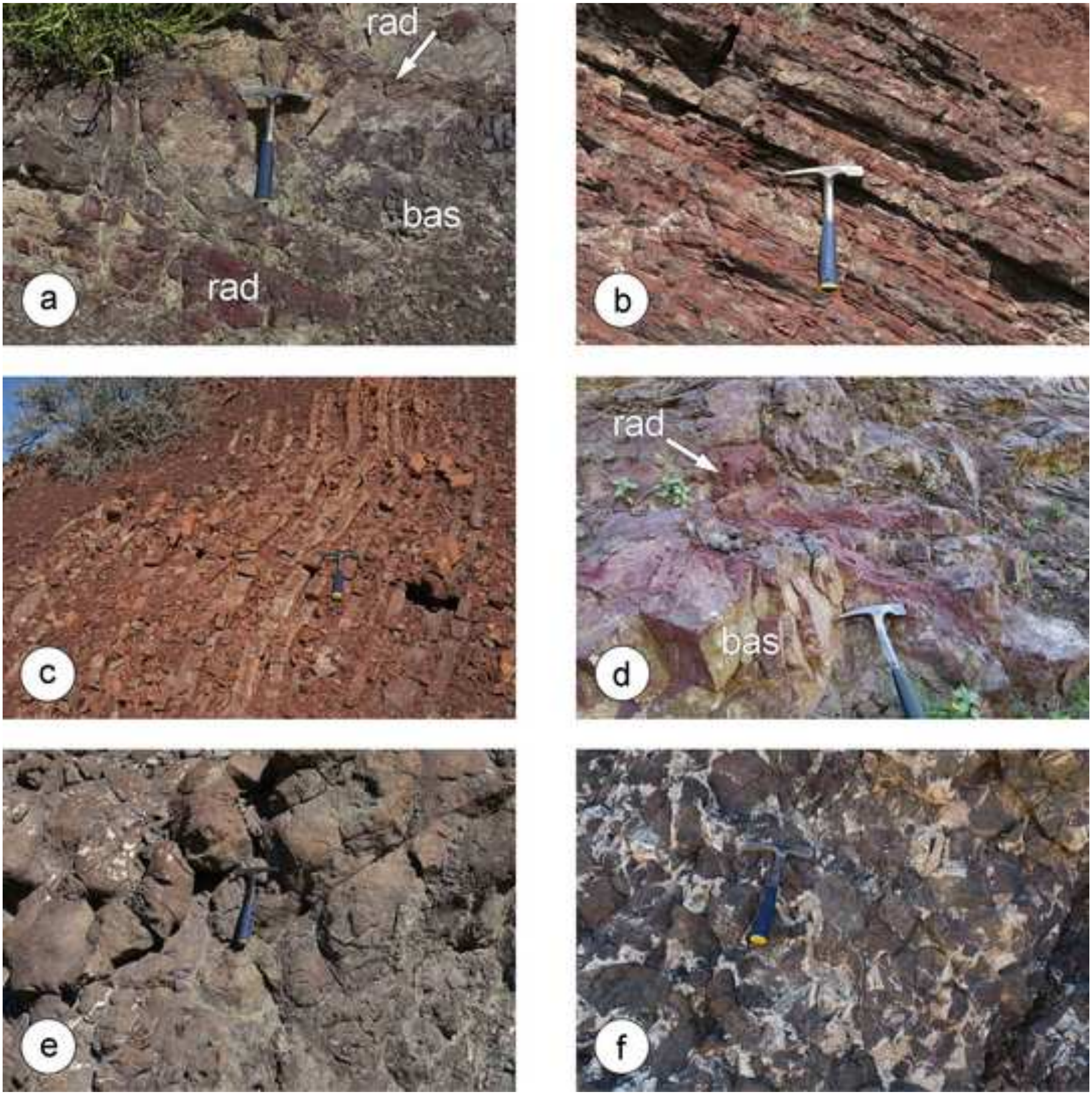

Figure 7 (only one in Black & White)

Click here to download high resolution image

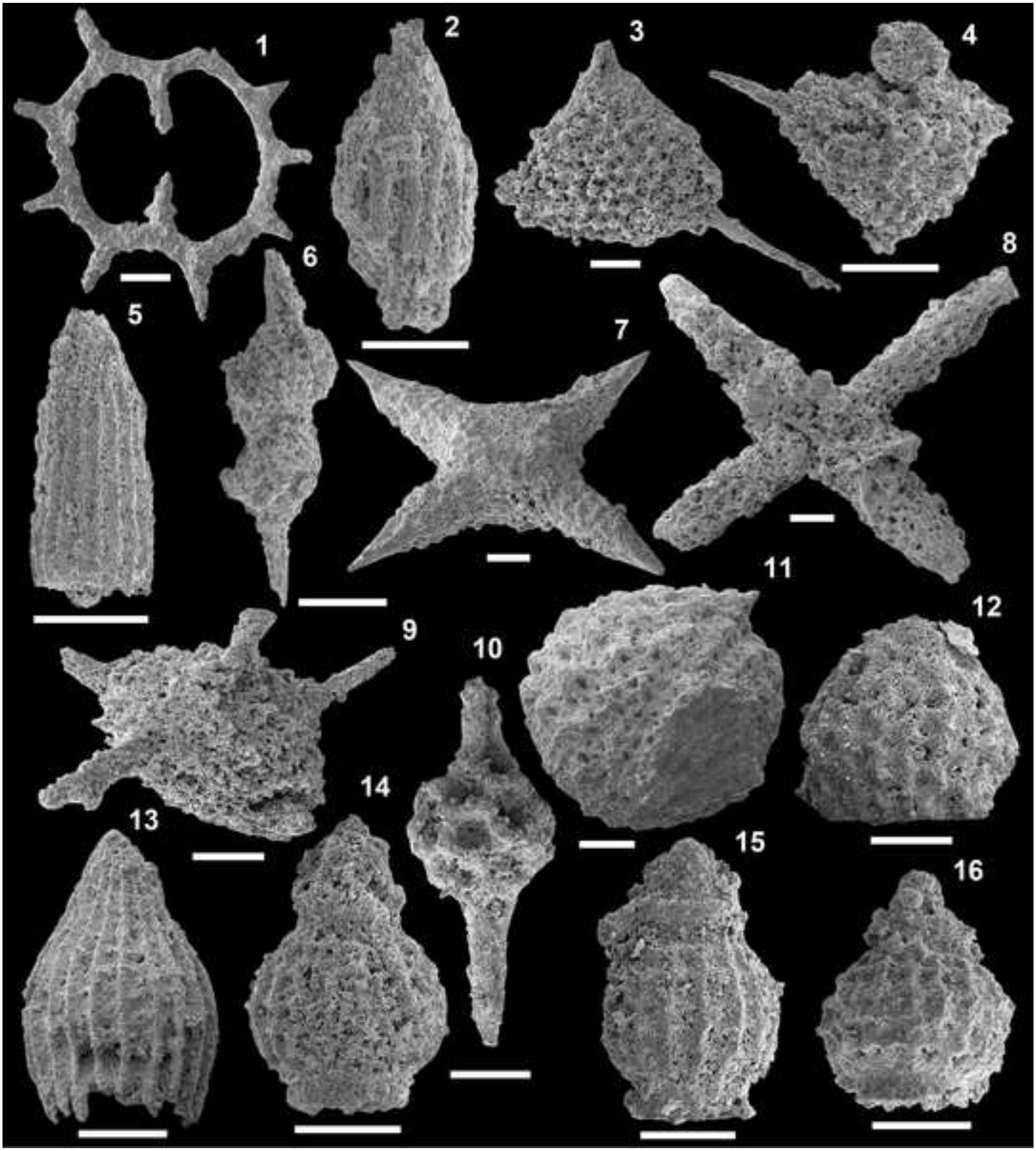

Figure 8 color
Click here to download high resolution image

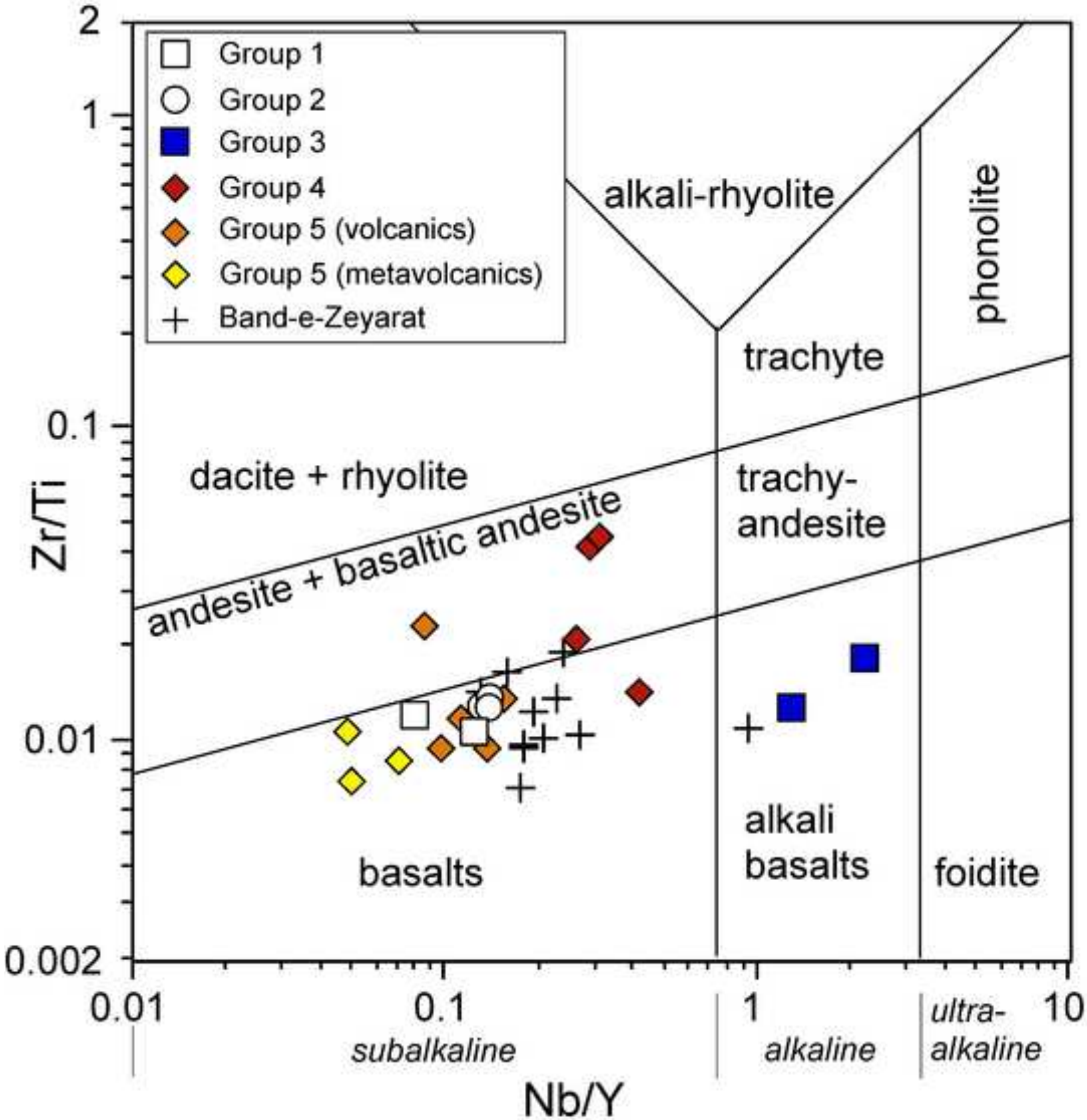

Figure 9 color

Click here to download high resolution image

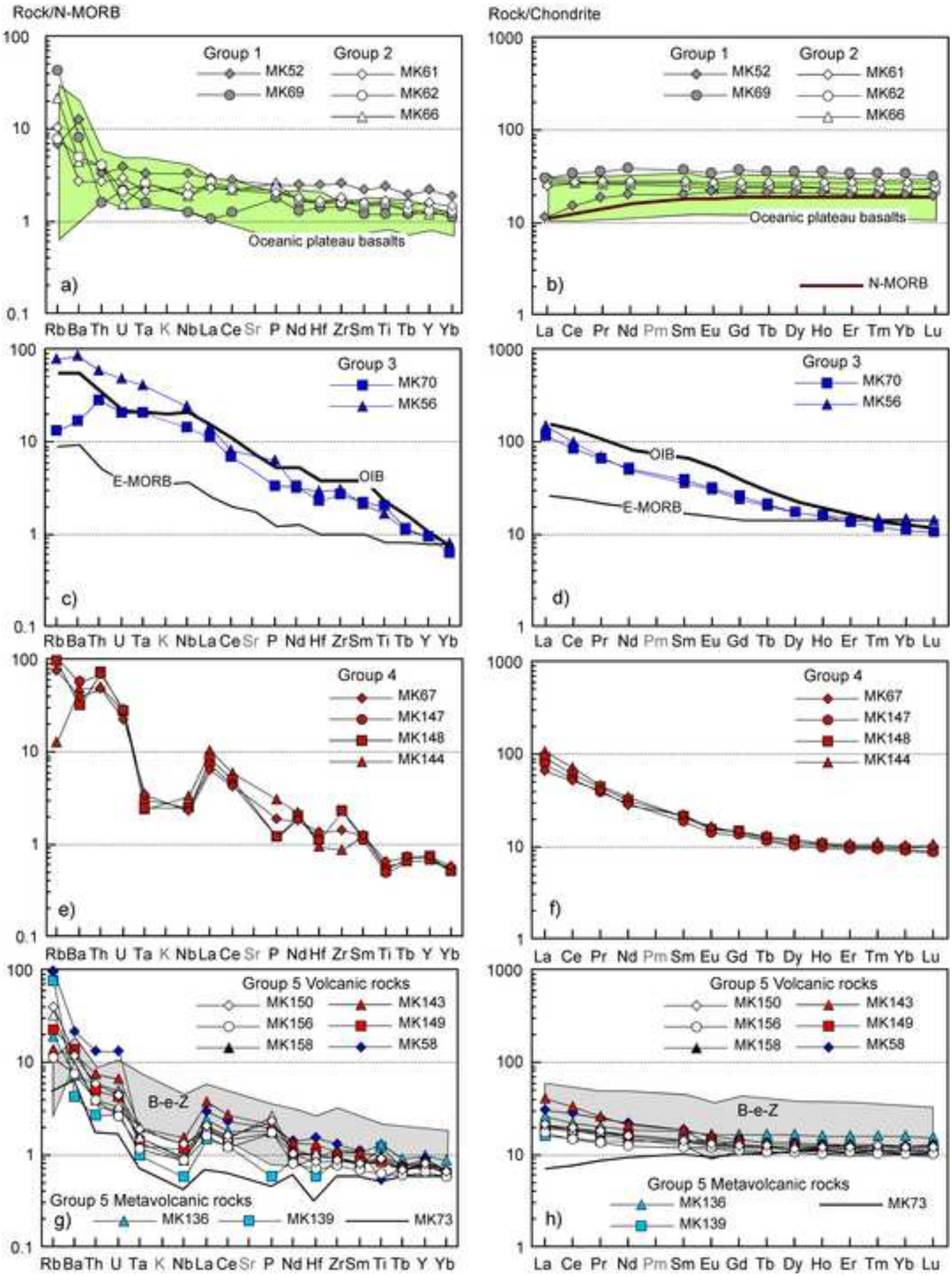

Figure 10 color

Click here to download high resolution image

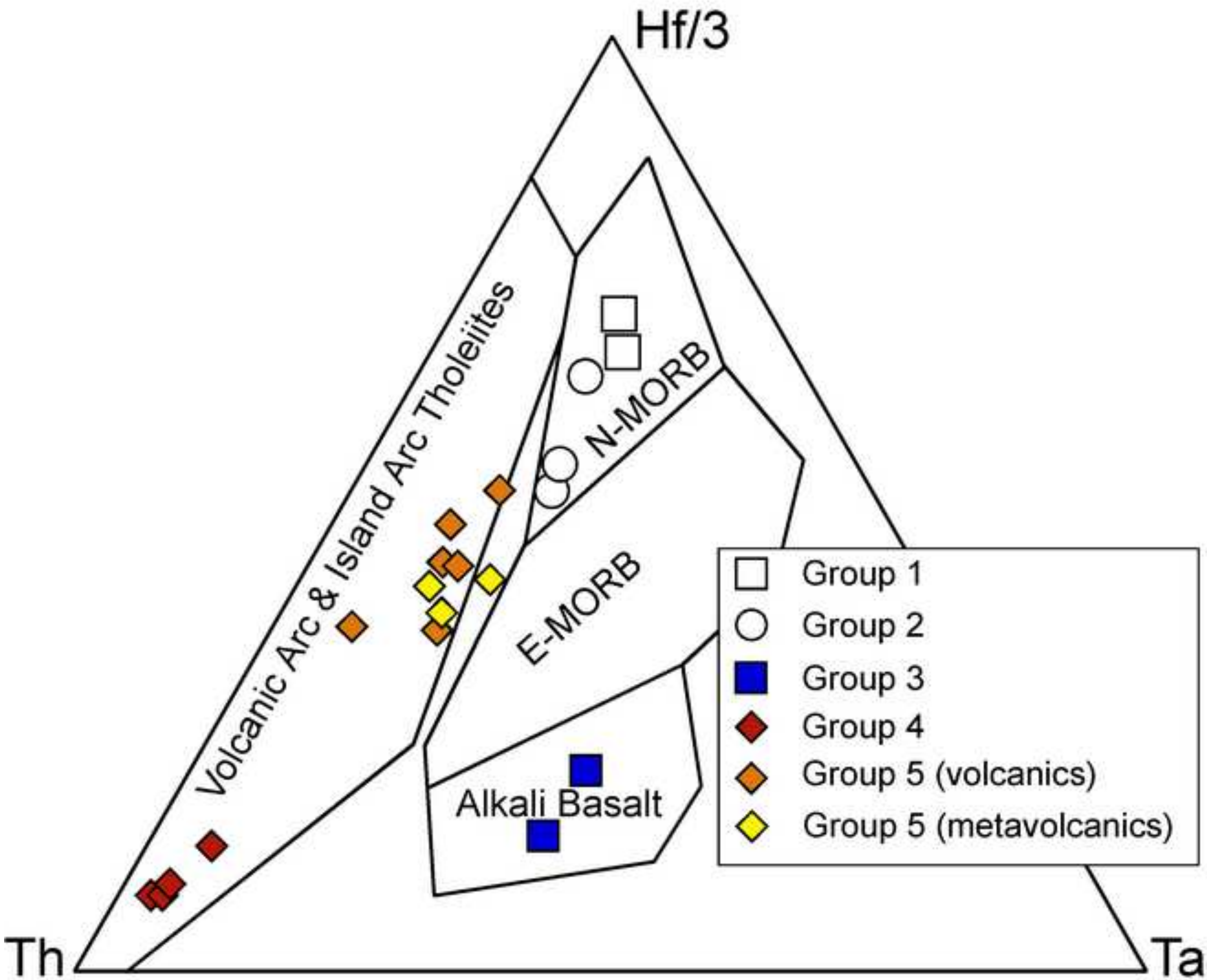

Figure 11 color

Click here to download high resolution image

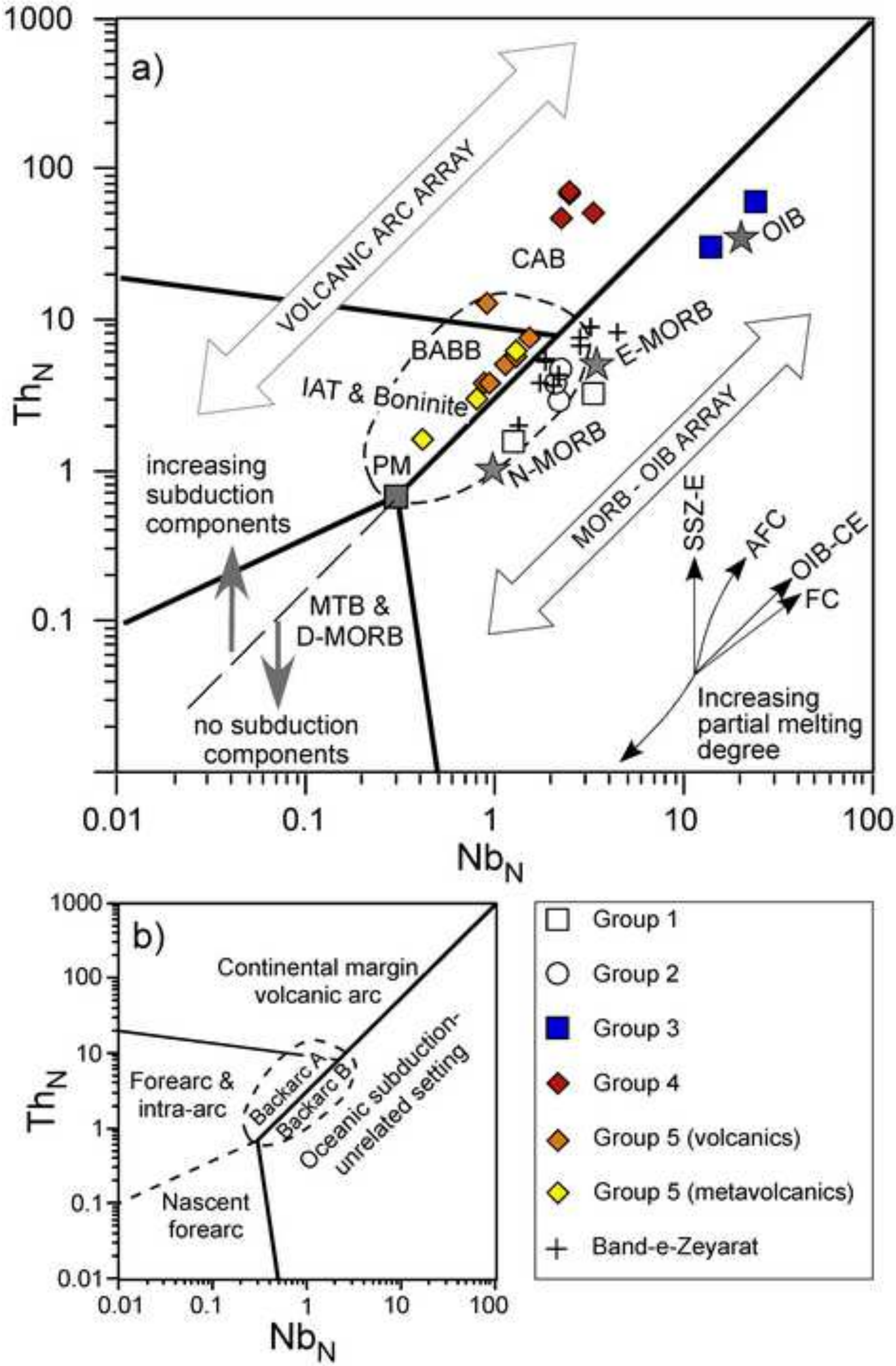

Figure 12 color

Click here to download high resolution image

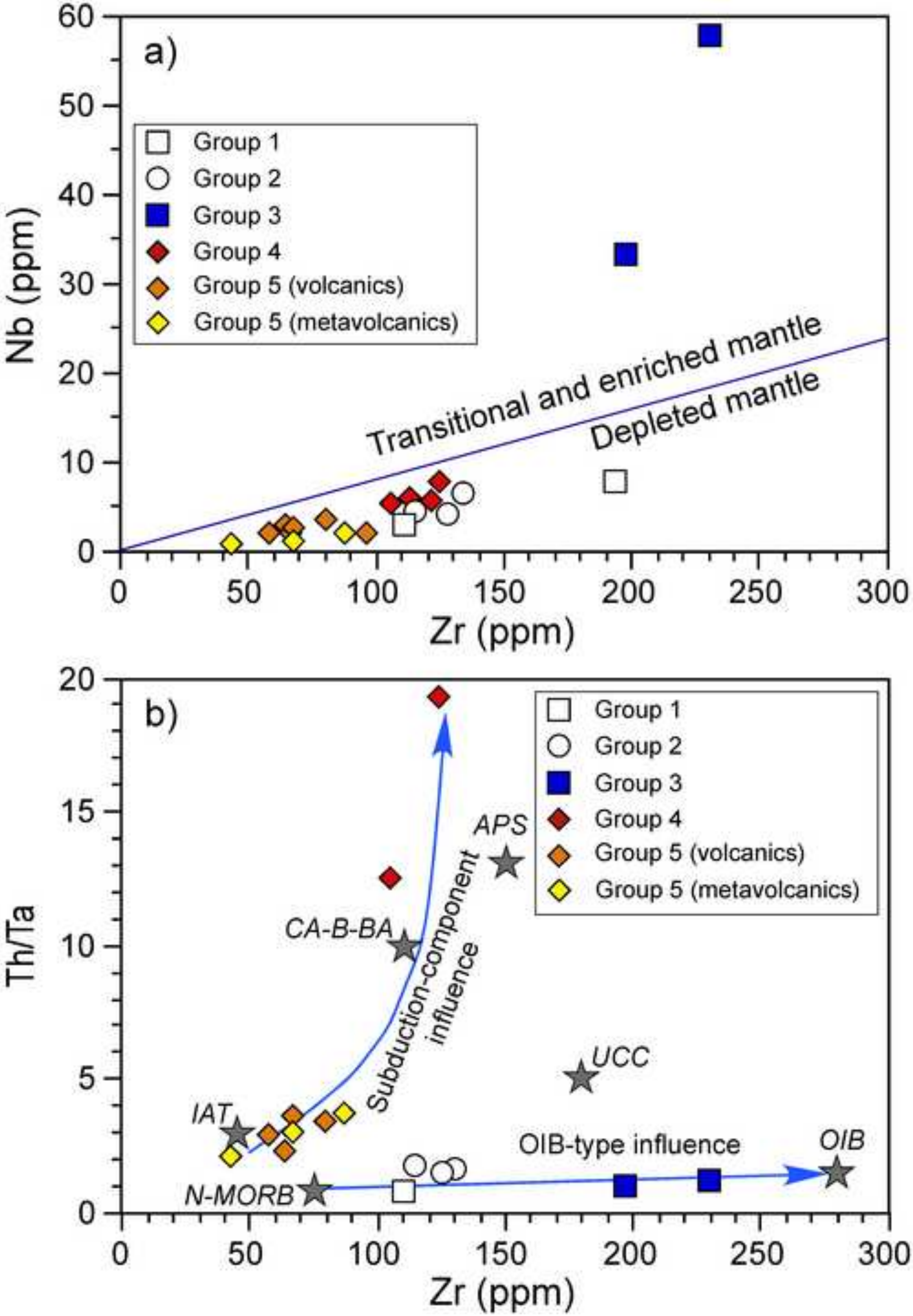

Figure 13 color

Click here to download high resolution image

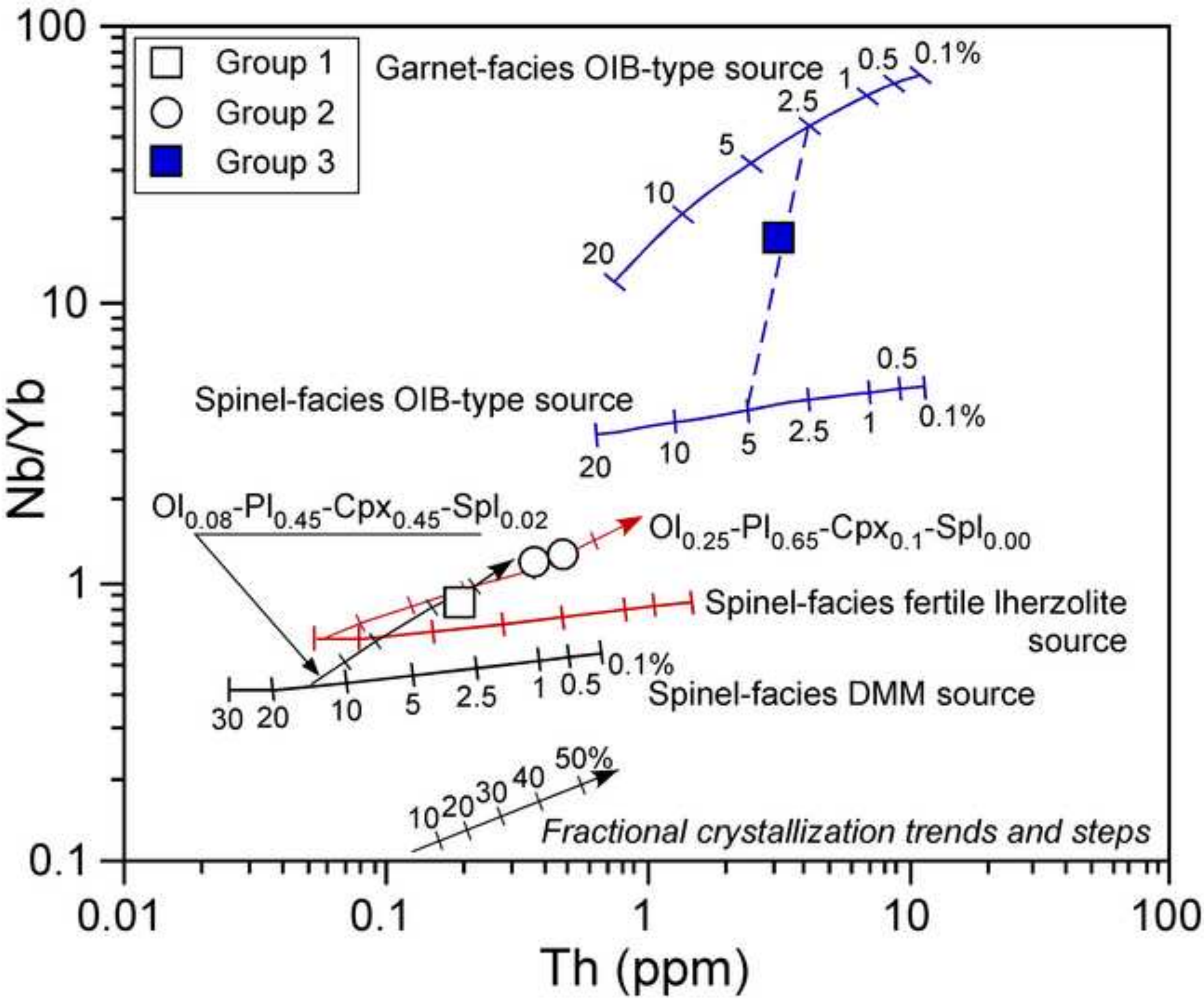

Figure 14 color
Click here to download high resolution image

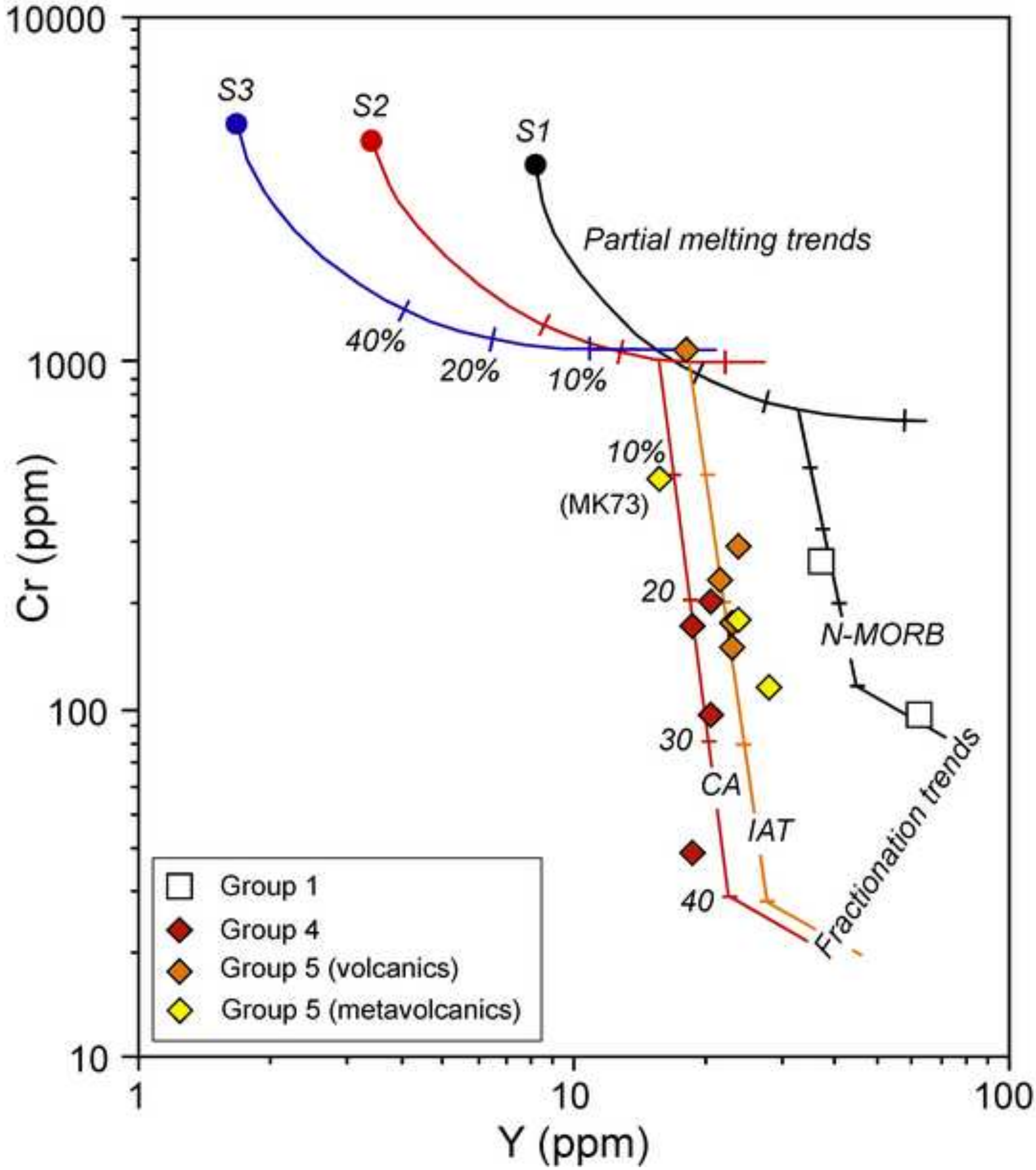

Figure 15 color
Click here to download high resolution image

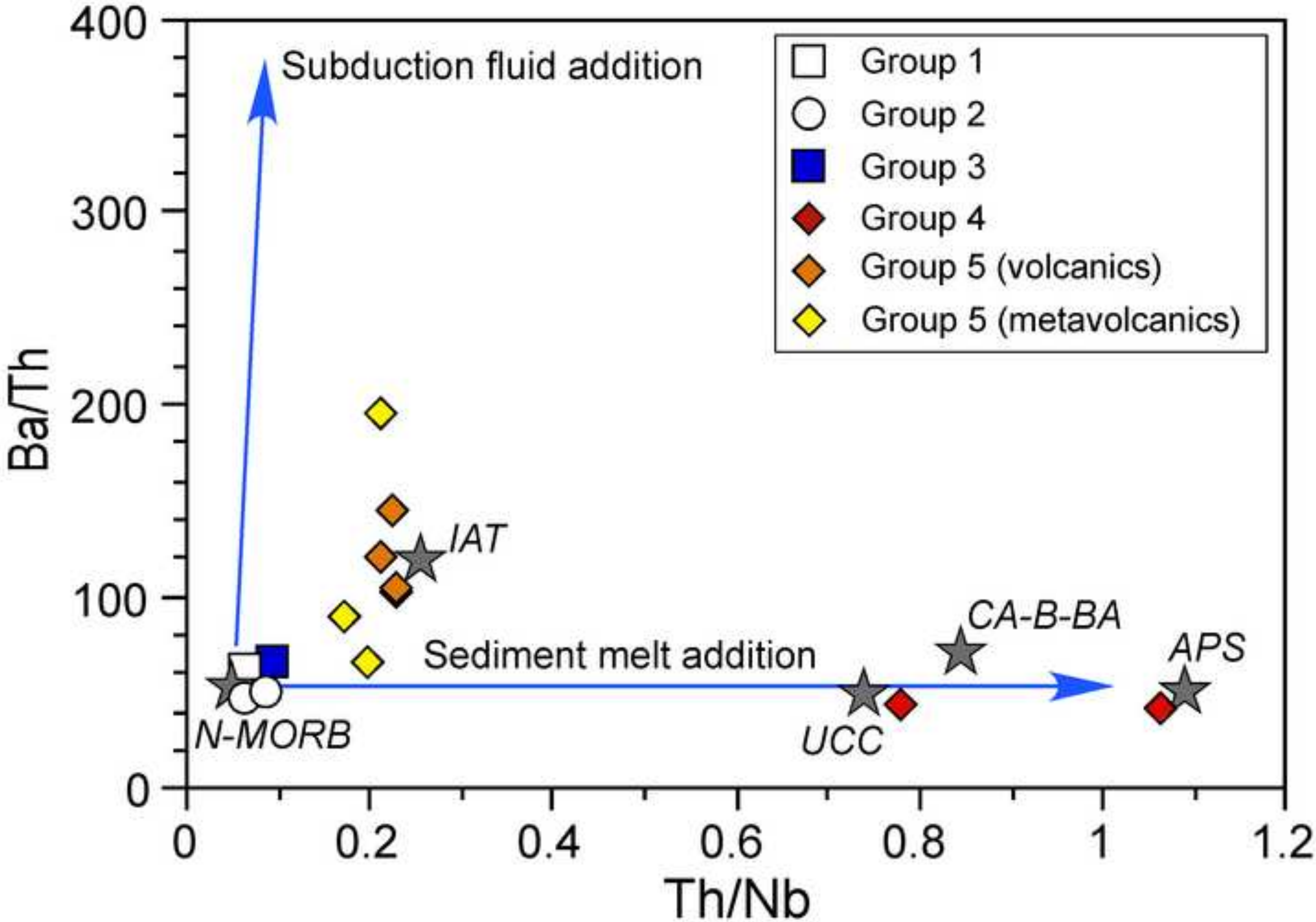

Figure 16 color

Click here to download high resolution image

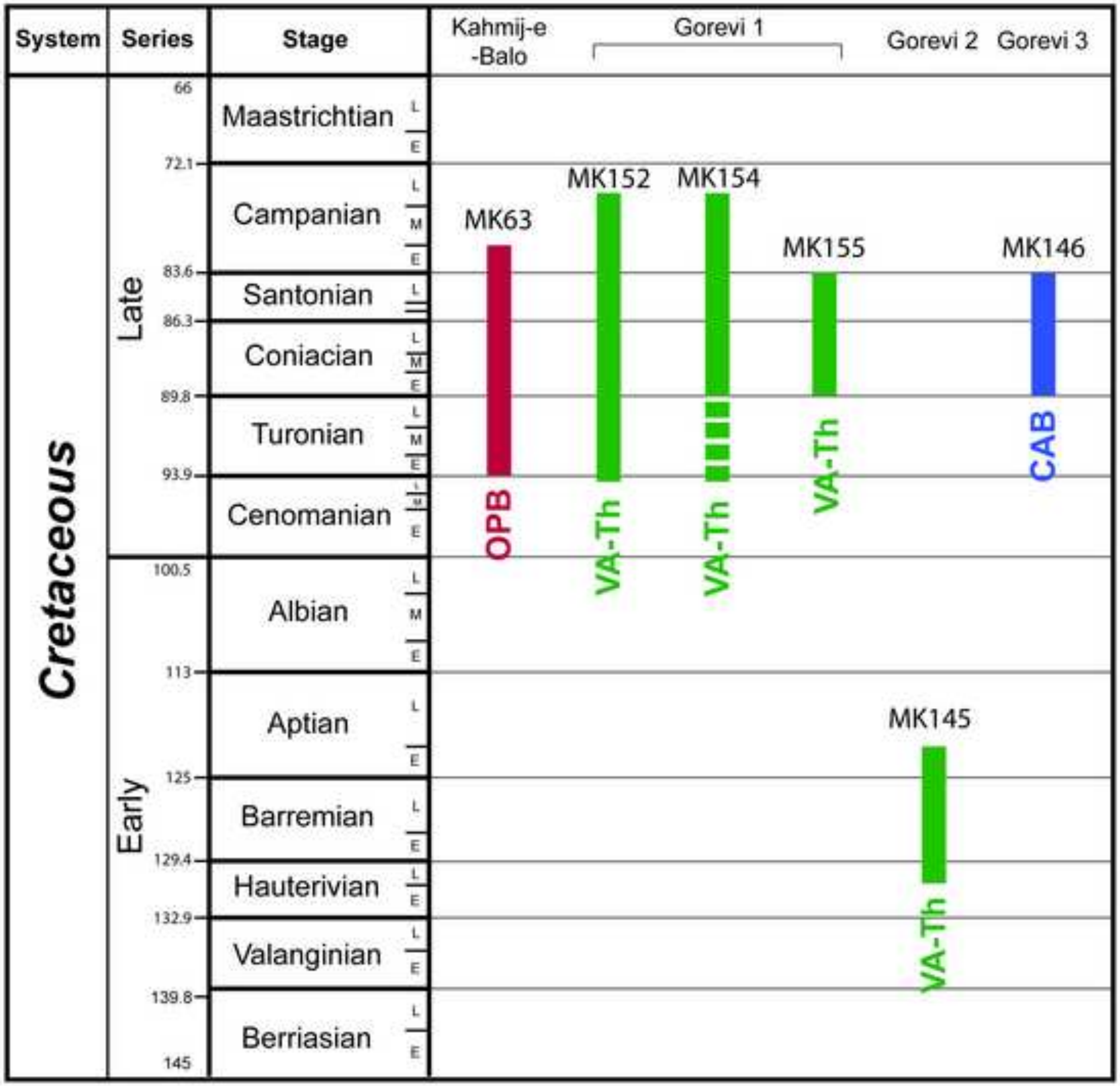

Figure 17 color
Click here to download high resolution image

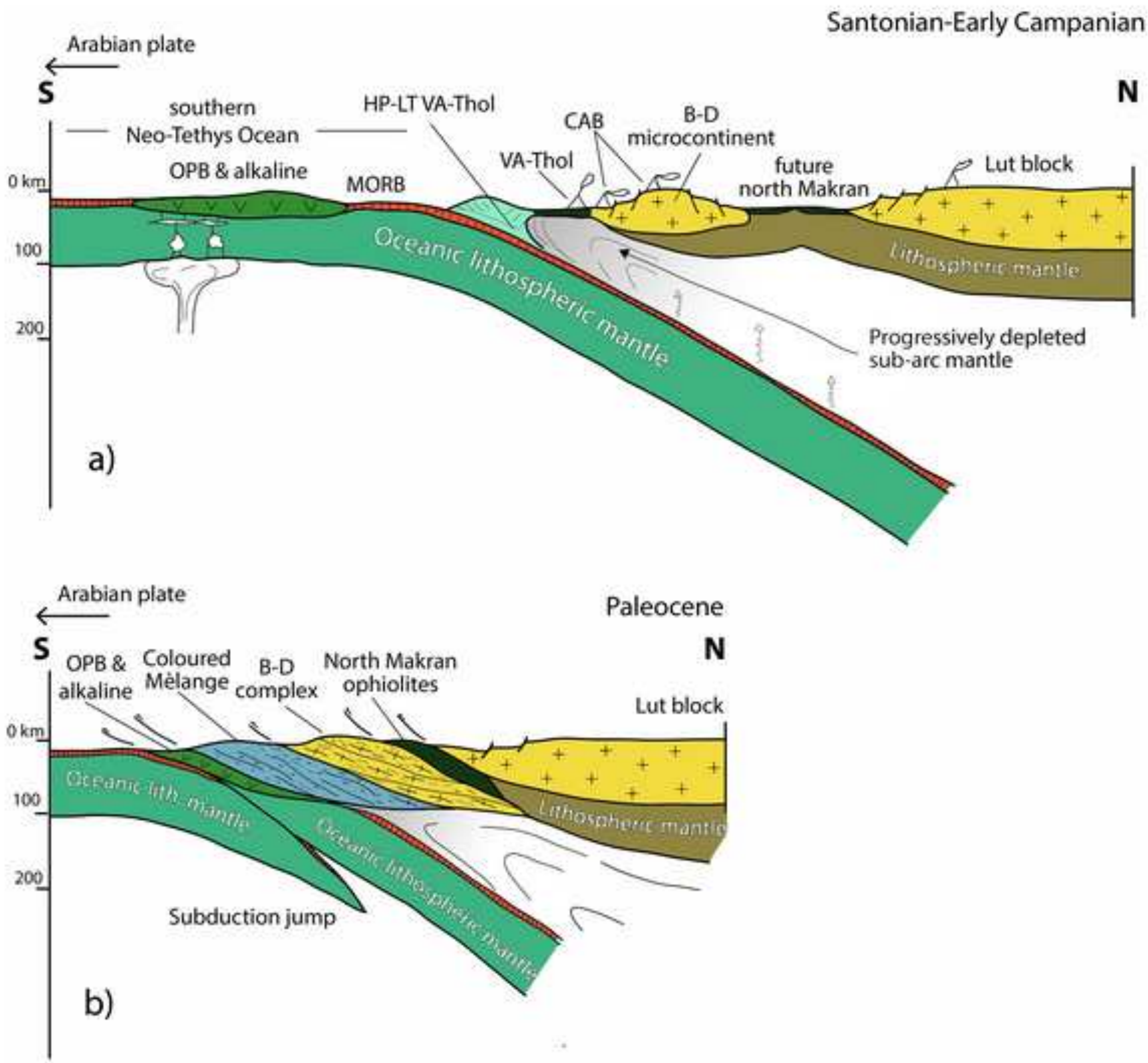

Figure 1 black & White

Click here to download high resolution image

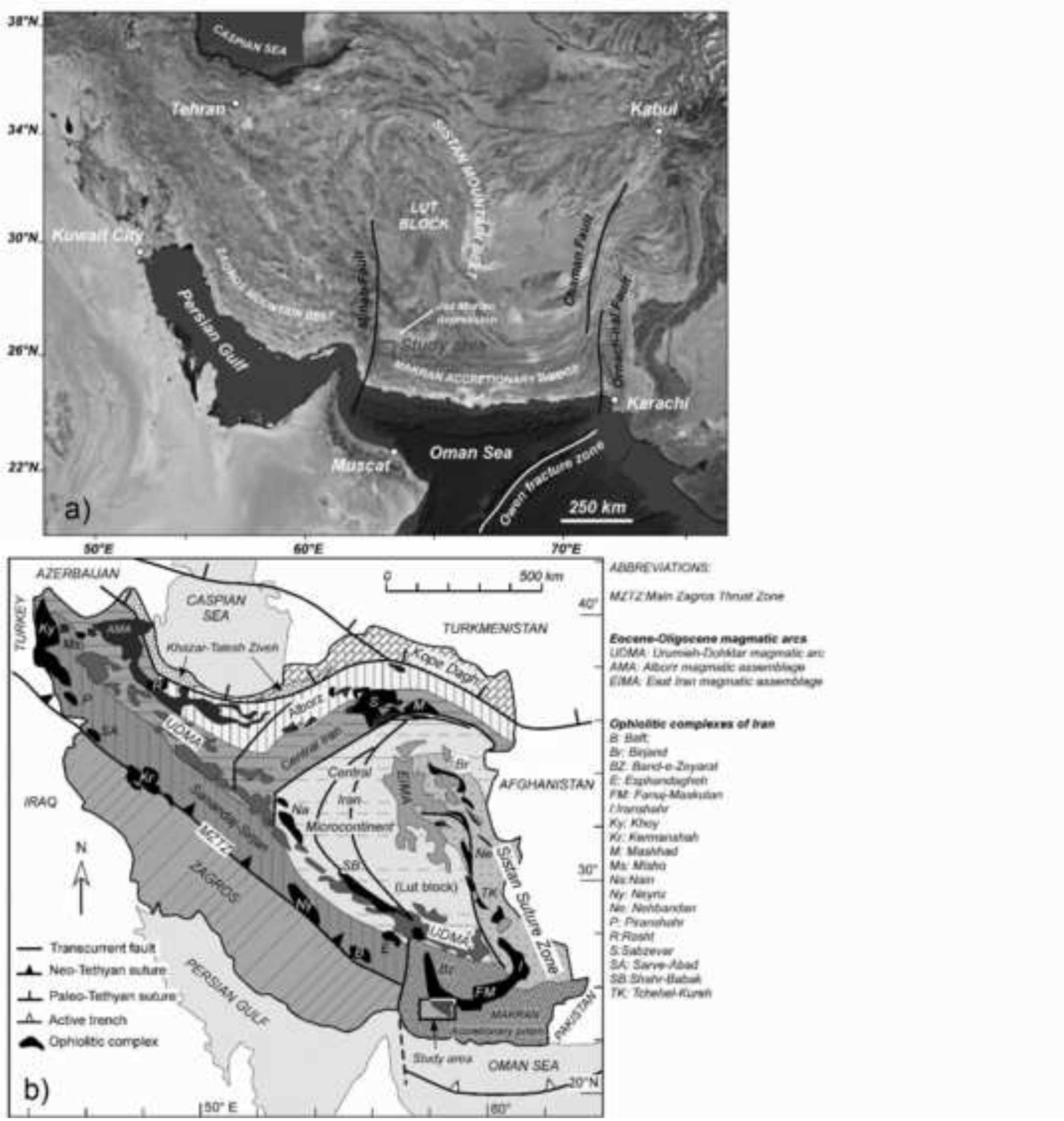

Figure 2 black & White

Click here to download high resolution image

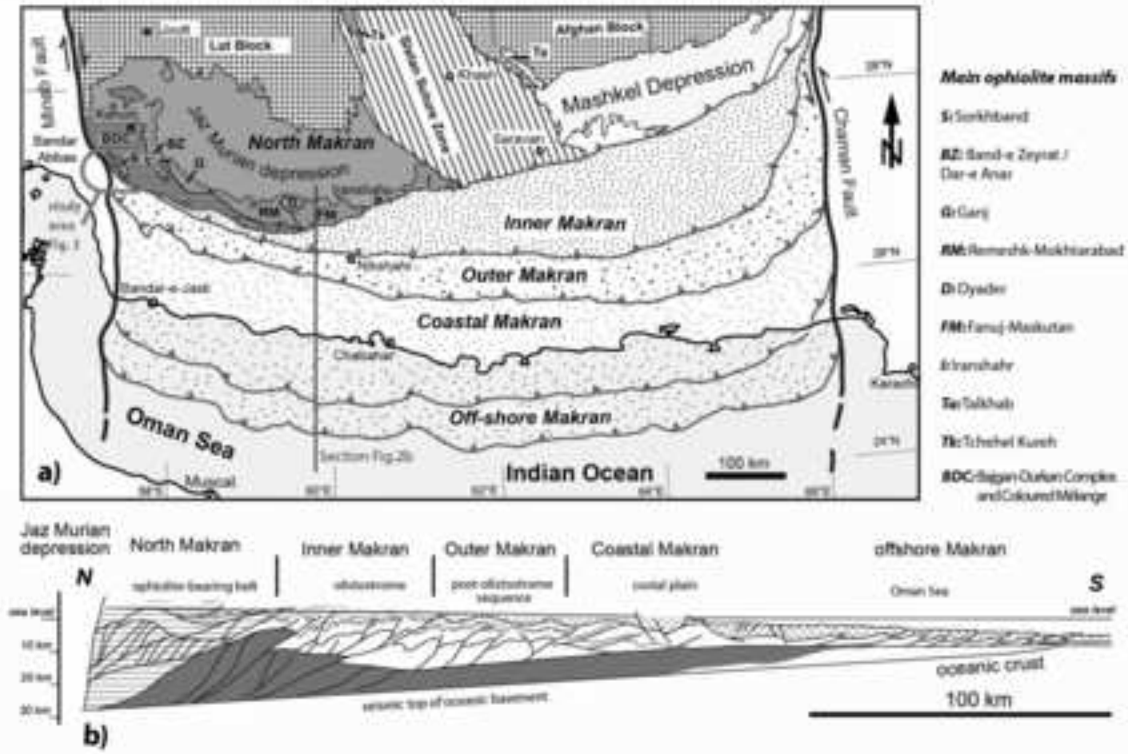

Figure 3 black & White

Click here to download high resolution image

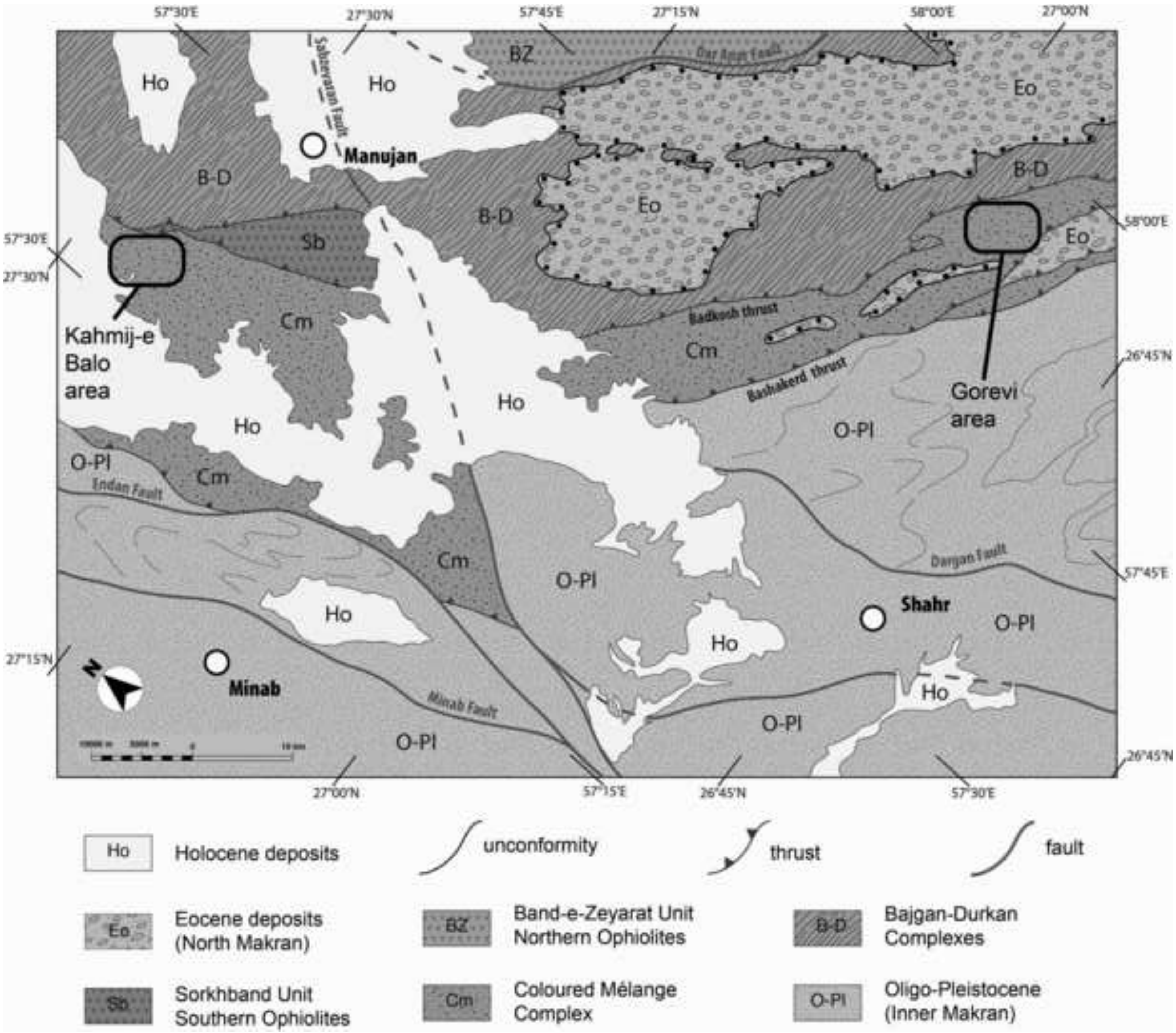

Figure 4 black & White

Click here to download high resolution image

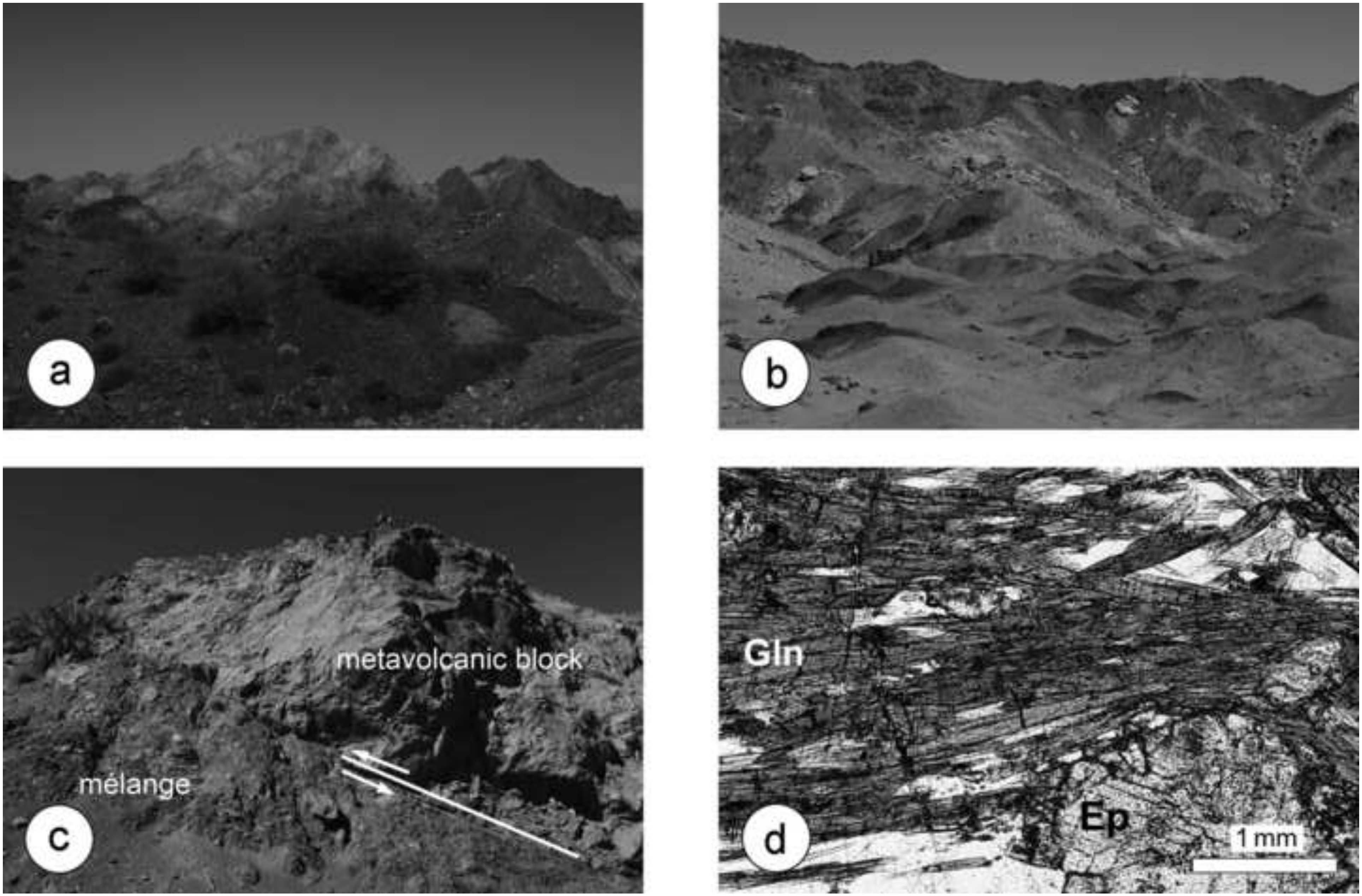

Figure 5 black & White

Click here to download high resolution image

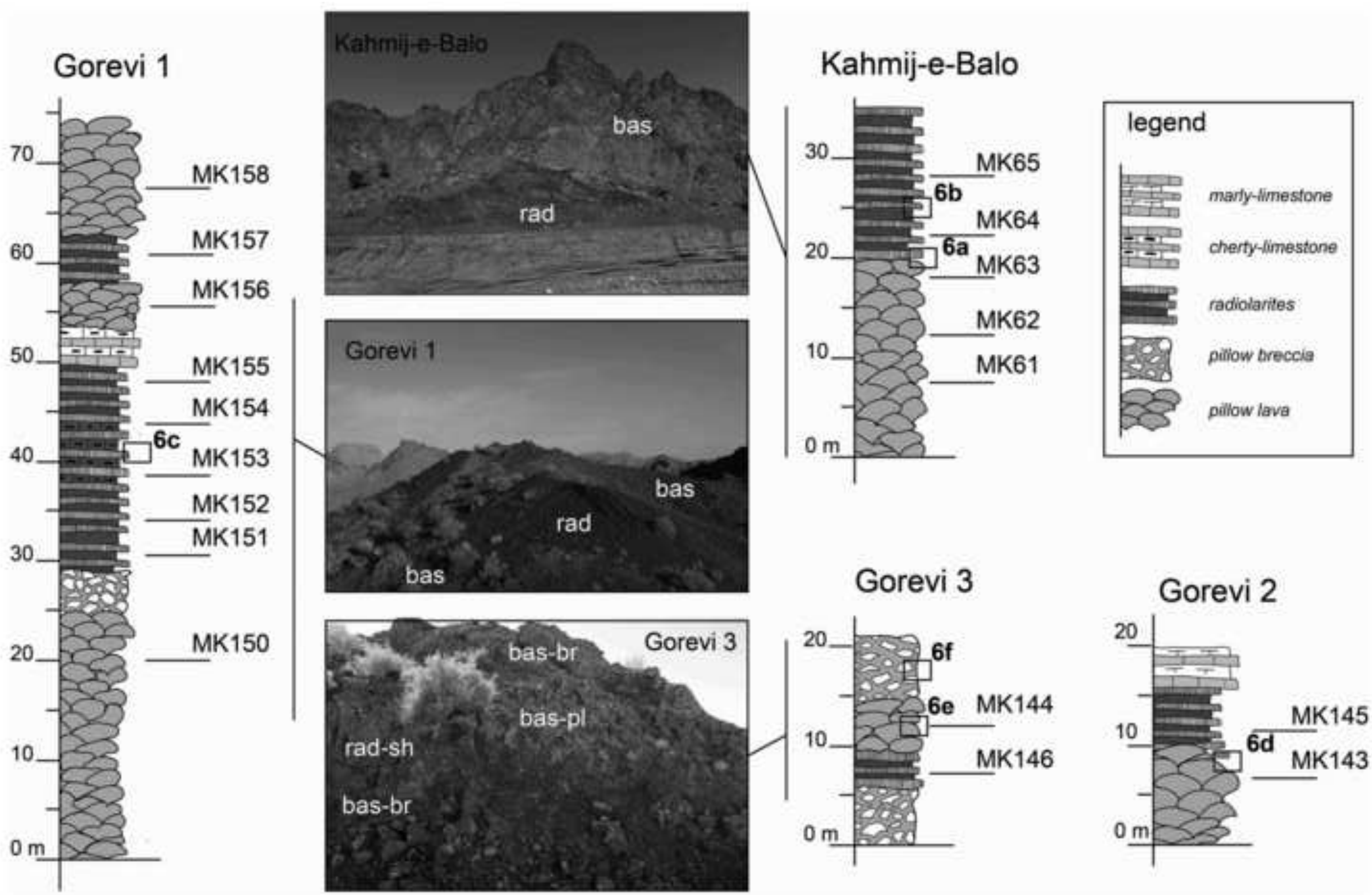

Figure 6 black & White
Click here to download high resolution image

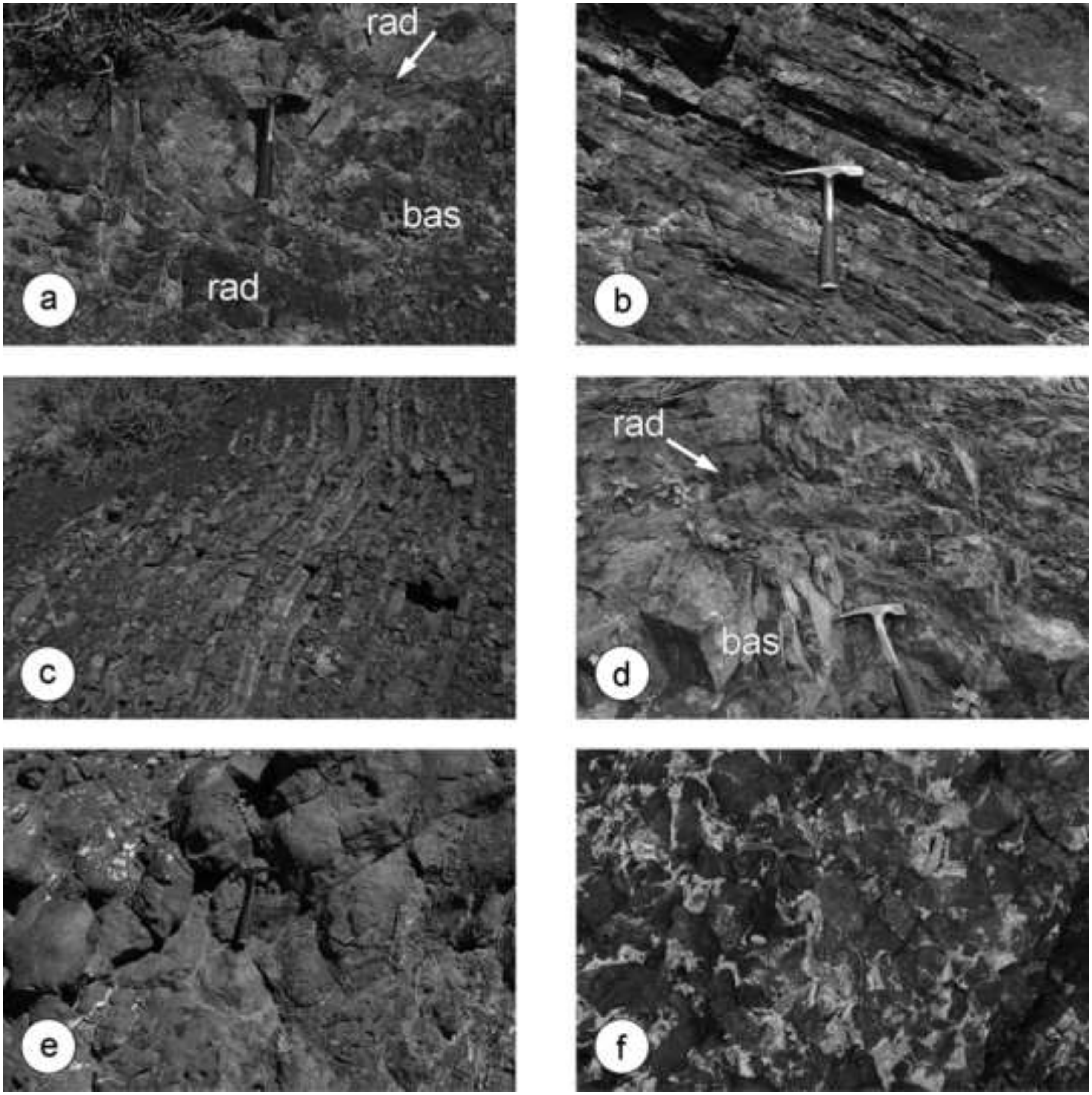

Figure 8 black & White
Click here to download high resolution image

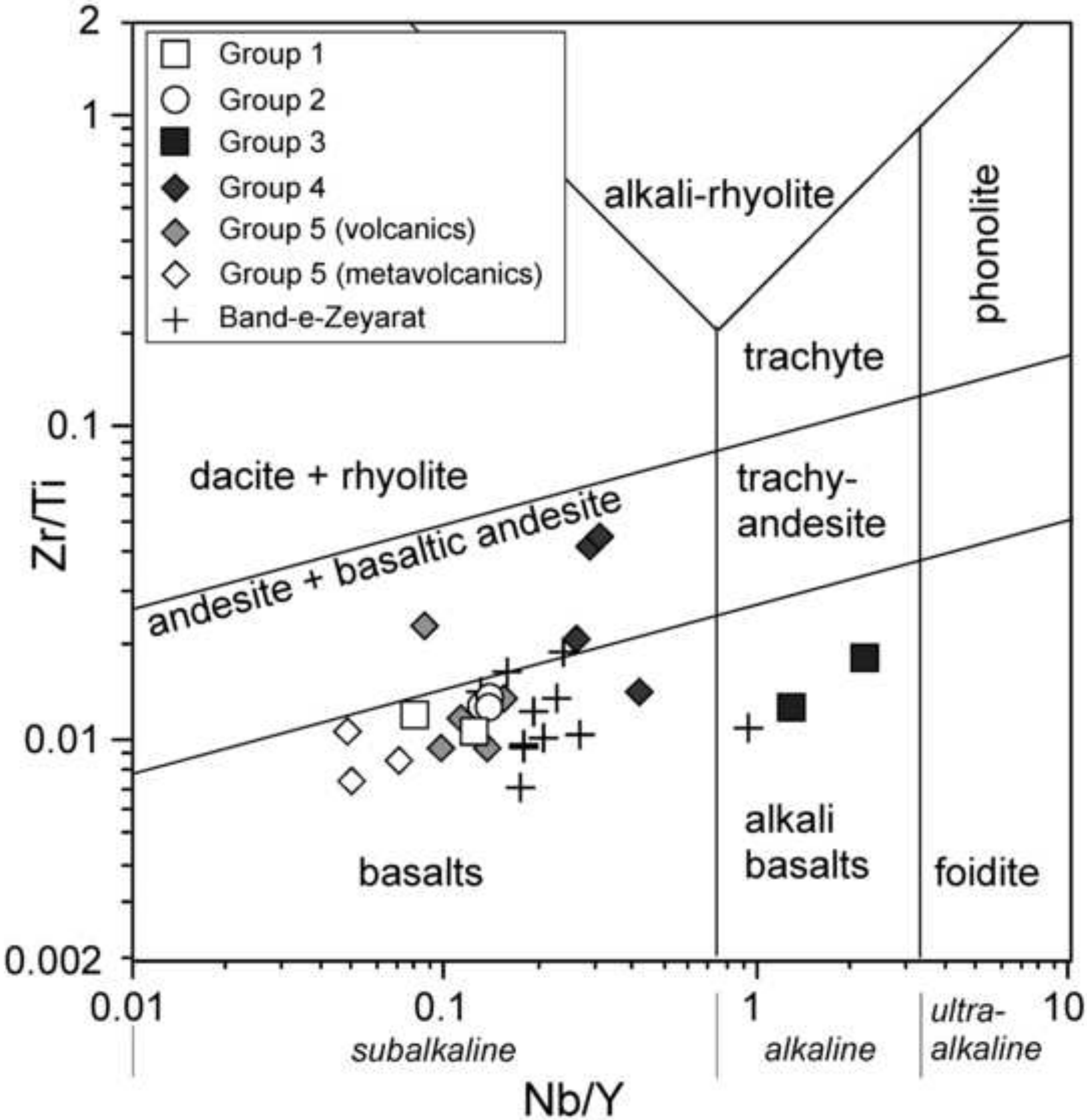

Figure 9 black & White

Click here to download high resolution image

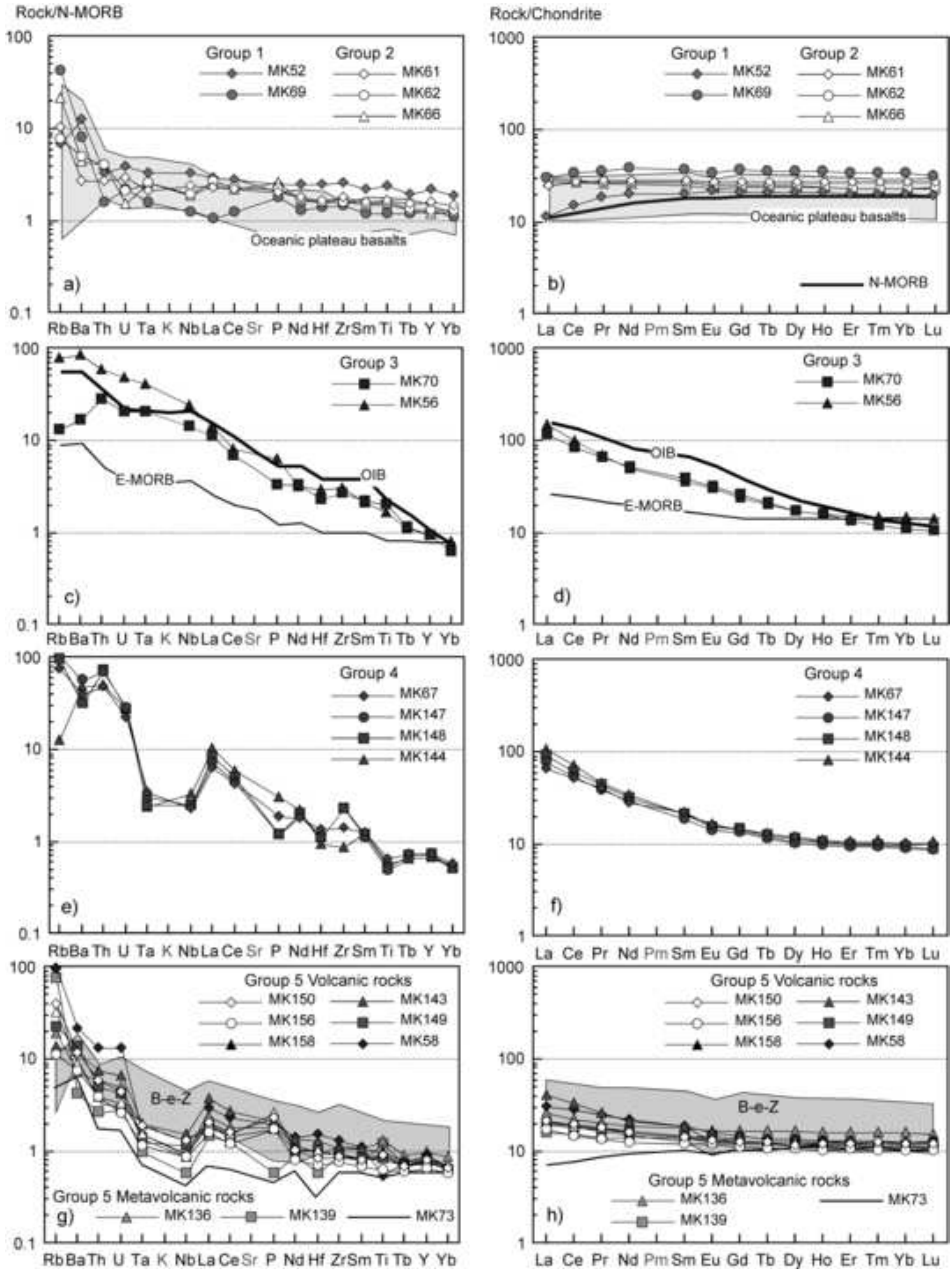

Figure 10 black & White

Click here to download high resolution image

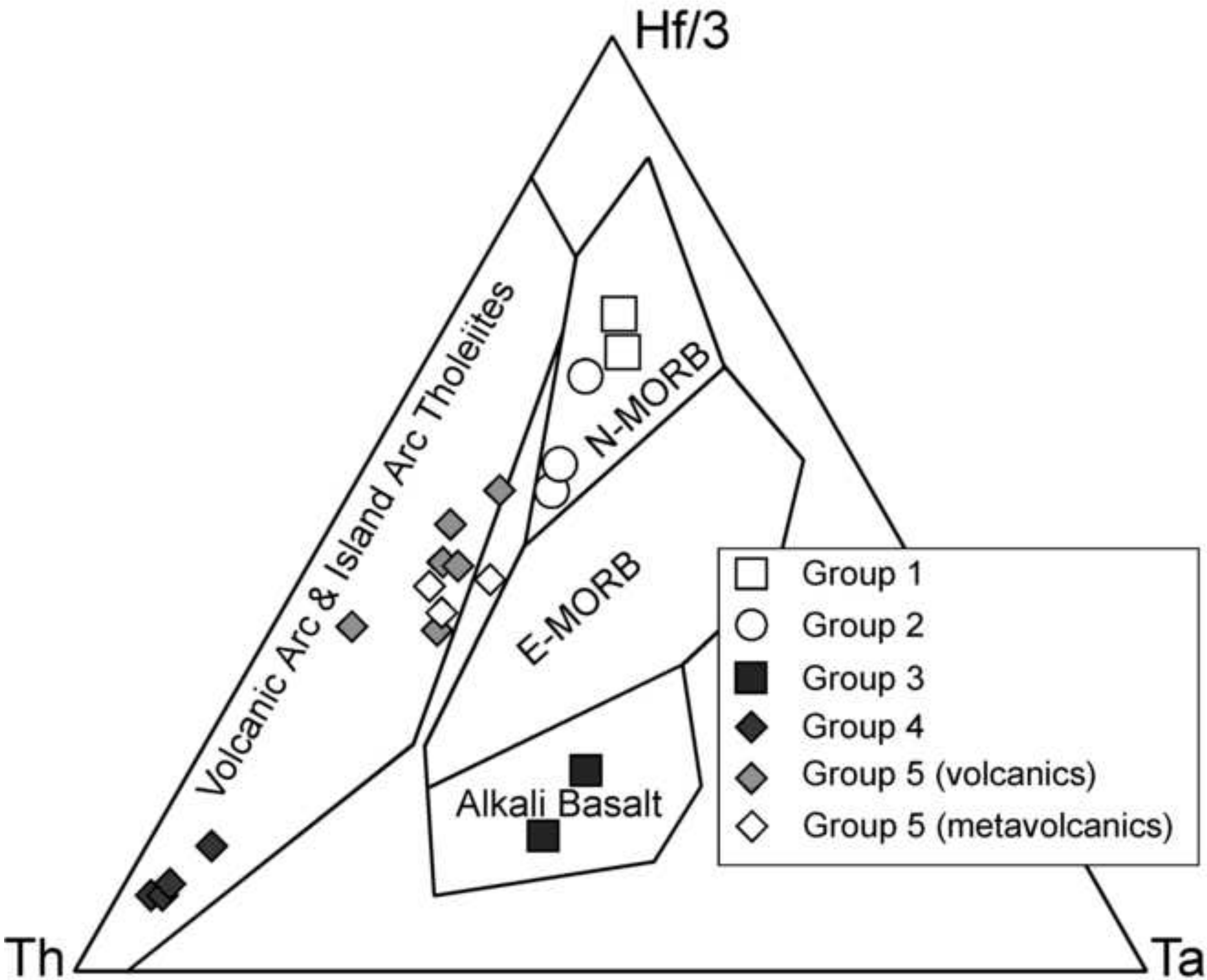

Figure 11 black & White

Click here to download high resolution image

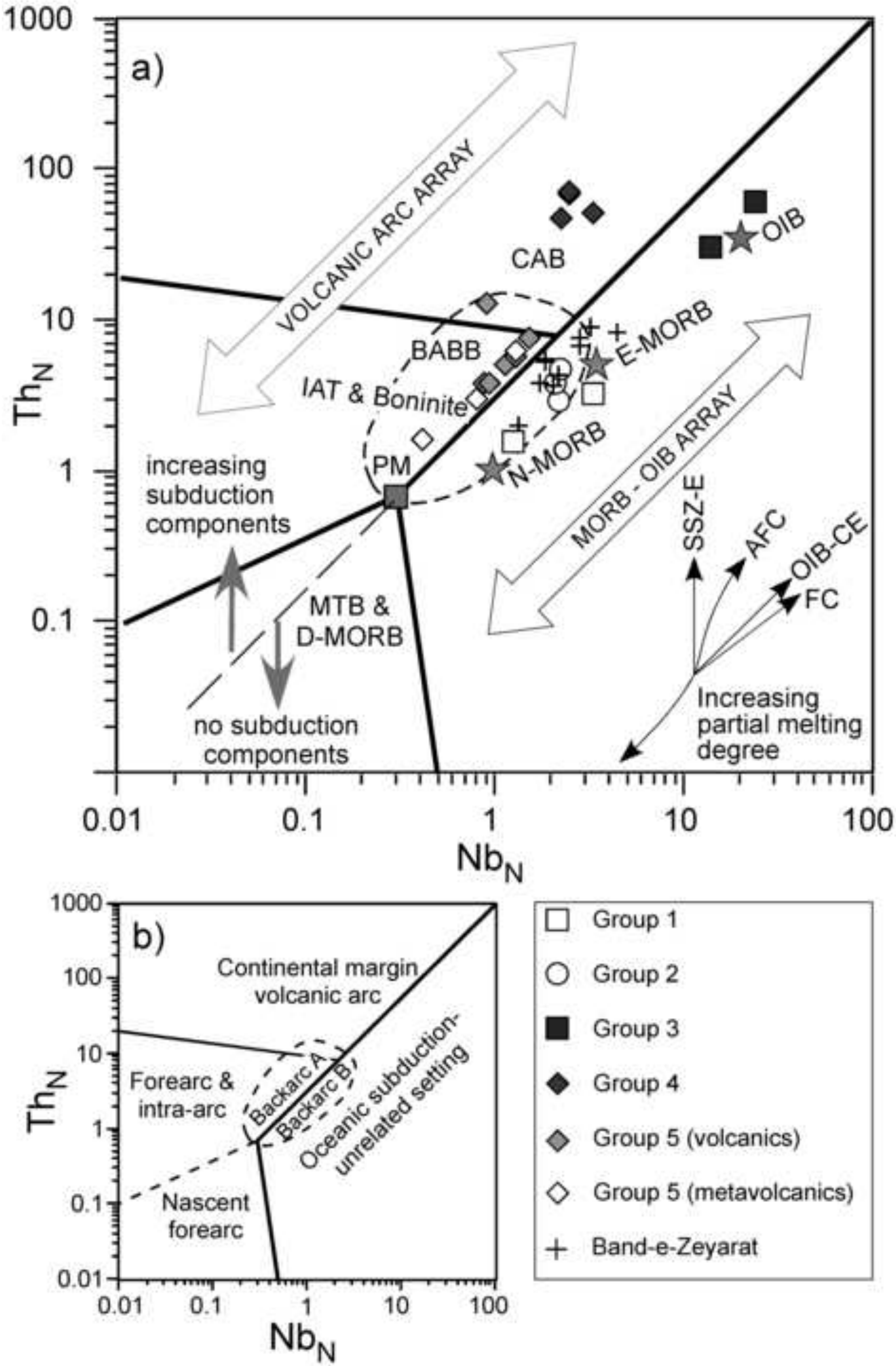

Figure 12 black & White

Click here to download high resolution image

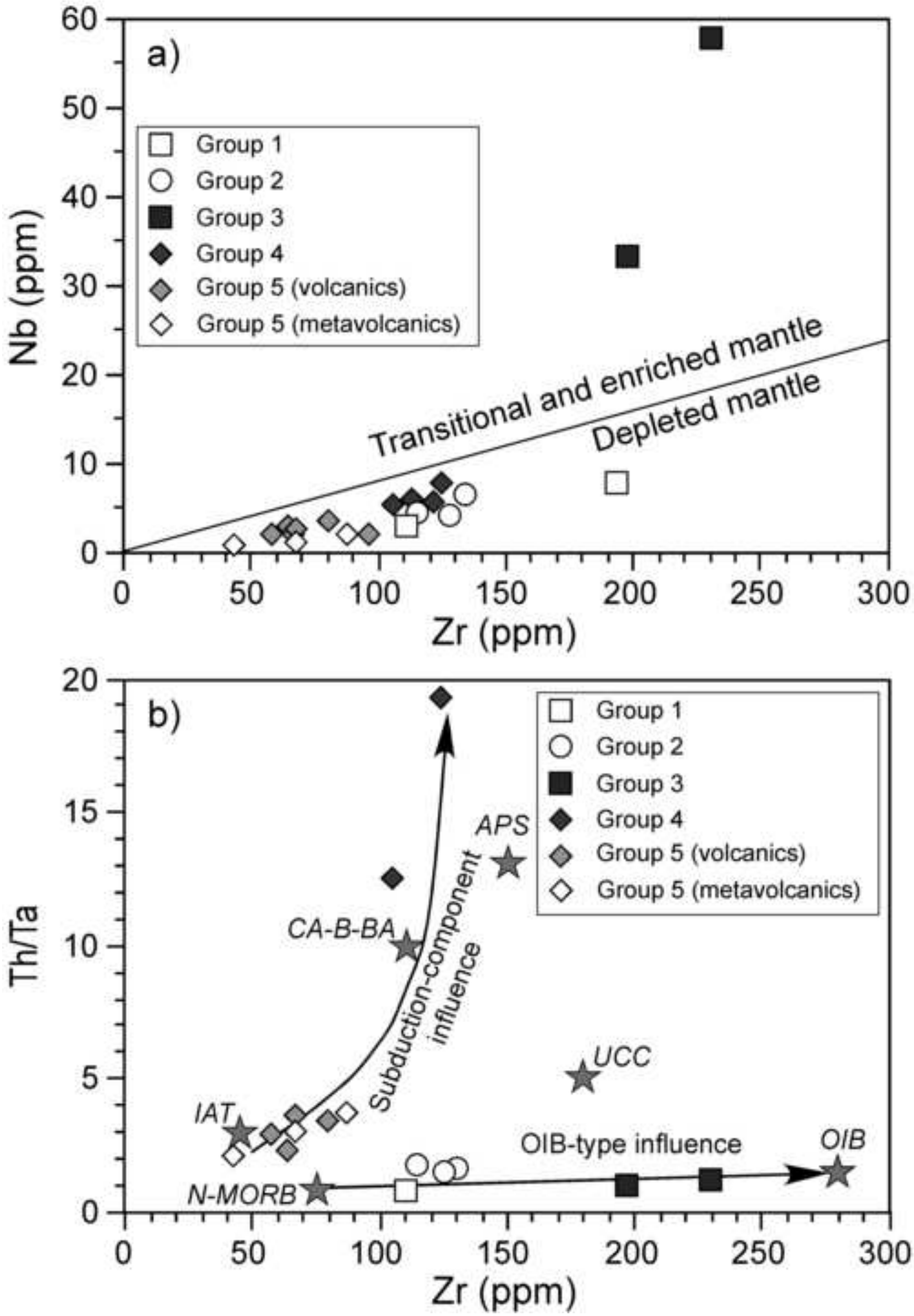

Figure 13 black & White

Click here to download high resolution image

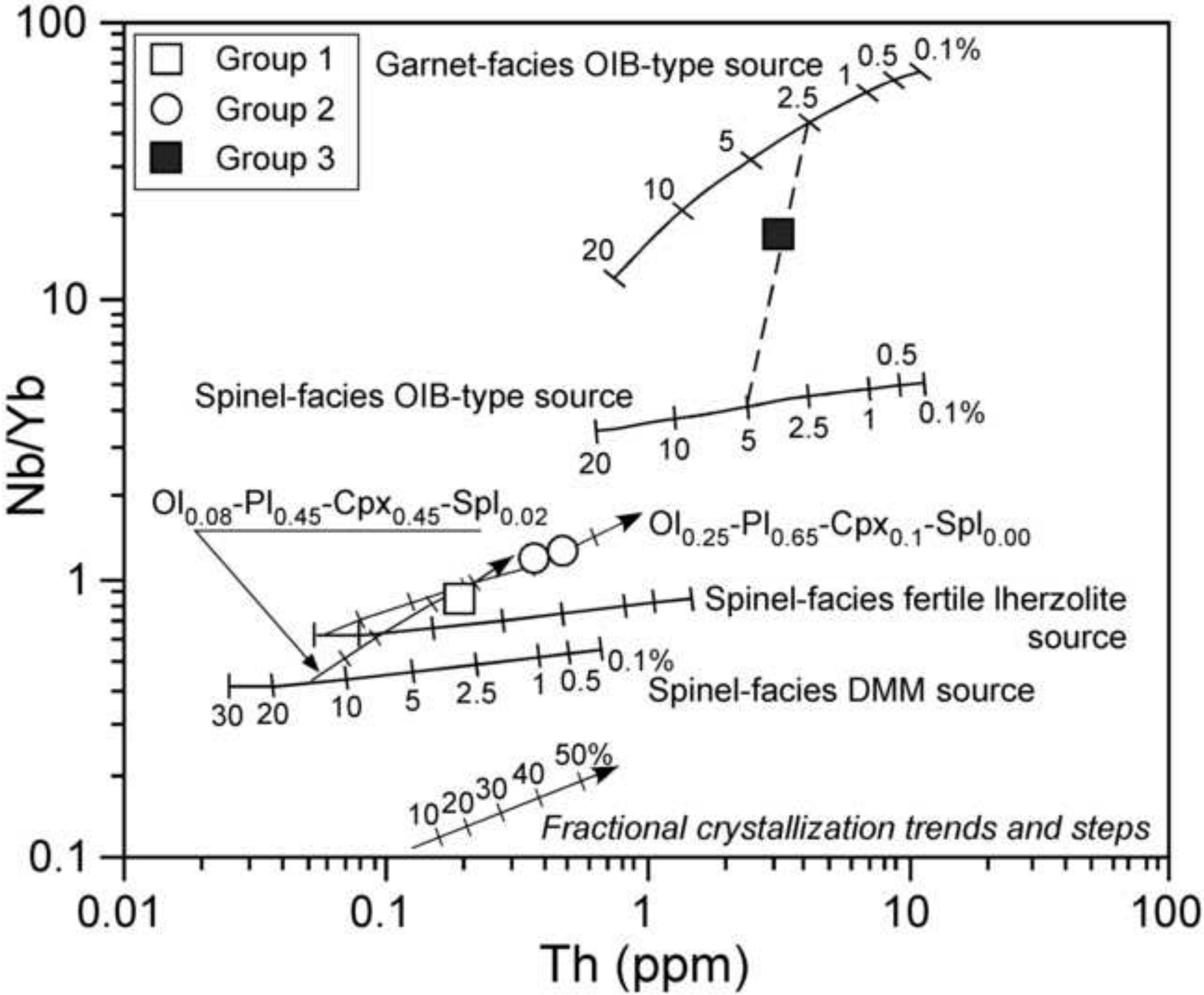

Figure 14 black & White

Click here to download high resolution image

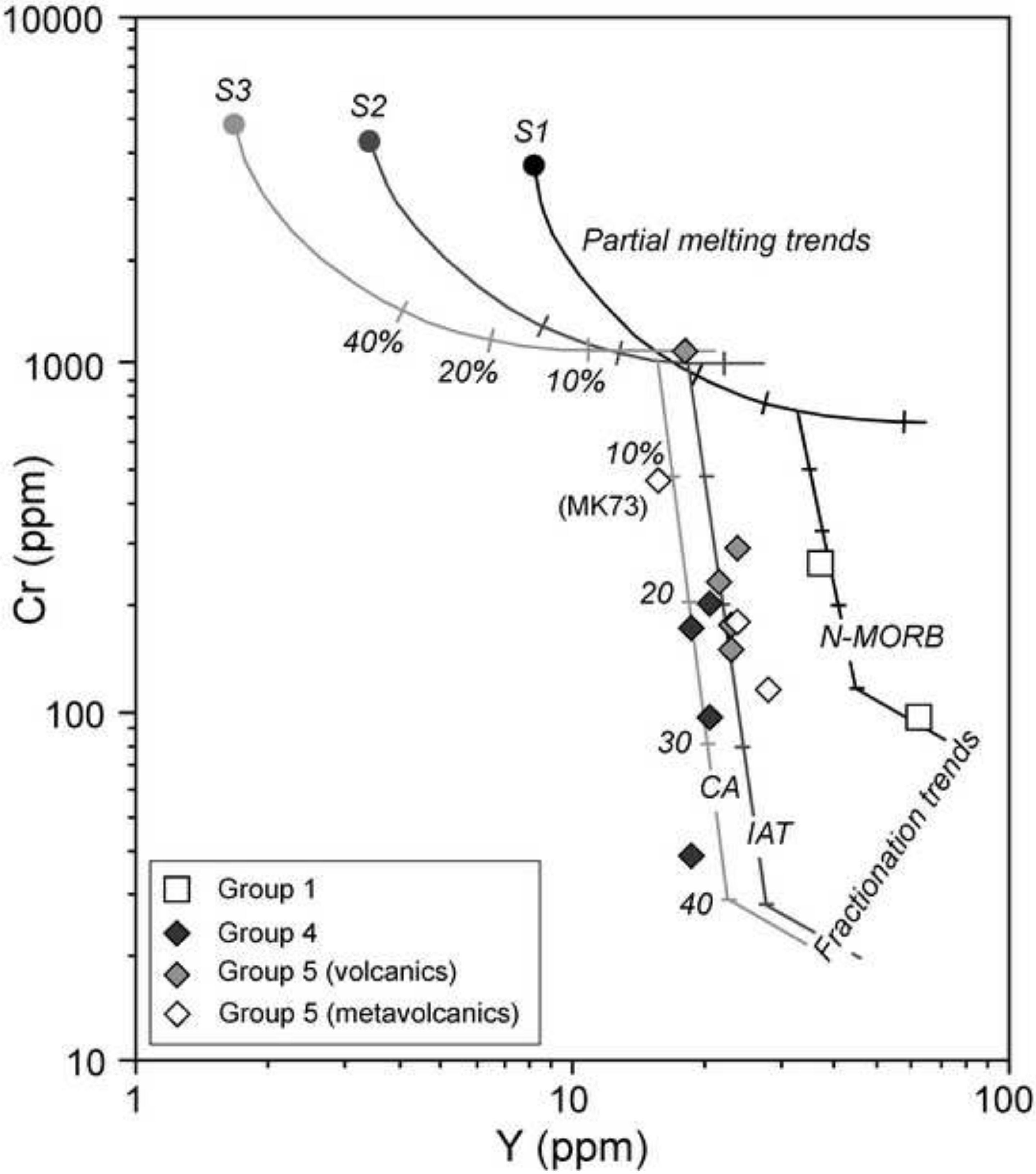

Figure 15 black & White

Click here to download high resolution image

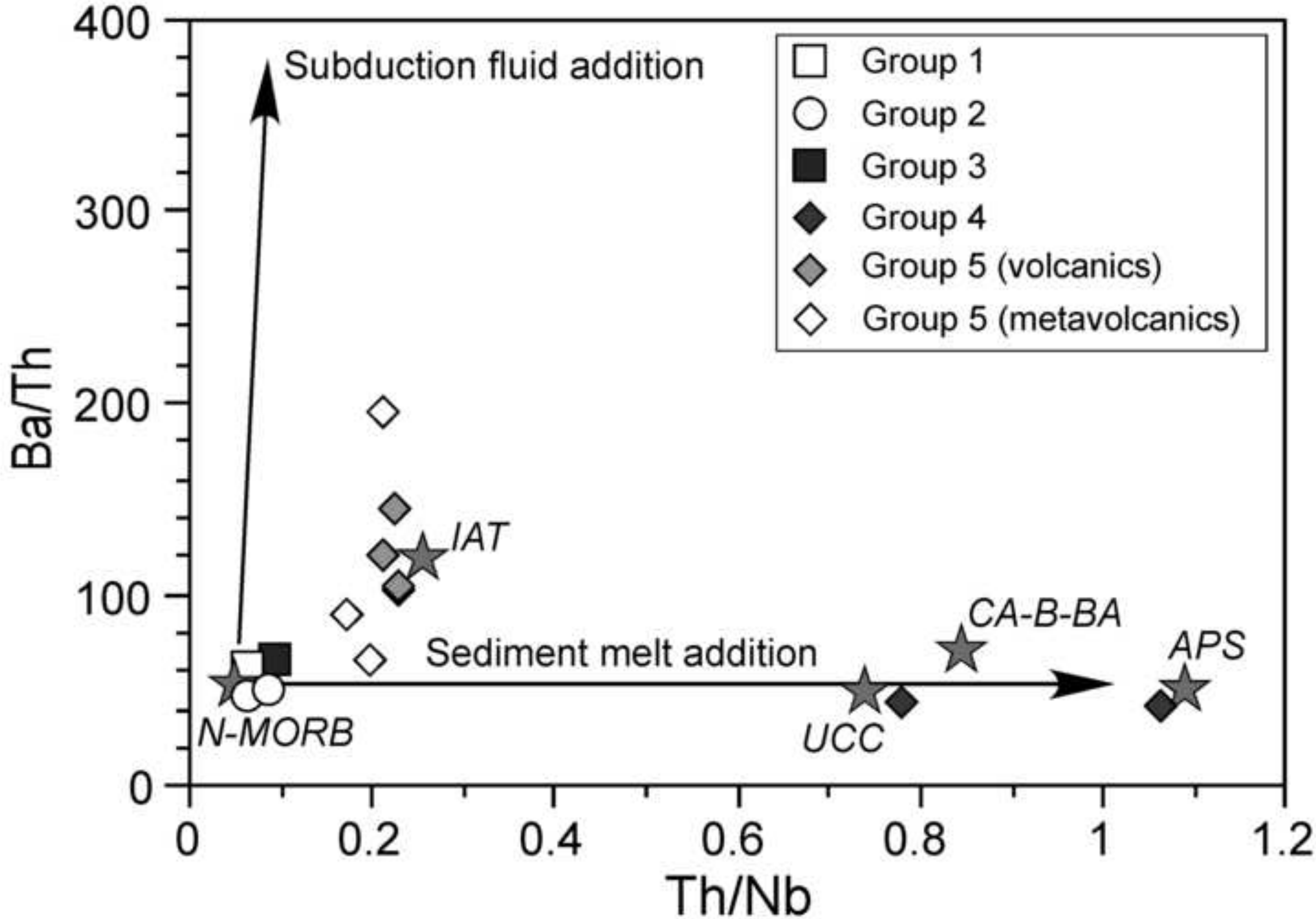

Figure 16 black & White

Click here to download high resolution image

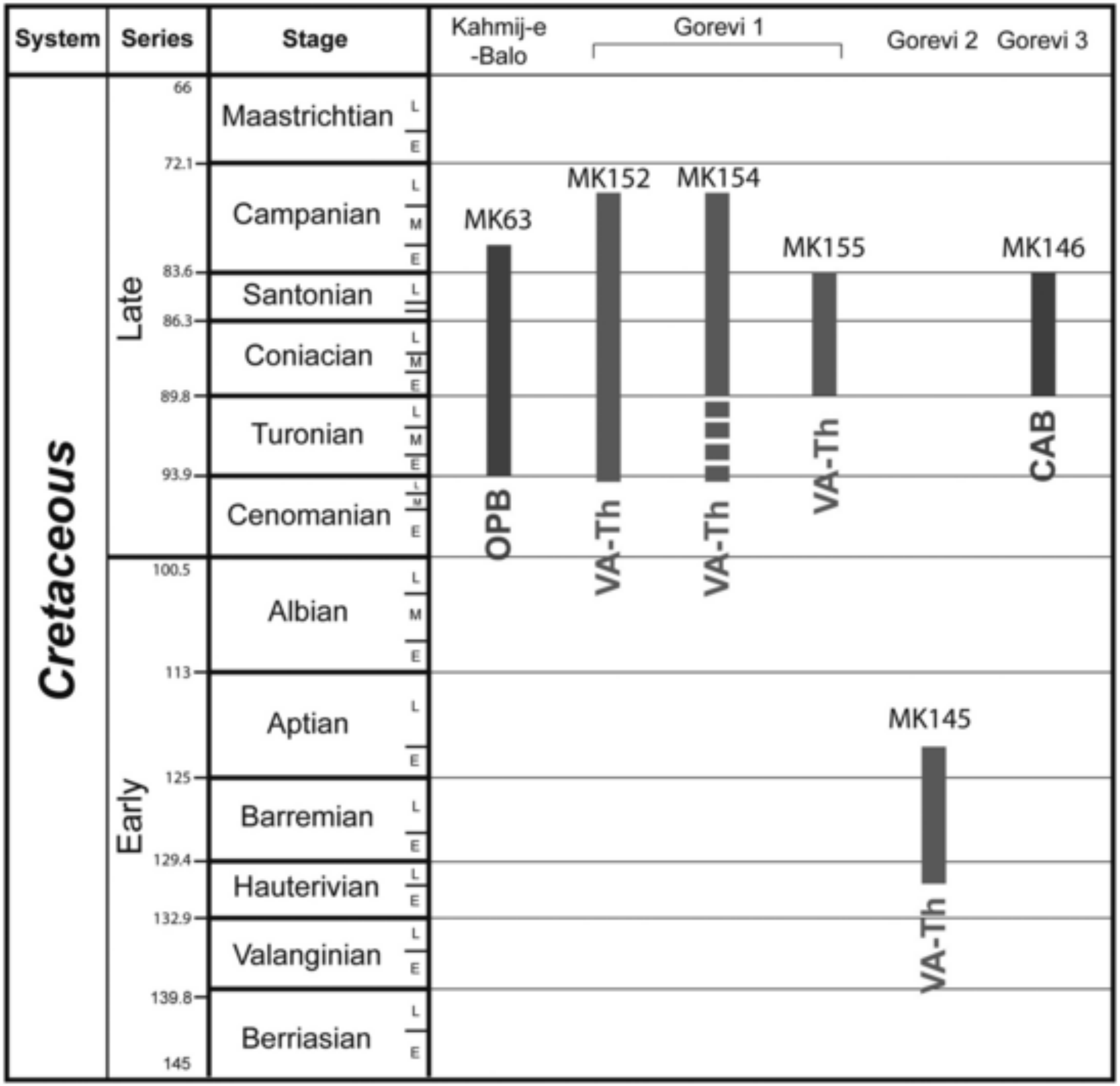

Figure 17 black & White

Click here to download high resolution image

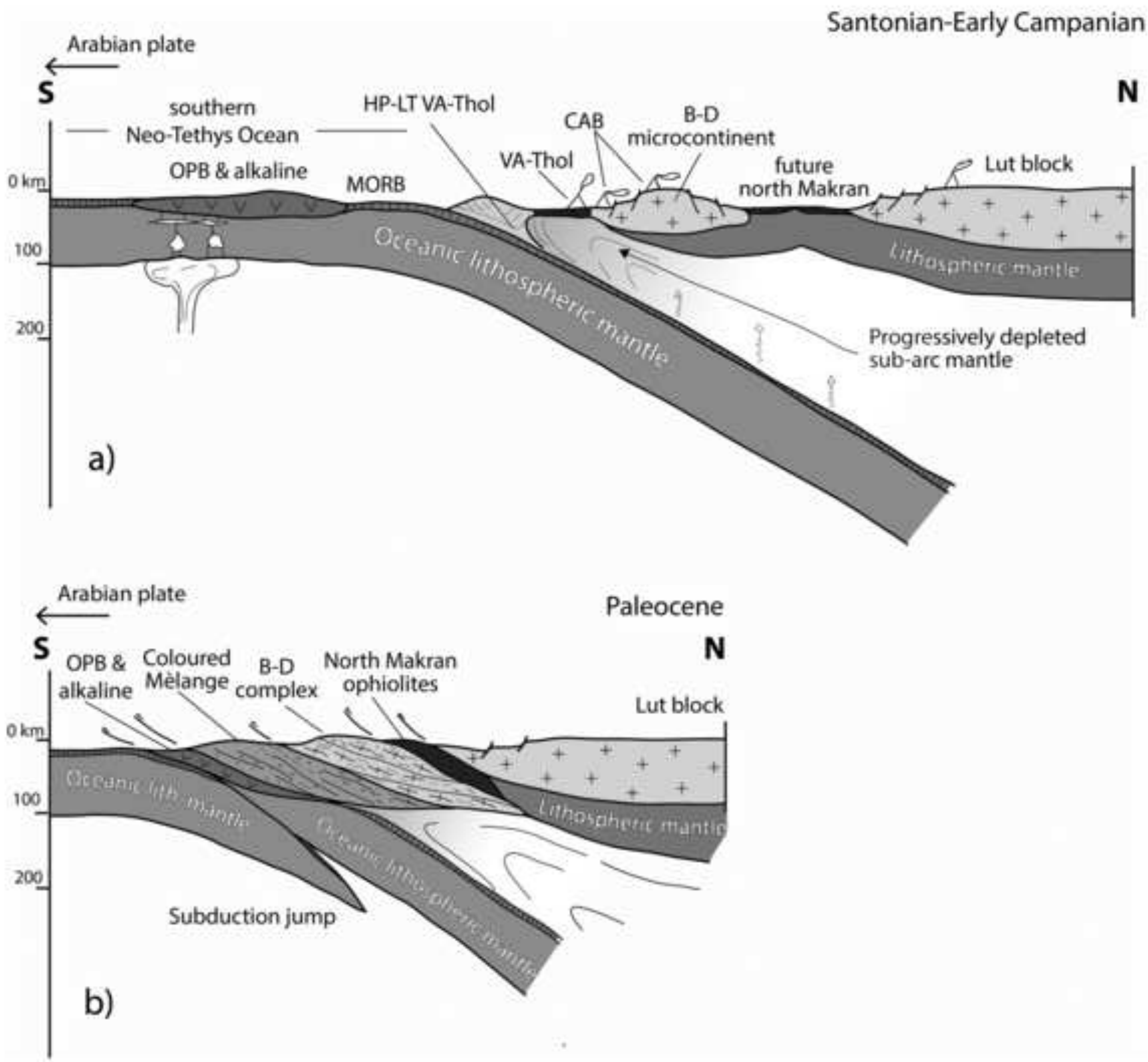

Table 1

Table 1.

Section				Kahmij-e-Balo						
Latitude (N)	27°26.6423’	27°26.6423’	27°26.9535’	27°28.2793’	27°28.2793’	27°27.8452’	27°27.8456’	27°27.5991’	27°27.5856’	27°27.0468’
Longitude (E)	57°4.7244’	57°4.7244’	57°4.9285’	57°17.8873’	57°17.8873’	57°18.6654’	57°18.6651’	57°19.5861’	57°20.0209’	57°20.6197’
Sample	MK52	MK56	MK58	MK61	MK62	MK66	MK67	MK69	MK70	MK73
Rock	bas	bas	dac	bas	bas	bas	bas and	Fe-bas	bas	metavolc
Group	Group 1	Group 3	Group 5	Group 2	Group 2	Group 2	Group 4	Group 1	Group 3	Group 5
Type	N-MORB	Alk	VA-Th	OPB	OPB	OPB	CA	N-MORB	Alk	VA-Th
Note	MLF	MLF	MLF	pillow	pillow	pillow	MLF	MLF	MLF	bas
Age				L Cr (Tu-Ca)	L Cr (Tu-Ca)					
XRF Analyses:										
SiO_2	44.65	50.86	68.70	50.23	45.08	49.81	52.61	51.4	43.52	50.30
TiO_2	1.41	2.04	0.66	2.11	1.92	1.95	0.79	2.95	2.54	0.64
Al_2O_3	15.56	18.75	12.32	12.88	14.21	14.25	14.18	11.34	12.21	10.18
Fe_2O_3	1.36	1.19	0.39	1.86	1.62	1.61	0.92	2.17	1.73	1.06
FeO	9.06	7.91	2.58	12.41	10.79	10.76	6.13	14.46	11.51	7.09
MnO	0.17	0.17	0.10	0.26	0.39	0.25	0.24	0.14	0.18	0.23
MgO	6.08	4.37	3.57	7.02	8.86	6.73	9.53	5.49	12.33	12.87
CaO	9.07	5.02	2.71	7.61	8.95	8.34	5.71	6.30	10.52	11.52
Na_2O	3.78	2.49	2.15	2.83	3.04	3.61	3.89	3.41	1.77	3.53
K_2O	1.05	3.27	2.64	0.18	0.03	0.50	1.69	0.05	0.42	0.09
P_2O_5	0.20	0.73	0.22	0.24	0.24	0.29	0.21	0.28	0.38	0.05
L.O.I.	7.52	3.01	3.86	2.32	4.69	1.64	4.03	1.94	2.79	2.42
Total	99.91	99.8	99.88	99.95	99.81	99.73	99.92	99.93	99.89	99.98
Mg#	54.5	49.6	71.2	50.2	59.4	52.7	73.5	40.4	65.6	76.4
Zn	122	95	51	108	150	114	91	121	108	66
Cu	50	43	4	34	33	21	71	47	85	27
Sc	30	16	13	37	44	36	14	45	40	27
Ga	15	18	12	21	21	18	15	17	19	11
Ni	134	104	6	39	41	61	49	30	73	85
Co	91	37	2	65	58	64	12	48	70	45
Cr	272	101	n.d.	126	367	263	100	99	76	480
V	126	163	63	320	346	297	160	448	332	224
Ba	12	534	134	17	32	28	247	37	205	41
Pb	12	13	17	10	14	12	16	6	8	7
ICP-MS Analyses:										
Rb	4.22	45.0	55.3	5.71	4.41	12.3	42.7	3.88	7.38	2.74
Sr	451	548	398	142	115	174	261	104	457	57.0
Y	36.7	26.3	25.1	42.0	36.0	33.9	20.7	62.3	26.0	20.1
Zr	110	231	96.3	134	119	128	106	194	198	43.6
La	2.70	36.2	7.38	5.90	6.91	6.32	15.7	7.32	27.8	1.70
Ce	9.46	60.4	17.6	16.42	17.6	16.7	31.5	21.1	52.2	4.74
Pr	1.78	6.71	2.36	2.68	2.64	2.51	3.82	3.48	6.44	0.84
Nd	9.41	23.5	10.5	13.15	12.83	12.0	13.4	18.1	24.5	4.39
Sm	3.17	5.57	2.89	4.29	4.13	3.90	3.33	5.8	5.95	1.55
Eu	1.28	1.76	0.733	1.56	1.43	1.36	0.945	2.00	1.87	0.544
Gd	4.35	4.87	3.08	5.68	5.15	4.90	2.99	7.61	5.35	2.12
Tb	0.801	0.757	0.516	1.04	0.928	0.892	0.489	1.34	0.790	0.386
Dy	5.41	4.46	3.39	6.99	6.30	6.12	3.01	9.20	4.47	2.78
Ho	1.18	0.920	0.740	1.55	1.37	1.34	0.623	2.03	0.892	0.62
Er	3.38	2.57	2.08	4.51	3.90	3.82	1.77	5.85	2.25	1.77
Tm	0.521	0.383	0.325	0.696	0.601	0.591	0.269	0.878	0.311	0.279
Yb	3.46	2.48	2.13	4.54	3.95	3.89	1.75	5.81	1.90	1.77
Lu	0.501	0.366	0.327	0.692	0.603	0.580	0.261	0.806	0.275	0.271
Nb	2.95	57.7	2.12	2.62	4.53	4.32	5.39	7.75	33.1	0.990
Hf	2.90	6.11	3.13	3.39	3.34	3.25	2.79	5.06	4.79	0.660
Ta	0.208	5.37	0.207	0.282	0.345	0.342	0.455	0.444	2.79	0.093
Th	0.190	7.14	1.56	0.321	0.454	0.487	5.72	0.397	3.12	0.208
U	0.104	2.31	0.628	0.141	0.099	0.073	1.07	0.188	0.968	0.078
Ti/V	47	78	65	40	35	40	31	40	47	18
Zr/Y	3.00	8.79	3.84	2.51	2.52	2.97	5.12	3.11	7.63	2.17
Nb/Y	0.08	2.20	0.08	0.13	0.13	0.13	0.26	0.12	1.28	0.05
Nb/Zr	0.019	0.250	0.022	0.042	0.038	0.034	0.051	0.040	0.167	0.023
$(La/Sm)_N$	0.55	4.19	1.65	0.89	1.08	1.05	3.04	0.82	3.02	0.71
$(Sm/Yb)_N$	1.02	2.50	1.51	1.05	1.16	1.11	2.11	1.11	3.48	0.97
$(La/Yb)_N$	0.56	10.46	2.49	0.93	1.25	1.17	6.41	0.90	10.5	0.69

Table 1. (cont.)

Section			Gorevi 1						Gorevi 2	Gorevi 3
Latitude (N)	26°56.6259’	26°56.6259’	26°53.2789’	26°53.2789’	26°53.2789’	26°53.3702’	26°53.3702’	26°53.3706’	26°53.3256’	26°53.3702’
Longitude (E)	57°56.4407’	57°56.4407’	57°56.7885’	57°56.7885’	57°56.7885’	57°56.6880’	57°56.6880’	57°56.6875’	57°56.7333’	57°56.6880’
Sample	MK136	MK139	MK150	MK156	MK158	MK147	MK148	MK149	MK143	MK144
Rock	metavolc	metavolc	bas	bas	bas	and	dac	bas	bas	bas and
Group	Group 5	Group 5	Group 5	Group 5	Group 5	Group 4	Group 4	Group 5	Group 5	Group 4
Type	VA-Th	VA-Th	VA-Th	VA-Th	VA-Th	CA	CA	VA-Th	VA-Th	CA
Note	bas	bas and	pillow	pillow	pillow	MLF	MLF	pillow	pill. brec.	pill. brec.
Age			L Cr (lCe-Sa)	L Cr (Tu-Ca)					E Cr (Ha-Ap)	L Cr (Co-Sa)
XRF Analyses:										
SiO_2	46.11	54.89	49.09	44.18	51.68	58.20	59.89	47.43	45.70	53.43
TiO_2	1.65	1.49	1.11	0.79	1.17	0.59	0.65	1.00	1.18	0.72
Al_2O_3	13.93	12.32	14.22	11.54	14.70	12.13	12.26	12.04	14.51	16.71
Fe_2O_3	1.62	1.41	1.33	1.59	1.44	0.59	0.62	1.27	1.08	0.88
FeO	10.80	9.40	8.85	10.61	9.61	3.96	4.12	8.45	7.23	5.89
MnO	0.20	0.24	0.19	0.54	0.16	0.09	0.09	0.12	0.19	0.06
MgO	11.67	6.13	4.97	17.06	7.14	6.41	5.94	13.78	12.80	4.29
CaO	7.73	8.35	10.11	6.44	6.46	7.03	6.28	7.36	8.79	8.14
Na_2O	2.81	1.54	5.15	3.80	4.56	2.53	2.51	3.17	3.05	6.53
K_2O	0.70	1.91	1.94	0.45	1.78	1.44	1.56	1.10	0.61	0.45
P_2O_5	0.20	0.07	0.26	0.19	0.30	0.13	0.13	0.20	0.23	0.36
L.O.I.	2.52	2.24	2.63	2.90	0.95	6.58	5.85	4.03	4.57	2.28
Total	99.95	99.98	99.85	100.08	99.94	99.69	99.89	99.97	99.93	99.76
Mg#	65.8	53.7	50.0	74.1	57.0	74.3	72.0	74.4	75.9	56.5
Zn	97	91	46	92	70	50	51	67	71	49
Cu	86	48	14	6	12	22	20	32	83	64
Sc	27	33	20	22	25	11	14	27	27	17
Ga	16	15	13	9	12	11	11	10	20	18
Ni	55	52	50	372	68	68	63	63	135	4
Co	59	47	39	81	48	6	5	51	50	13
Cr	120	186	155	1120	184	180	210	244	302	40
V	296	216	184	178	234	124	123	238	228	233
Ba	46	26	74	48	56	280	264	87	77	274
Pb	6	7	10	13	9	13	11	10	8	14
ICP-MS Analyses:										
Rb	10.8	42.5	22.3	6.34	18.2	58.0	53.9	12.4	7.84	7.25
Sr	323	448	220	154	223	137	147	278	417	604
Y	27.8	23.6	22.9	18.2	22.9	18.8	20.5	21.4	23.9	18.8
Zr	87.3	67.8	64.6	57.7	66.9	121	113	67.1	80.5	124
La	6.08	3.73	5.15	4.05	4.91	18.2	21.4	4.74	9.53	26.0
Ce	13.5	9.35	12.2	9.14	11.4	33.0	37.9	11.1	20.3	43.4
Pr	1.93	1.37	1.69	1.32	1.69	3.74	4.22	1.64	2.45	4.46
Nd	8.78	6.62	7.64	5.93	7.65	13.6	15.0	7.37	9.99	15.9
Sm	2.79	2.13	2.16	1.82	2.24	2.92	3.21	2.18	2.84	3.27
Eu	0.963	0.866	0.747	0.706	0.776	0.837	0.890	0.736	0.936	0.983
Gd	3.47	2.77	2.55	2.31	2.62	2.78	3.03	2.51	2.99	2.87
Tb	0.617	0.499	0.463	0.407	0.474	0.433	0.478	0.459	0.514	0.444
Dy	4.16	3.14	3.00	2.70	3.20	2.65	2.91	2.99	3.41	2.71
Ho	0.924	0.682	0.680	0.591	0.703	0.548	0.597	0.652	0.749	0.604
Er	2.63	2.00	2.01	1.74	2.06	1.55	1.66	1.91	2.15	1.69
Tm	0.404	0.295	0.315	0.267	0.317	0.239	0.253	0.288	0.330	0.263
Yb	2.68	1.94	2.04	1.75	2.13	1.54	1.60	1.89	2.18	1.70
Lu	0.396	0.281	0.312	0.261	0.323	0.222	0.232	0.283	0.320	0.257
Nb	2.88	1.63	3.07	2.04	2.20	5.86	5.94	2.65	3.66	7.90
Hf	1.94	1.19	1.70	1.43	2.13	2.24	2.30	2.09	2.72	1.93
Ta	0.178	0.128	0.25	0.156	0.202	0.400	0.330	0.163	0.259	0.317
Th	0.584	0.314	0.700	0.466	0.465	8.34	8.65	0.599	0.905	6.14
U	0.231	0.135	0.209	0.122	0.154	1.32	1.32	0.199	0.313	1.28
Ti/V	34	42	37	27	30	31	34	26	32	19
Zr/Y	3.14	2.87	2.83	3.18	2.92	6.45	5.50	3.13	3.37	6.60
Nb/Y	0.07	0.05	0.13	0.11	0.10	0.31	0.29	0.12	0.15	0.42
Nb/Zr	0.024	0.017	0.047	0.045	0.033	0.048	0.053	0.039	0.045	0.064
$(La/Sm)_N$	1.41	1.13	1.54	1.44	1.42	4.03	4.29	1.40	2.16	5.14
$(Sm/Yb)_N$	1.16	1.22	1.17	1.15	1.17	2.11	2.24	1.28	1.45	2.13
$(La/Yb)_N$	1.63	1.38	1.81	1.66	1.66	8.51	9.61	1.8	3.14	10.96

Supplementary Appendix

Click here to download e-component: Saccani_et_al_Makran_Appendix.pdf